Universidade de São Paulo
Instituto de Física

Dinâmica de fluidos em modelos de rede de poros: aplicações usando o Método de Redes de Boltzmann

Vladivostok Franz Suxo Mamani

Orientador: Prof. Dr. Caetano Rodrigues Miranda

Tese de doutorado apresentada ao Instituto de Física da Universidade de São Paulo, como requisito parcial para a obtenção do título de Doutor em Ciências.

Banca Examinadora:
Prof. Dr. Caetano Rodrigues Miranda - Orientador (IFUSP)
Prof. Dr. Adriano Mesquita Alencar (IFUSP)
Prof. Dr. Rafael dos Santos Gioria (EPUSP)
Prof. Dr. Luís Fernando Mercier Franco (UNICAMP)
Dr. Rodrigo Surmas (Petrobras)

São Paulo
2023

FICHA CATALOGRÁFICA
Preparada pelo Serviço de Biblioteca e Informação
do Instituto de Física da Universidade de São Paulo

Suxo Mamani, Vladivostok Franz

Dinâmica de fluidos em modelos de rede de poros: aplicações usando o Método de Redes de Boltzmann / Fluid dynamics in pore network models: applications using the Lattice Boltzmann Method. São Paulo, 2023.

Tese (Doutorado) - Universidade de São Paulo. Instituto de Física. Depto. de Física dos Materiais e Mecânica

Orientador: Prof. Dr. Caetano Rodrigues Miranda.

Área de Concentração: Física da Matéria Condensada

Unitermos: 1. Física computacional; 2. Dinâmica dos fluídos; 3. Mecânica dos fluídos computacional.

USP/IF/SBI-092/2023

University of São Paulo
Physics Institute

Fluid dynamics in pore network models: applications using the Lattice Boltzmann Method

Vladivostok Franz Suxo Mamani

Supervisor: Prof. Dr. Caetano Rodrigues Miranda

Thesis submitted to the Physics Institute of the University of São Paulo in partial fulfillment of the requirements for the degree of Doctor of Science.

Examining Committee:
Prof. Dr. Caetano Rodrigues Miranda - Supervisor (IFUSP)
Prof. Dr. Adriano Mesquita Alencar (IFUSP)
Prof. Dr. Rafael dos Santos Gioria (EPUSP)
Prof. Dr. Luís Fernando Mercier Franco (UNICAMP)
Dr. Rodrigo Surmas (Petrobras)

São Paulo
2023

"*Imperfection is beauty, madness is genius and it's better to be absolutely ridiculous than absolutely boring.*"

Marilyn Monroe

Abstract

A critical problem in fluid dynamics in porous media is describing the delay in fluid flow as it passes through the internal porous network. Capillary phenomena become predominant at the micrometre scale and significantly affect fluid displacement and petroleum recovery in porous media, such as porous rocks or artificial devices formed by heterogeneous microchannels with distinct wettability. Depending on the wettability and heterogeneity of the walls, fluid flow can be retarded and confined in the micropores. Here, the general objective is to determine the relationship between the quantity of fluid trapped within a micrometric porous medium based on i) the random geometric characteristics or ii) the wettable physical properties of the porous medium. This thesis focused on describing the i) porous media and ii) its fluid dynamics at the pore scale to model these phenomena. A natural porous medium is emulated using a Pore Network Model (PNM) formed by randomly distributed circles as solid walls to quantify the degree of randomness in the porous structure. This characterisation follows the adoption of the Voronoi diagram within the PNM, which uses the circle's positions as a starting point. Performing a statistical analysis of the Voronoi polygons allows for calculating the Shannon entropy, which measures pore randomness. Moreover, Lattice Boltzmann Method (LBM) simulations using the Explicit Force method are applied to address single-fluid flow or oil recovery by fluid injection because they can model multi-component flows in porous media with heterogeneous wettability at the micrometric scale. Initially, we studied the oil extraction by varying the shape, size, and configuration of the obstacles forming the hydrophilic PNM. Our results indicate that square shapes and small circles displace more oil, while random configurations retain a certain amount of oil. Furthermore, for the same porous structure, we observed that the addition of nanoparticles in the injected fluid improves oil recovery. To investigate the effect of randomness on fluid flow, we have designed PNMs based on circles ranging from perfectly ordered to fully disordered models. Additionally, we have examined the effects of size and porosity by varying the radius and the number of circles, respectively. Our simulations demonstrate that entropic information is directly related to the degree of tortuosity and permeability. The more disordered the obstacles or the higher entropic the PNM, the more the flow experiences more significant tortuosity and improved permeability. Based on the PNMs from the previous case, we study the effect of randomness on the oil recovery process. Our results show that entropic information is closely related to the amount of trapped oil. In other words, more disordered obstacles or PNMs with higher entropy lead to an increase in the amount of oil trapped in the random pore networks. Finally, the effect of heterogeneous wettability on the oil recovery process is studied. To uncouple the effects of geometric structure, PNMs are designed with ordered circles but with hydrophobic and hydrophilic materials in varying proportions. Our results show that the hydrophilic surfaces of a PNM facilitate the oil recovery process, while the hydrophobic ones tend to obstruct the process. In conclusion, a purely physical process, such as the oil-trapped quantity or how tortuous or permeable a flow is, can be inferred from an essentially geometric characteristic, such as the morphology-topology of the porous media quantified by the Shannon entropy.

Keywords: Lattice Boltzmann Method ; Pore Network Models ; Shannon Entropy ; Oil Recovery.

Resumo

Um problema crítico na dinâmica de fluidos em meios porosos é descrever o atraso no fluxo de fluido à medida que passa pela rede porosa interna. Fenômenos capilares tornam-se predominantes na escala micrométrica e afetam significativamente o deslocamento de fluidos e a recuperação de petróleo em meios porosos, como rochas porosas ou dispositivos artificiais formados por microcanais heterogêneos com diferentes molhabilidades. Dependendo da molhabilidade e heterogeneidade das paredes, o fluxo do fluido pode ser retardado e confinado nos microporos. Aqui, o objetivo geral é determinar a relação entre a quantidade de fluido retida em um meio poroso micrométrico com base em suas i) características geométricas aleatórias ou ii) propriedades físicas molháveis do meio poroso. Precisamos descrever i) meios porosos e ii) sua dinâmica de fluidos na escala dos poros para modelar esses fenômenos. Para quantificar o grau de aleatoriedade presente na estrutura porosa, um meio poroso natural é emulado usando um Modelo de Rede de Poros (PNM) formado por círculos distribuídos aleatoriamente como paredes sólidas. Um diagrama de Voronoi dentro do PNM usa as posições dos círculos como ponto de partida. Realizar uma análise estatística dos polígonos de Voronoi permite o cálculo da entropia de Shannon, que fornece uma medida de aleatoriedade dos poros. Para abordar o fluxo de fluido simples ou a recuperação de petróleo por injeção de fluido, são aplicadas simulações do Método Lattice Boltzmann (LBM) usando o método da Força Explícita, pois podem modelar fluxos multicomponentes em meios porosos com molhabilidade heterogênea na escala micrométrica. Inicialmente, estudamos a extração de petróleo variando a forma, tamanho e configuração dos obstáculos que formam o PNM hidrofílico. Nossos resultados indicam que formas quadradas e pequenos círculos deslocam mais petróleo, enquanto configurações aleatórias retêm uma certa quantidade de petróleo. Além disso, para a mesma estrutura porosa, observamos que a adição de nanopartículas no fluido injetado melhora a recuperação do óleo. Para investigar o efeito da aleatoriedade no fluxo de fluido simples, projetamos PNMs com base em círculos que variam de modelos perfeitamente ordenados à modelos completamente desordenados. Nossas simulações demonstram que a informação entrópica está diretamente relacionada ao grau de tortuosidade e permeabilidade. Quanto mais desordenados os obstáculos ou quanto mais entropia o PNM, o fluxo experimenta maior tortuosidade e permeabilidade aprimorada. A partir das PNMs geradas, estudamos o efeito da aleatoriedade no processo de recuperação de petróleo. Nossos resultados mostram que a informação entrópica está intimamente relacionada à quantidade de petróleo retido. Em outras palavras, obstáculos mais desordenados ou PNMs com entropia mais alta levam a um aumento na quantidade de petróleo retido nas redes de poros aleatórios. Finalmente, estudamos o efeito da molhabilidade heterogênea no processo de recuperação de petróleo. Para mitigar os efeitos da estrutura geométrica, os PNMs são projetados com círculos ordenados, mas com materiais hidrofóbicos e hidrofílicos em proporções variadas. Nossos resultados mostram que as superfícies hidrofílicas de um PNM facilitam o processo de recuperação de petróleo, enquanto as hidrofóbicas tendem a obstruir o processo. Em conclusão, um processo puramente físico, como a quantidade de petróleo retida ou o quão tortuoso ou permeável é um fluxo, pode ser inferido a partir de uma característica essencialmente geométrica, como a morfologia-topologia dos meios porosos quantificada pela entropia de Shannon.

Palavras-chaves: Método de Redes de Boltzmann ; Modelos de Rede de Poros ; Entropia de Shannon ; Recuperação Melhorada de Óleo.

Acknowledgements

I must give special thanks and sincere to my advisor Caetano R. Miranda for accepting to do this thesis under his direction. Your support and confidence in my work and their ability to guide my ideas has been an invaluable contribution not only in the development of this thesis, but also in my development as a researcher. Own ideas, always framed in orientation and rigor, have been key to the good work we have done together, which can not be conceived without its ever timely participation. I am also grateful for having always provided the means to carry out all the activities proposed for the development of this thesis.

I want to express my sincere thanks to *Research Group SAMPA* for the significant contribution and active participation in the development of this thesis. I must emphasize, above all, availability and patience which made our discussions are beneficially both scientific and personal. No doubt that their involvement has enriched the work done and also has meant the emergence of a friendship.

Mainly, I want to thank Alexsandro Kirch for their direct collaboration on the Lattice Boltzmann Method and Molecular Dynamics necessary for conducting this research.

A very special thanks is due to the understanding, patience and encouragement received from my family.

This study was financed in part by the Coordenação de Aperfeiçoamento de Pessoal de Nível Superior - Brasil (CAPES) - Finance Code 001

Thus, I gratefully acknowledge the financial support from CAPES, CNPq, Petrobras and Repsol Sinopec Brasil funding agencies.

The same acknowledge is extended to the computing time provided on the Superintendencia de Tecnologia da Informação da Universidade de São Paulo.

To everyone, thank you very much ...

Contents

Acknowledgements **iv**

1 Introduction **1**
1.1 Motivation . . . 1
1.2 Computational simulations . . . 4
1.3 Objectives . . . 6
1.4 Thesis structure . . . 7

2 Lattice Boltzmann Method **8**
2.1 Introduction . . . 9
2.2 Liouville equation . . . 11
2.3 Kinetic model . . . 13
2.4 Boltzmann transport equation . . . 15
2.5 Boltzmann equation . . . 17
2.5.1 The BGKW model for the collision term . . . 17
2.5.2 Incorporation of external force fields . . . 18
2.5.3 The approximate Boltzmann transport equation . . . 19
2.6 Lattice Boltzmann Method . . . 20
2.6.1 Equilibrium distribution function . . . 23
2.6.2 Bridge between micro and macro scales . . . 24
2.7 LBM implementation in Fluid Dynamics . . . 26
2.8 Explicit Force method . . . 27
2.8.1 Incorporation of Forces . . . 30
2.8.2 Taxila-LBM package . . . 31

3 Characterization of Pore Network Models **32**
3.1 Introduction . . . 33
3.2 Random Pore Network Models (PNMs) . . . 34
3.2.1 Voronoi diagram . . . 36
3.3 Shannon entropy . . . 37
3.3.1 Shannon entropy of a Voronoi diagram . . . 38

3.3.2 Characterization of a PNM using Shannon entropy 39
3.4 Petrophysical parameters of porous media 40
3.4.1 Porosity 41
3.4.2 Tortuosity and permeability in microfluidics 41
3.4.3 Hydraulic tortuosity 42
3.4.4 Darcy permeability 44

4 Enhanced Oil Recovery in PNMs 46
4.1 Introduction 47
4.2 Methodology 49
4.2.1 Pore Netwok Models (PNMs) 50
4.2.2 Oil extraction process in PNMs 50
4.3 Results 52
4.3.1 Pore estructure effect in oil extraction 53
4.3.2 Nanoparticles effect in EOR process 56
4.4 Conclusions 58

5 Randomness Effect of the PNMs on Fluid Dynamics 60
5.1 Introduction 61
5.2 Fluid dynamics in multiscale 62
5.3 Methodology 63
5.3.1 Design of PNMs under study 64
5.3.2 Fluid dynamics in PNMs 66
5.4 Results 68
5.5 Conclusions 72

6 Randomness Effect of the Pore Network Models on Oil Recovery 74
6.1 Introduction 75
6.2 Methodology 76
6.3 Oil recovery from random PNMs 77
6.4 Results 79
6.5 Conclusions 81

7 Effects of Heterogeneity Porous Media on Oil Extraction 83
7.1 Introduction 84
7.2 Methodology 85
7.2.1 Experimental data 86
7.2.2 Mapping experimental data to LBM simulations 87

7.3 Oil recovery in heterogeneous PNMs . . . 88
7.3.1 Case study . . . 88
7.3.2 Results . . . 89
7.4 Conclusions . . . 90

8 Conclusions and Perspectives **92**
8.1 Conclusions . . . 92
8.2 Perspectives . . . 94

A Boltzmann Lattice **96**
A.1 One dimensional . . . 96
A.2 Two dimensional . . . 97
A.3 Three dimensional . . . 98

B Boundary Conditions **99**
B.1 Boundary periodic . . . 99
B.2 Bounce-back boundary . . . 100
B.3 Dirichlet boundary . . . 101

C Simulation parameters **104**
C.1 Characteristic scale . . . 104
C.2 Taxila-LBM values . . . 105
C.3 Example: Molecular Dynamics data . . . 107

Bibliography **109**

List of Figures

2.1 Schematic representation of various methodological approaches at different scales in space-time. From the quantum model to the continuum through the atomistic and mesoscopic. Picture adapted from (Kirch et al., 2020). 9
2.2 Methodological approaches (diverse models) to perform fluid dynamics simulations at different scales. 10
2.3 Dynamics of microscopic point particles. a) Position and moment before and after applying forces on a single particle. b) Particles probability density function in phase space. 14
2.4 Phase space discretization process: Position discretization and subsequent momentum discretization. 20
2.5 LBM algorithm: Main steps for the systematic application of the LBM methodology. 25
2.6 Schematic representation of a thermodynamic equilibrium process due to *interfacial tension* as a driving force. Case: a water droplet immersed in air that **a)** initially has a square shape and **c)** becomes circular when the system reaches equilibrium. 28
2.7 Schematic representation of the *wettability* phenomenon expressed and quantified through the *contact angle*. Case: a water droplet immersed in air and scattered over a solid horizontal surface with **a)** hydrophobic and **b)** hydrophilic properties. 29

3.1 The illustration shows the effect of *randomness* and *wettability* of porous media on fluid dynamics. Case: flow or streamline (red arrow) in a porous medium that **a)** initially is structurally ordered, **b)** then the streamline is visibly affected by the obstacles randomness and **c)** finally also by the walls wettability. 34
3.2 Schematic of a Voronoi diagram: Voronoi diagram from a set of points called nuclei (blue points) and a Voronoi cell with its respective nucleus $\boldsymbol{c}_i$ (red point) surrounded by neighboring cells $\boldsymbol{c}_j$. 36

3.3 Scheme of a discrete probability distribution function $f_{(x_i^*)}$: Definition of expected value $\langle x \rangle$ and properties of $f_{(x_i^*)}$. 37
3.4 Design and statistical analysis of PNMs. **a)** Voronoi diagrams generated within a PNM: First, from 64 points distributed randomly without restriction, second, using non-superimposed circles and finally, adding the restriction of a small space between circles. **b)** Distribution functions and their respective entropy compared to the Gamma distribution function. The functions and values are the average of 1000 different random configurations in the three types of PNMs. 39
3.5 Tortuosity in a channel of constant narrow width at different angles of inclination. **a)** Fluid velocity field in the inclined channels. **b)** Normalized stationary velocity relative to the case of greater inclination. **c)** Comparison between analytical tortuosity and simulated hydraulic tortuosity. 42
3.6 Hagen-Poiseuille flow by fluid injection. **a)** Scheme of a channel formed by parallel plates. **b)** Fluid velocity field in the channel. **c)** Normalized stationary velocity. **d)** Comparison of results between the analytical and simulated velocity field, where the simulated profile belongs to the channel center $(L/2)$. 44

4.1 Basic porous structures formed by geometric objects and designed to have the same porosity value ($\phi = 0.68$), where the gray regions represent a solid area and the white color represents the porous space. Porous structures according to solid objects are classified into: **a)** different shapes, **b)** different sizes and **c)** different random locations. . . 49
4.2 Oil extraction process in PNMs with obstacles of different form (oil: black region, brine: cyan region and clay: gray region). **a)** Snapshot of oil extraction at time $t = 12.8\,\mu s$. **b)** Percentage of oil extraction during the brine injection time. 51
4.3 Oil extraction process in PNMs with circular obstacles of different sizes (oil: black region, brine: cyan region and clay: gray region). **a)** Snapshot of oil extraction at time $t = 8.5\,\mu s$. **b)** Percentage of oil extraction during the brine injection time. 52
4.4 Oil extraction process in PNMs with small circular obstacles of different random location. **a)** Snapshot of oil extraction at time $t = 22.8\,\mu s$. **b)** Percentage of oil extraction during the brine injection time. 53

4.5 Enhanced oil recovery by using different nanoparticles in a PNM with small circular obstacles of random configuration. **a)** Snapshot of enhanced oil recovery at time $t = 11.2\,\mu s$. **b)** Percentage of oil extraction during the brine injection time. 55
4.6 Enhanced oil recovery in dead-end porous media, where the figures show snapshot when fluid flow reaches stationary state $t > 12\,\mu s$ (oil: black region, brine: cyan region and clay: gray region). The oil recovery amount using **a)** brine without NPs, **b)** brine with NP-H, **c)** brine with NP-SA and **d)** brine with NP-PEG2 are 5.2, 7.3, 10.4 and 13.7% respectively. 56
4.7 Enhanced oil recovery in a three-dimensional PNM formed by orderedly located spheres (oil: black region, brine: cyan region and clay: gray region), cases: brine without nanoparticles and with three types of nanoparticle, NP-H, NP-SA and NP-PEG2. **a)** Snapshot of enhanced oil recovery. **b)** Oil extraction as a function of time. 57

5.1 Designs of two-dimensional PNMs formed by a random distribution of circular geometric objects (obstacles) but without overlapping objects, where the gray regions represent the solid structure and the rest is the pore space (white region). The random PNMs are classified as: **a)** Obstacle disorder variation, **b)** System entropic variation, **c)** Obstacle size variation and **d)** System porosity variation. 63
5.2 *Obstacle disorder variation*: Design and statistical analysis of PNMs that present an obstacle disorder in five successive steps. **a)** Voronoi diagrams generated within a PNM. **b)** Probability functions for each disorder degree. **c)** The (averange) Shannon entropy for each disorder degree and its respective spectrum or possible entropy values. 65
5.3 *Obstacle size variation*: Design and statistical analysis of PNMs formed by obstacles of five different sizes. **a)** Voronoi diagrams generated within a PNM. **b)** Probability functions for each size. **c)** The Shannon entropy of constant value $H = 1.90$ for each size and its respective spectrum or possible entropy values. 67
5.4 *System porosity variation*: Design and statistical analysis of PNMs that have five different porosities based on the obstacle number. **a)** Voronoi diagrams generated within a PNM. **b)** Probability functions for each porosity. **c)** The Shannon entropy of constant value $H = 1.90$ for each porosity and its respective spectrum or possible entropy values. 67

5.5 *Obstacle disorder effect*: Disorder degree effect on fluid dynamics. **a)** Snapshot of the velocity field of the fluid flow at steady state. **b)** Disorder degree effect on the tortuosity of PNMs. **c)** Disorder degree effect on the permeability of PNMs. 69
5.6 *System entropy effect*: Entropy variation effect on fluid dynamics. **a)** Snapshot of the velocity field of the fluid flow at steady state. **b)** Entropy variation effect on the tortuosity of PNMs. **c)** Entropy variation effect on the permeability of PNMs. 69
5.7 *Ostacle size effect*: Size variation effect on fluid dynamics. **a)** Snapshot of the velocity field of the fluid flow at steady state. **b)** Size variation effect on the tortuosity of PNMs. **c)** Size variation effect on the permeability of PNMs. 72
5.8 *System porosity effect*: Porosity variation effect on fluid dynamics. **a)** Snapshot of the velocity field of the fluid flow at steady state. **b)** Porosity variation effect on the tortuosity of PNMs. **c)** Porosity variation effect on the permeability of PNMs. 73

6.1 *Obstacle disorder effect*: Disorder degree effect on oil recovery process. **a)** Final snapshot of the oil recovery process. **b)** Percentage of oil extracted as a function of time. **c)** Relationship between the percentage of oil extracted and the disorder degree. 78
6.2 *System entropy effect*: Entropy variation effect on oil recovery process. **a)** Final snapshot of the oil recovery process. **b)** Percentage of oil extracted as a function of time. **c)** Relationship between the percentage of oil extracted and the system entropy. 79
6.3 *Ostacle size effect*: Size variation effect on oil recovery process. **a)** Final snapshot of the oil recovery process. **b)** Percentage of oil extracted as a function of time. **c)** Relationship between the percentage of oil extracted and the obstacle size. 81
6.4 *System porosity effect*: Porosity variation effect on oil recovery process. **a)** Final snapshot of the oil recovery process. **b)** Percentage of oil extracted as a function of time. **c)** Relationship between the percentage of oil extracted and the system porosity. 82

7.1 Experimental data mapping that generates input parameters for LBM simulations. Final snapshot of LBM simulations for an oil bubble in the middle of water and confined by two parallel plates, cases: **a)** hydrophilic and **b)** hydrophobic. 87
7.2 Oil recovery by water injection on the left side into PNMs with varied wettability for 4 time steps (oil: black region, water: cyan region, hydrophobic: orange region and hydrophilic: gray region), cases: **a)** Hydrophobic, **c)** Hydrophilic and **b)** Heterogeneous (mixed). 88
7.3 *Heterogeneity effect*: Heterogeneity effect on oil recovery process. **a)** Final snapshot of the oil recovery. **b)** Percentage of oil extracted as a function of time. **c)** Relationship between the percentage of oil extracted and percentage of heterogeneity. 89

A.1 One-dimensional configuration of Boltzmann lattices and their respective statistical weights, cases: A and B. 97
A.2 Two-dimensional configuration of Boltzmann lattices and their respective statistical weights, cases: D_2Q_4, D_2Q_5 and D_2Q_9. 97
A.3 Three-dimensional configuration of Boltzmann lattices and their respective statistical weights, cases: D_3Q_{19} and D_3Q_{27}. 98

B.1 Streaming process between nodes far from the system boundary. **a)** Central node (red arrows) that interacts with its neighbors (blue arrows) at time t. **b)** End of the interaction process between the central node and its neighbors at time $t + \Delta t$. 100
B.2 Streaming process in the presence of periodic boundary condition. **a)** A node (red arrows) that interacts with its neighbors (blue arrows) through the periodic boundary (located on the right) at time t. **b)** End of interaction process between the node and its neighbors $(t + \Delta t)$. 101
B.3 Continuous model to discrete model 102
B.4 Process streaming in the presence of a Dirichlet boundary (boundary velocity) that has a velocity $\boldsymbol{v}_o = v_x\hat{\imath} + v_y\hat{\jmath}$. **a)** A node (red arrows) interacts with its neighbors (blue arrows) and the velocity boundary at time t. **b)** is the intermediate step before the completion of the process. **c)** End of process, interactions missing in the node is completed by solving the equations relating macroscopic and microscopic quantities $(t + \Delta t)$. 103

C.1 Scheme for obtaining the characteristic scale Γ of a system based on physical magnitudes and simulation parameters, case: study of fluid dynamics using the LBM methodology. 105
C.2 Scheme of the conversion of physical magnitudes to dimensionless simulation parameters and their subsequent conversion to values of the Taxila-LBM software. 106

List of Tables

2.1 Comparison of continuum and kinetic models expressed by the Navier-Stokes equation and the Boltzmann equation respectively. . . . 19
2.2 List of lattice dimension values for different lattice configurations in: 1D, 2D and 3D. 24

7.1 Summary of data from experimental measurements of oil recovery processes by water injection, into glass porous media with walls covered by a thin hydrophilic or hydrophobic layer. 86
7.2 Summary of the input parameters for the LBM simulations that come from the mapping of experimental data (see Tab. 7.1). 86

C.1 Summary of molecular dynamics simulations performed for the case of a brine solution (with and without nanoparticles) in contact with oil confined between surfaces of the montmorillonite clay. 107
C.2 Summary of the molecular dynamics mapped parameters for the Explicit Force model and LBM simulations. 108

List of Abbreviations

PDE	**P**artial **D**ifferential **E**quations
FDM	**F**inite **D**ifference **M**ethod
FVM	**F**inite **V**olume **M**ethod
FEM	**F**inite **E**lement **M**ethod
CFD	**C**omputational **F**luid **D**ynamics
LBM	**L**attice **B**oltzmann **M**ethod
BGK	**B**hatnagar **G**ross **K**rook
BGKW	**B**hatnagar **G**ross **K**rook **W**elander
PNM	**P**ore **N**etwork **M**odels
API	**A**merican **P**etroleum **I**nstitute
MMT	**M**ont**M**orilloni**T**e
MD	**M**olecular **D**ynamics
NP	**N**ano**P**article
no-NP	(without) **N**ano**P**article
NP-H	**N**ano**P**article **H**ydroxylated
NP-SA	**N**ano**P**article **S**ulfonic **A**cid
NP-PEG2	**N**ano**P**article **P**oly**E**thylene**G**lycol

Physical Constants

Velocity of Light	$c_o = 2.99792458 \times 10^8\, m/s$ (exact)
Velocity of Sound	$c_s = 343\, m/s$ (in Air at $20\,^{\circ}$C and $760\, mm$Hg)
Boltzmann constant	$k_B = 1.38064852 \times 10^{-23}$ J/K

List of Symbols

ρ	density	kg/m^3
μ	dynamic viscosity	$kg/(m \cdot s)$
ν	kinematic viscosity	m^2/s
γ	interfacial tension	kg/s^2
θ	contact angle	$^{\circ}$
$\boldsymbol{v}$	velocity field	m/s
p	pressure profile	$kg/(m \cdot s^2)$
$\boldsymbol{v}_{\mathrm{o}}$	injection velocity	m/s
f	distribution function	
f^{eq}	equilibrium distribution function	
f^{F}	force distribution function	
Ω_{col}	collision operator	
Ω_{for}	force operator	
τ	relaxation time	
ω	collision frequency	
H	Shannon entropy	
ϕ	porosity	
τ	tortuosity	
k	permeability	mD

For to my parents, brothers and nephews

for their love, endless support
and encouragement. . .

Chapter 1

Introduction

1.1 Motivation

Petroleum recovery

Reservoir characteristics are critical in oil extraction, influencing the feasibility, efficiency, and strategies for recovering oil from underground reservoirs. Higher porosity generally means more space for oil to accumulate, while increased permeability allows oil to flow more easily through the rock. In addition, reservoirs are often heterogeneous and formed by various rocks, meaning they have varying characteristics at different locations. Understanding the random distribution of porosity, permeability, and fluid content is crucial for optimising extraction (Islam et al., 2016). Crude oil production from natural reservoirs typically (and currently) involves up to three distinct phases: primary, secondary, and tertiary. These phases are designed to maximise crude oil recovery from the reservoir, each employing different techniques and methods (Morrow, 1990).

Primary recovery is the initial phase of crude oil production. It relies on the natural reservoir energy to drive oil to the surface. This energy can come from the reservoir's pressure or natural forces, such as gas expansion or water drive. During primary recovery, oil is typically displaced and flows to the surface under its reservoir pressure. The efficiency of primary recovery varies depending on the reservoir characteristics but often recovers only a fraction of the total oil in place. Primary recovery is the most straightforward and least costly phase but is often insufficient to extract a significant portion of the oil (Vishnyakov et al., 2020). *Secondary recovery* follows primary recovery when the natural reservoir energy becomes insufficient to continue lifting oil to the surface effectively. One standard method used in secondary recovery is waterflooding. Water is injected into the reservoir to maintain pressure, displace

oil, and push it towards production wells. This helps to increase the percentage of oil recovered from the reservoir. Other secondary recovery techniques may include gas injection (e.g., CO_2 or natural gas) to maintain pressure or improve oil mobility (Vishnyakov et al., 2020).

Tertiary recovery, also known as Enhanced Oil Recovery (EOR), is the final phase of crude oil production and is employed when primary and secondary methods have been exhausted. EOR techniques are designed to recover additional oil trapped in the reservoir. They inject various substances into the reservoir to alter the properties of oil present and injection fluid, reduce its viscosity, or displace it from rock pores more effectively (Lake et al., 2014). Standard EOR methods include steam injection (e.g., steam flooding), chemical injection (e.g., polymer or surfactant flooding), and gas injection (e.g., CO_2 flooding). Each method has specific advantages and applications depending on the reservoir characteristics. EOR methods can significantly increase the percentage of oil recovery from the reservoir but are more complex and expensive than primary and secondary recovery (Alamooti and Malekabadi, 2018).

The EOR using nanoparticles is an innovative approach to improve the efficiency of recovering crude oil from reservoirs. Nanoparticles, which are particles with sizes typically less than 100 nanometers, are used in EOR to alter the properties of crude oil and the reservoir rock, making it easier to displace and recover the oil. Specifically, nanoparticles can alter the wettability of reservoir rock surfaces, making them more water-wet. This change in wettability helps to release oil that might be trapped in the rock pores (Sheng, 2020). In addition, nanoparticles can also interact with crude oil and reduce its viscosity. Lowering the oil viscosity makes it flow more easily through the reservoir rock, increasing the chances of recovery (Pereira, Lara, and Miranda, 2016).

Each reservoir is unique, and a detailed assessment of its characteristics is essential for successful oil extraction. Thus, choosing phase(s) to implement in a particular reservoir depends on factors like reservoir characteristics, economics, environmental considerations, and available technology. Primary, secondary, and tertiary recovery methods may be employed to maximise oil recovery while ensuring efficient and sustainable production.

Microchannels and microfluidics

Microfluidics is a multidisciplinary field of science and technology that deals with fluid behaviour, manipulation, and control at the microscale, typically in channels with dimensions ranging from micrometers to millimeters (Bruus, 2008). It involves the precise handling of small volumes of liquids, gases, or suspensions in microfabricated systems, often referred to as microfluidic chips (lab-on-a-chip) or micro total analysis systems (μ-tas), which are miniaturised platforms that integrate and automate various laboratory functions and processes onto a single chip. These devices have gained immense popularity in analytical chemistry, biotechnology, and biomedical engineering due to their ability to perform a wide range of laboratory operations on a small scale (Mark et al., 2010).

Lab-on-a-chip technology in microfluidics has revolutionised various fields by offering miniaturised and integrated solutions for laboratory processes. These microdevices, often containing complex microchannels, have diverse applications, from the biomedical diagnostics pharmaceuticals industry to chemical and environmental monitoring (Yilmaz and Yilmaz, 2018). Additionally, technology is finding novel applications in EOR by enabling miniaturised and highly controlled experiments that mimic subsurface conditions. These devices facilitate the study of fluid behaviour, wettability effects, and interfacial tension within porous media at the microscale, allowing for a better understanding of EOR mechanisms. The microchannels can simulate reservoir conditions, investigate the impact of various injection fluids, and optimise recovery strategies cost-effectively and timelessly. In addition, they enable real-time monitoring of fluid displacement processes, making it possible to fine-tune EOR methods and improve their effectiveness (Fani et al., 2022).

Understanding and controlling the effects of microchannel structure on flow behaviour is crucial for designing and optimising microfluidic devices for various applications, including lab-on-a-chip systems, microreactors, and microscale heat exchangers. Manufacturers and designers use computational modelling, experimental techniques, and microfabrication methods to tailor microchannel structures to meet specific flow requirements. On the other hand, wettability effects in microfluidics are a fundamental consideration in the design and operation of microfluidic devices and systems. Researchers and engineers often leverage these effects to achieve specific fluid handling and manipulation goals in various applications, including diagnostics, biotechnology, chemistry, and materials science.

1.2 Computational simulations

The third approach

Because of the impending development of computers dedicated to solving scientific problems, computer simulation is often referred to as the third approach to scientific research. Computer simulations are a complementary and alternative computational methodology approach to traditional experimental and theoretical sciences (Kaufmann and Smarr, 1995). It involves using computer programs and mathematical models to mimic real-world processes, systems, or phenomena in a virtual, controlled environment. This allows researchers to explore and analyse complex scenarios, make predictions, and gain insights that might be challenging, costly, or impossible to achieve through pure experimentation or theoretical calculations.

Computational simulation applications span various disciplines, from physics and engineering to biology and social sciences. In physics and engineering, simulations are used to model fluid dynamics, structural behaviour, and electromagnetic phenomena, aiding in designing and optimising aircraft, buildings, and electronic devices (Durán, 2018). In biology and medicine, simulations help understand complex biochemical processes, drug interactions, and disease spread, contributing to drug discovery. Simulations also play a crucial role in climate modelling, economics, and urban planning, enabling researchers and policymakers to explore scenarios, make predictions, and assess the impact of various decisions.

Computational fluid dynamics

Computational Fluid Dynamics (CFD) is a branch of fluid mechanics that uses numerical methods and algorithms to simulate and analyse the behaviour of fluids, such as gases and liquids, as they interact with various objects and boundaries (Chung et al., 2002). CFD allows engineers and scientists to model and understand complex fluid flow phenomena, making it a valuable tool in various industries, including aerospace, automotive, energy, environmental science, and petroleum (Bates, Lane, and Ferguson, 2005). CFD simulations provide insights that are often difficult or impossible to obtain through experiments alone, making them valuable tools for research, design, and problem-solving in various fields.

CFD is a systematic approach to model and analysing fluid flow by mathematically formulating the governing equations, such as the Navier-Stokes equations, which are then discretised (Temam, 2001). Mesh generation divides the computational domain into discrete elements, and numerical techniques like finite difference, finite element, or finite volume methods approximate solutions (Drazin, Riley, and Society, 2006). Proper boundary conditions are essential in defining fluid interactions at domain boundaries. CFD software and high-performance computing are employed to solve these equations iteratively, simulating fluid flow, heat transfer, and turbulence. Visualisation tools are used to interpret results, providing insights into flow patterns, pressure, temperature distributions, and other critical parameters, aiding engineers and scientists in optimising designs and processes.

Lattice Boltzmann method

The Lattice Boltzmann Method (LBM) is a computational approach for simulating fluid flow and other physical phenomena. It has gained popularity as an alternative to traditional CFD methods due to its simplicity and efficiency, particularly for modelling complex fluid systems. LBM is based on a microscopic description of fluid flow, where the fluid is divided into discrete particles that move and collide on a grid (Cercignani, 2013). This particle-based approach allows LBM to capture and interpret capillary phenomena as microscopic interactions. LBM is inherently suited for mesoscale simulations, an intermediate scale between the microscopic and macroscopic levels. Instead of tracking individual molecules or particles (microscale), it represents fluid behaviour using distribution functions on a lattice grid (Mohamad, 2011).

The LBM offers several advantages for simulating fluid flow and related phenomena. Its inherent simplicity and parallelizability make it an attractive choice for high-performance computing, enabling simulations of complex, multi-scale fluid dynamics on modern computing platforms (Körner et al., 2006). LBM lattice-based approach provides natural handling of irregular geometries and complex boundaries, making it well-suited for applications involving porous media, microfluidics, and complex flow as turbulence phenomena (Aidun and Clausen, 2010). LBM is also employed in predicting heat and mass transfer in engineering processes and assessing environmental factors, such as pollutant dispersion. Additionally, LBM excels in simulating multiphase and multicomponent flows, including interface dynamics and phase separation.

LBM simulations are extensively applied in oil recovery to optimise the extraction of hydrocarbons from subsurface reservoirs (Liu, Zhang, and Ghahfarokhi, 2021). These simulations involve complex mathematical models considering reservoir geometry, fluid properties, and production strategies. They enable engineers to predict and analyse reservoir behaviour, optimise drilling and production techniques, and design EOR processes like waterflooding and gas injection with surfactants (Pereira, Lara, and Miranda, 2016). By simulating various scenarios, computational simulations help maximise oil recovery, reduce production costs, and minimise environmental impact. They make them indispensable tools for the oil and gas industry to pursue efficient and sustainable hydrocarbon extraction.

1.3 Objectives

The general objective is twofold: to determine the relationship between the quantity of oil trapped within a micrometric porous medium and the **1)** geometric characteristics or **2)** physical properties of the porous medium. Specifically, geometry refers to the randomness of the pore network, and physics pertains to the heterogeneous wettability of the pore surfaces. In oil recovery through fluid injection, LBM simulations using the Explicit Force method are applied to handle multi-component flows and heterogeneous porous media. In the first case, Molecular Dynamics data serve as input parameters for LBM simulations, with clay as the porous medium and the injected fluid is brine (in four different solutions of nanoparticles). In the second case, experimental measurement data are employed, where the injection fluid is water, and the porous medium is either hydrophobic or hydrophilic crystal.

The specific objective is to quantify the degree of randomness present in the pore structure of a porous medium. For this purpose, a natural porous medium is emulated using a Pore Network Model (PNM) formed by randomly distributed circles as solid walls. In our case, the coordinates of the circular centers form a set of obstacles to fluid flow, in contrast to networks of narrow channels formed by the connection between coordinates. A Voronoi diagram within the PNM uses the coordinates of circular centers as a starting point, forming polygons around the circles. By performing a statistical analysis of the Voronoi polygons, the Shannon entropy of the PNM is calculated, providing a measure of pore randomness. Since the entropy value serves as a unique parameter for random PNMs, the study focuses on assessing the effect of randomness on three cases: **a)** tortuosity, **b)** permeability and **c)** oil recovery. Then,

within random PNMs sharing the same entropy value, the effect of circle size and system porosity on these same three cases is Investigated. Finally, the effect of the degree of heterogeneity on oil recovery is studied using ordered (non-random) heterogeneous PNMs composed of diverse hydrophobic and hydrophilic portions.

1.4 Thesis structure

The thesis follows this structure: first we present the motivations and theoretical background, then the methodology for the study and finally, the method is applied to the proposed systems of interest. The chapters are:

Chap. 1 Introduction: The motivations and background of the study, along with the primary objectives.

Chap. 2 Lattice Boltzmann Method: Development of the LBM methodology and the Explicit Forces method.

Chap. 3 Characterization of Pore Network Models: Development of the Shannon entropy of PNMs and petrophysical parameters.

Chap. 4 Oil Extraction in Pore Network Models: Study of oil extraction in simple PNMs and the using of nanoparticles in EOR.

Chap. 5 Effects of Randomness Porous Media on Fluid Dynamics: Study of randomness in PNMs on tortuosity and permeability.

Chap. 6 Effects of Randomness Porous Media on Oil Recovery: Study of randomness in PNMs on oil recovery.

Chap. 7 Effects of Heterogeneity Porous Media on Oil Recovery: Study of heterogeneity in PNMs on oil recovery.

Chap. 8 Conclusions and Perspectives: Summary of the main results obtained and prospects for further studies.

Chapter 2

Lattice Boltzmann Method

Abstract

This chapter presents a Computational Fluid Dynamics (CFD) method called the Lattice Boltzmann Method (LBM) derived from kinetic theory. The LBM methodology is a numerical technique for simulating fluid dynamics and modelling complex fluid behaviours. It has gained popularity in various fields due to its unique characteristics and advantages over traditional CFD methods based on the Navier-Stokes equations. Instead of solving the Navier-Stokes equations directly, the LBM simulates the density/velocity of fluids through flow and collision processes in a discrete lattice, where reticular cells or pseudoparticles emulate fluid flow. This allows for a more direct and intuitive simulation of fluid flow at a microscopic level. LBM is inherently parallelisable, making it well-suited for modern high-performance computing architectures. The grid-based nature of LBM allows for straightforward distribution of computation across multiple processors or cores, enabling faster simulations for complex fluid scenarios. Since it operates on a discrete lattice grid, LBM can easily handle complex geometries, such as irregular shapes and porous media. This is in contrast to some traditional CFD methods that require complex meshing and refinement techniques to represent complex geometries accurately. LBM can be adapted to handle a wide range of fluid behaviours, from incompressible flows to some compressible cases and from laminar to turbulent flows, simply by modifying the collision rules in the lattice cells. This adaptability makes it a versatile method for various fluid simulation scenarios. It also naturally handles multiphase flows, where multiple fluid phases interact with each other, such as liquid-gas interfaces or droplet formation. Various methodologies address multiphase flows such as Shan-Chen, colour gradient or free energy. Specifically, here we present the Explicit Force method with its software, Taxila-LBM, to address multiphase/multicomponent systems in homogeneous/heterogeneous porous media.

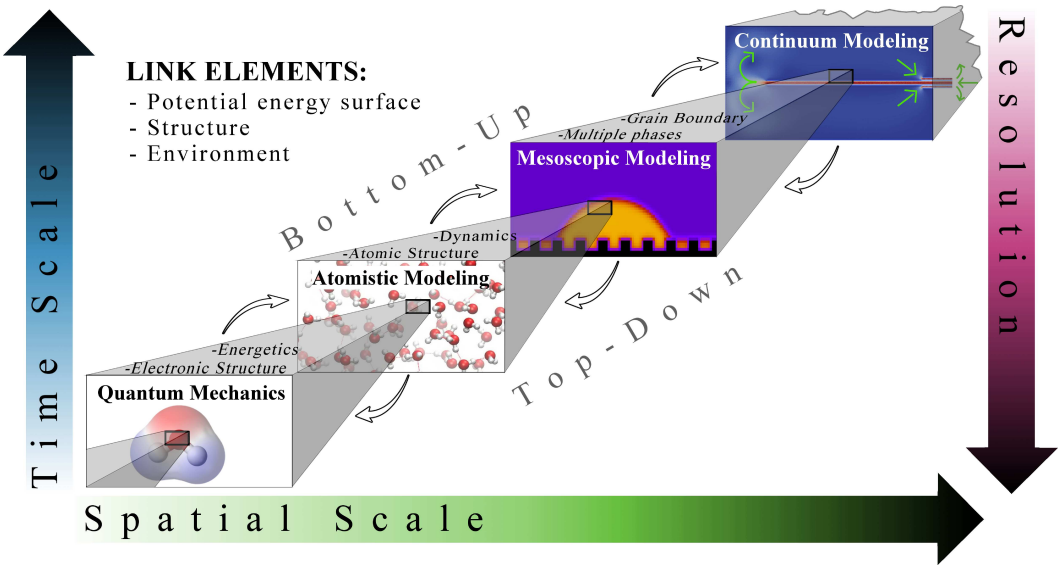

FIGURE 2.1: Schematic representation of various methodological approaches at different scales in space-time. From the quantum model to the continuum through the atomistic and mesoscopic. Picture adapted from (Kirch et al., 2020).

2.1 Introduction

Oil reservoirs have a complex geometric structure and a heterogeneous composition. In addition, several fluids in different proportions or phases can move or be confined inside a region. The natural reservoirs exhibit behaviours or characteristics that vary over time and space scales (Popov et al., 2009). The structure is formed by diverse rock pore sizes ranging from the nanoscale to the macroscale. Alternatively, fluid displacement encompasses various phenomena, from molecular interactions at the smallest scales to large-scale flow patterns in macroscopic systems (Drikakis, Frank, and Tabor, 2019). A multiscale approach is necessary when a single-scale model, such as the oil recovery process, cannot accurately describe the phenomenon of interest. As illustrated in Fig. 2.1, a multiscale computational model is a mathematical and computational framework that simulates and analyses complex systems or phenomena at multiple space-time scales. Each methodology addresses a particular time and length scale, and various resolutions can be linked through either a hierarchical (top-down/bottom-up) or simultaneous multiscale strategy.

In the continuum model, a system is defined by the principal physical quantities, mass, momentum, and energy that can be described using Partial Differential Equations (PDEs), such as the Navier-Stokes equations that model fluid dynamics (Landau and Lifshits, 1959). However, there are only analytical solutions for simple

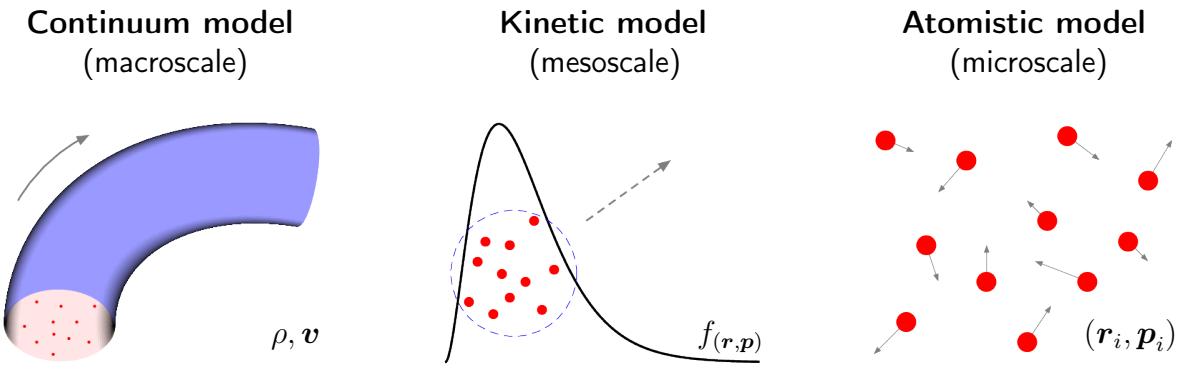

FIGURE 2.2: Methodological approaches (diverse models) to perform fluid dynamics simulations at different scales.

cases. At the same time, for more realistic situations, the modelling equations can only generate approximate solutions due to the equation's non-linearity, the system's irregular geometry or the boundary conditions' complexity (Drazin, Riley, and Society, 2006; Galdi, 2011). As a consequence, various numerical strategies were developed, such as the Finite Difference Method (FDM), the Finite Volume Method (FVM) and the Finite Element Method (FEM). These essentially convert the PDE into an algebraic equations system (Scheid, 1988), where generally, the system is solved iteratively until the results are according to the required precision (Press, 2007).

Molecular Dynamics (MD) is another computational simulation methodology to study fluids at the atomistic level. In this context, fluids can refer to liquids or gases, and the goal is to understand their properties, interactions and behaviour at the atomic or molecular scale (Allen and Tildesley, 1989). The atomistic approach is governed by Newton's laws expressed in the Hamilton-Jacobi formalism and empirical intermolecular interactions such as the Lennard Jones potential, van der Waals forces or electrostatic fields (Leach, 2001). The temporal evolution of the position and momentum of each particle is described by differential equations that are solved numerically through the Verlet algorithm (Omelyan, Mryglod, and Folk, 2002). MD applied to fluid dynamics can help to understand complex flow behaviours, explore fluids in the presence of solid material, and complement experimental observations that are difficult or inaccessible in a laboratory. However, the simulations are limited by the system size and the time scale because emulating a system beyond nanometer dimensions requires high computational cost and longer simulation time.

The kinetic model developed by Ludwig Boltzmann bridges the gap between continuum and atomistic models that operate at extreme scales (see Fig. 2.2).

This model operates on the mesoscopic scale and describes the system's macroscopic properties based on the collective behaviour of microscopic particles described by kinetic equations (Mohamad, 2011). For example, the Boltzmann equation describes the evolution of the velocity distribution, explaining macroscopic properties such as pressure, temperature and viscosity. The LBM coming from the kinetic theory can be approached through numerical analysis and computational simulations. The equations arising from these numerical techniques can be locally solved, thus enabling efficient parallel computation (Succi, 2001). This chapter presents the formalism of the LBM methodology applied to CFD. Specifically, the explicit force method addresses multiphase or multicomponent fluids of heterogeneous composition and complex geometry on porous media (Porter et al., 2012).

2.2 Liouville equation

The kinetic theory was independently developed by Maxwell and Boltzmann. Both contributions provided a significant foundation for understanding the behavior of gases. Gibbs introduced the idea of a statistical ensemble to describe a macroscopic system from a microscopic perspective, which was fundamental to the connection between thermodynamics and statistical mechanics (Cercignani, 1988). The system under consideration is the state of a gas that can be specified by $3N$ canonical coordinates: $q_1, q_2, \ldots, q_{3N}$ and their respective conjugate moments: $p_1, p_2, \ldots, p_{3N}$. The system's phase space represents the $6N$-dimensional space or degrees of freedom expressed by $\Gamma = \{q_i, p_i\}$. A state of the entire system formed by N particles represents a point in Γ space referred to as the representative point (Soto, 2016). This contrasts the kinetic model developed from individual particles in a 6-dimensional space or degrees of freedom.

A very large (infinite) number of states of the gas corresponds to a given macroscopic condition of the gas. For example, the condition that the gas is contained in a specific volume is compatible with an infinite number of ways of distributing the molecules within the volume; that is, we would not be able to distinguish between two gases that exist in different states, but that satisfy the same macroscopic conditions (Harris, 2004). Thus, when we speak of gas under certain macroscopic conditions, we are not referring to a single system but to a collection of systems identical in composition and macroscopic condition but existing in different states.

According to Gibbs, we call such a collection of systems an ensemble that is expressed geometrically by a distribution of representative points in Γ space, which is generally a continuous distribution and can be conveniently described by a total density function $\mathcal{F}_{(\boldsymbol{q},\boldsymbol{p},t)}$, defined as follows:

$$\mathcal{F}_{(\boldsymbol{q},\boldsymbol{p},t)}\, d^{3N}\boldsymbol{q}\, d^{3N}\boldsymbol{p} \tag{2.1}$$

where $(\boldsymbol{q},\boldsymbol{p})$ is an abbreviation for $(q_1, q_2, \ldots, q_{3N}; p_1, p_2, \ldots, p_{3N})$. Then, Eq. 2.1 is the number of representative points at time t contained in the infinitesimal volume element $d^{3N}\boldsymbol{q}\, d^{3N}\boldsymbol{p}$ of the Γ space centred on the point $(\boldsymbol{q},\boldsymbol{p})$.

Given $\mathcal{F}_{(\boldsymbol{q},\boldsymbol{p},t)}$ at an instant t, the motion dynamics determines the subsequent values $t+\Delta t$. Let $\mathcal{H}_{(\boldsymbol{q},\boldsymbol{p})}$ be the Hamiltonian of a collection of systems (Gibbs ensemble). The equations that govern the motion of the systems are given by:

$$\left.\begin{aligned} \dot{q}_i &= \frac{\partial \mathcal{H}}{\partial p_i} \\ \dot{p}_i &= -\frac{\partial \mathcal{H}}{\partial q_i} \end{aligned}\right\} \qquad i = 1, 2, \ldots, 3N \tag{2.2}$$

If we assume that the Hamiltonian does not depend on time derivatives, the Eqs. 2.2 are invariant in time and determine the motion of a representative point for the entire collection of systems. Therefore, the geometric locus of a representative point is either a simple closed curve or a curve that never crosses itself, implying that the geometric locus of two distinct representative points never intersects.

Considering the phase space composed of the position-momentum coordinates of all the identical molecules of a certain gas $(\boldsymbol{q},\boldsymbol{p})$, the system state at a time t can be represented through the total density function $(\mathcal{F})$, expressed as follows:

$$\mathcal{F}_{(\boldsymbol{q},\boldsymbol{p},t)} = \delta_{(q_1 - q_{1(t)})}\delta_{(q_2 - q_{2(t)})} \ldots \delta_{(q_{3N} - q_{3N(t)})}\delta_{(p_1 - p_{1(t)})}\delta_{(p_2 - p_{2(t)})} \ldots \delta_{(p_{3N} - p_{3N(t)})} \tag{2.3}$$

where the parametric functions $q_{i(t)}$ and $p_{i(t)}$ are solutions of Eq. 2.2 for each gas molecule with index i, that is, a Dirac delta function represents a point or point function in Γ space (Bradt and Olbert, 2008; Surmas, 2010).

Then, from a process of derivation of the function $\mathcal{F}$ (see, Eq. 2.3) with respect to the variables q_i, p_i and t, we can obtain the so-called Liouville equation that is presented below:

$$\frac{\partial \mathcal{F}}{\partial t} + \sum_{i=1}^{3N} \left(\dot{q}_i \frac{\partial \mathcal{F}}{\partial q_i} + \dot{p}_i \frac{\partial \mathcal{F}}{\partial p_i} \right) = 0 \tag{2.4}$$

where the solution describes the path of the function $\mathcal{F}$ over the phase space $(\boldsymbol{q}, \boldsymbol{p})$ driven by the functions $\dot{q}_{i(t)}$ and $\dot{p}_{i(t)}$ that are related to velocity and force respectively.

2.3 Kinetic model

According to the continuous hypothesis, density, pressure, velocity, and temperature describe the fluid flow on a macroscopic scale. Microscopic details, such as the representation of the fluid molecules and the molecular interactions, are irrelevant as long as the constitutive relationships between mass, moment and energy are adequately defined in the system modelling equations (Degond, Pareschi, and Russo, 2012). Nevertheless, to clarify the details of the boundary conditions, we must decrease the scale sufficiently until we can model the fluid flow as a set of molecules/particles without any distinguishable internal structure but represented by material points (Bellomo and Pulvirenti, 2013). Therefore, due to the characteristics imposed on the particle model, the particle motion is governed by Newtonian dynamics, that is:

$$\left.\begin{aligned} \boldsymbol{p} &= m \frac{d\boldsymbol{r}}{dt} \\ \boldsymbol{F} &= \frac{d\boldsymbol{p}}{dt} \end{aligned}\right\} \tag{2.5}$$

where $\boldsymbol{r}$ and $\boldsymbol{p}$ represent the position and momentum of a single particle of mass m respectively, and $\boldsymbol{F}$ represents the total force applied on the particle due to the gravitational force, the presence of other particles or solid walls (see, Fig. 2.3 a). However, for this atomistic description to apply, we must know a priori the interaction forces between two homogeneous/heterogeneous particles, as well as the interaction between a particle and the solid wall (Jeans, 1982).

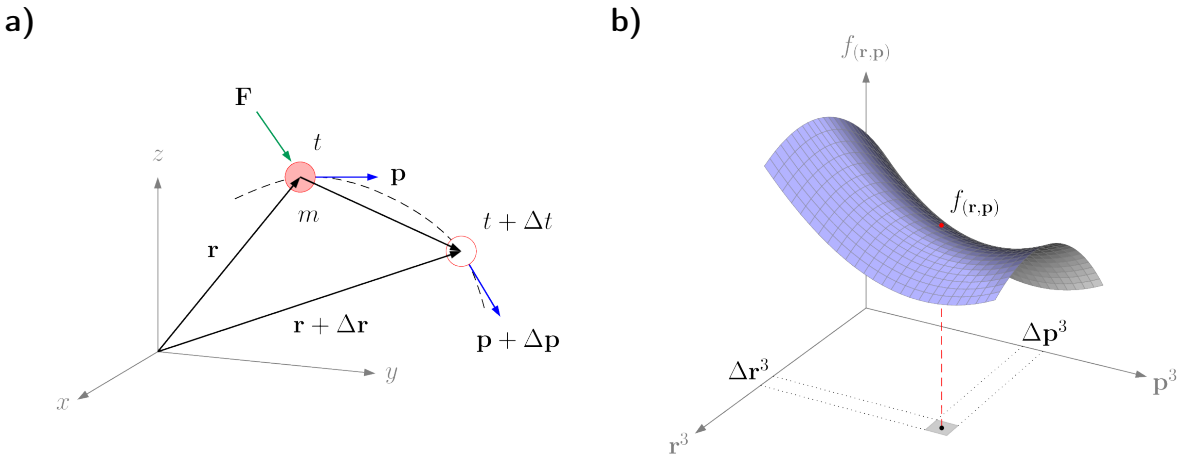

FIGURE 2.3: Dynamics of microscopic point particles. a) Position and moment before and after applying forces on a single particle. b) Particles probability density function in phase space.

In a multiscale analysis, we must recognise the differences between the boundary conditions applied to the continuous and atomistic model. On a macroscopic scale, parameters such as density, velocity, pressure, and temperature can be directly imposed at the system boundary. In contrast, on a microscopic scale, macroscopic parameters at the boundary are determined by statistical averages of microscopic interparticle interactions that emulate the fluid and the solid edge (Cercignani, 2013). However, calculating macroscopic parameters at the boundary requires modelling a large number of particles to obtain reliable results, which means a high computational cost regarding the simulation time and data storage (Cercignani, 2014). Although a supercomputer could perform the simulation, the results would be contaminated due to the errors in determining the position and momentum of many particles because the computational error accumulated each time step increases.

If instead of following the evolution of each particle of a particular system, our interest is to study the microscopic behaviour of different systems, but with similar macroscopic characteristics, such as the number of particles or the total energy, we can describe the microscopic systems using concepts of Statistical Mechanics that operates on an intermediate mathematical scale called mesoscopic (Pathria and Beale, 2011). In the kinetic model formulation, although the details of the interactions between the particles are simplified, the atomistic details relevant to the continuous description of the fluids, flow is conserved. Nevertheless, the particle's trajectory in the phase space $(\boldsymbol{r}^3, \boldsymbol{p}^3)$ is unknown, where all the degrees of freedom of the particle's movement are ignored except for translational (Mohamad, 2011). Therefore, considering the atomistic

and continuous conditions imposed, a system can be described by the function $f_{(\boldsymbol{r},\boldsymbol{p},t)}$, defined as:

$$dN = f_{(\boldsymbol{r},\boldsymbol{p},t)}\, d\boldsymbol{r}^3\, d\boldsymbol{p}^3 \tag{2.6}$$

where dN is the number of particles at instant t located inside the infinitesimal hypervolume of the phase space $dV = d\boldsymbol{r}^3 d\boldsymbol{p}^3$, $f_{(\boldsymbol{r},\boldsymbol{p},t)}$ represents the probability density function of the particles (see Fig. 2.3 b).

Initially, Boltzmann derived the kinetic model by considering a monatomic gas composed of rigid spheres called the Boltzmann gas. The number of molecules is very large ($N \to \infty$), the mass of each molecule is very small ($m \to 0$), and the diameter of each molecule is negligible ($d \to 0$). However, the value of the total mass ($\approx mN$) and the number of collisions ($\approx d^2N$) are not null values (Krüger et al., 2016). A fluid that obeys the Boltzmann model description comprises an infinite number of identical point particles that interact with each other through a short-range potential. Then, the potential generates only binary collisions in a period long enough for the collisions to affect the flow dynamics.

2.4 Boltzmann transport equation

Rather than performing statistical analysis of all individual positions and moments of each particle in Γ space of the Liouville equation (see Sec. 2.2), the Boltzmann transport equation is based on the probability of the number of particles present in a region of phase space (see Eq. 2.6). Especifically, $f_{(\boldsymbol{r},\boldsymbol{p},t)}$ is the probability of finding particles located between $\boldsymbol{r}$ and $\boldsymbol{r} + \Delta\boldsymbol{r}$ with momentum between $\boldsymbol{p}$ and $\boldsymbol{p} + \Delta\boldsymbol{p}$ at time t. If an external force $\boldsymbol{F}$ acts on a particle m, the particle momentum will change from $\boldsymbol{p}$ to $\boldsymbol{p} + \boldsymbol{F}\Delta t$ and the position from $\boldsymbol{r}$ to $\boldsymbol{r} + (\boldsymbol{p}/m)\Delta t$ according to Newtonian dynamics (see Fig. 2.3 a and Eq. 2.5).

In particular, if there are no collisions between particles during a time Δt, the number of particles N present in $\Delta\boldsymbol{r}^3\Delta\boldsymbol{p}^3$ remains constant, regardless of whether an external force is applied or not (see Fig. 2.3 b and Eq. 2.6), that is:

$$
\begin{aligned}
\Delta N &= 0 \\
N_{(t+\Delta t)} - N_{(t)} &= 0 \\
f_{(\boldsymbol{r}+\Delta\boldsymbol{r},\boldsymbol{p}+\Delta\boldsymbol{p},t+\Delta t)}\Delta\boldsymbol{r}^3\Delta\boldsymbol{p}^3 - f_{(\boldsymbol{r},\boldsymbol{p},t)}\Delta\boldsymbol{r}^3\Delta\boldsymbol{p}^3 &= 0 \\
\left[f_{(\boldsymbol{r}+\Delta\boldsymbol{r},\boldsymbol{p}+\Delta\boldsymbol{p},t+\Delta t)} - f_{(\boldsymbol{r},\boldsymbol{p},t)}\right]\Delta\boldsymbol{r}^3\Delta\boldsymbol{p}^3 &= 0 \\
f_{(\boldsymbol{r}+\Delta\boldsymbol{r},\boldsymbol{p}+\Delta\boldsymbol{p},t+\Delta t)} - f_{(\boldsymbol{r},\boldsymbol{p},t)} &= 0 \\
\Delta f &= 0
\end{aligned} \tag{2.7}
$$

In general, if collisions between particles occur, the rate of change between the final and initial states of the distribution function ($\Delta f/\Delta t$) will be nonzero and equal to a term called the collision operator (Ω). Then, applying the limit $\Delta t \to 0$ we can obtain the Boltzmann transport equation (Mohamad, 2011), as shown below:

$$
\begin{aligned}
\lim_{\Delta t\to 0}\frac{\Delta f}{\Delta t} &= \Omega \\
\frac{df_{(\boldsymbol{r},\boldsymbol{p},t)}}{dt} &= \Omega_{(f)} \\
\frac{1}{dt}\left(\frac{\partial f}{\partial \boldsymbol{r}}d\boldsymbol{r} + \frac{\partial f}{\partial \boldsymbol{p}}d\boldsymbol{p} + \frac{\partial f}{\partial t}dt\right) &= \Omega \\
\frac{\partial f}{\partial t} + \frac{d\boldsymbol{r}}{dt}\frac{\partial f}{\partial \boldsymbol{r}} + \frac{d\boldsymbol{p}}{dt}\frac{\partial f}{\partial \boldsymbol{p}} &= \Omega \\
\frac{\partial f}{\partial t} + \boldsymbol{v}\frac{\partial f}{\partial \boldsymbol{r}} + \boldsymbol{F}\frac{\partial f}{\partial \boldsymbol{p}} &= \Omega \\
\frac{\partial f}{\partial t} + \frac{1}{m}\boldsymbol{p}\cdot\nabla_{\boldsymbol{r}} f + \boldsymbol{F}\cdot\nabla_{\boldsymbol{p}} f &= \Omega
\end{aligned} \tag{2.8}
$$

where the nabla operators $\nabla_{\boldsymbol{r}}$ and $\nabla_{\boldsymbol{p}}$ correspond to the position and momentum vector, respectively. Making $\Omega = 0$, the Eq. 2.8 is mathematically equivalent to Liouville equation (Eq. 2.4).

The Boltzmann transport equation is integro-differential and does not have an analytical solution (see Eq. 2.8), only approximate solutions based on the mathematical expression of Ω that describes the collision process according to some statistical distribution (Succi, 2001). The microscopic momentum change $\Delta \boldsymbol{p}$ must necessarily satisfy the macroscopic conservation equations during the collision between particles (Sukop and Thorne, 2007), that is:

$$\left.\begin{aligned} \rho_{(\boldsymbol{r},t)} &= m \int_{\mathbb{R}^3} f_{(\boldsymbol{r},\boldsymbol{p},t)}\, d\boldsymbol{p}^3 \\ \rho_{(\boldsymbol{r},t)}\, \boldsymbol{v}_{(\boldsymbol{r},t)} &= \int_{\mathbb{R}^3} \boldsymbol{p}\, f_{(\boldsymbol{r},\boldsymbol{p},t)}\, d\boldsymbol{p}^3 \\ \rho_{(\boldsymbol{r},t)}\, \epsilon_{(\boldsymbol{r},t)} &= \frac{1}{2} \int_{\mathbb{R}^3} \boldsymbol{p}_{\mathrm{o}}^2\, f_{(\boldsymbol{r},\boldsymbol{p},t)}\, d\boldsymbol{p}^3 \end{aligned}\right\} \tag{2.9}$$

where ρ, $\boldsymbol{v}$ and ϵ are the fluid's density, velocity and energy, respectively, while $\boldsymbol{p}_{\mathrm{o}} = \boldsymbol{p} - m\boldsymbol{v}$ is the particle momentum relative to the fluid. In summary, the macroscopic conservation of mass, momentum and energy are closely related to the microscopic information m and $\boldsymbol{p}$ (see Eq. 2.9).

2.5 Boltzmann equation

There are two especial cases in the Boltzmann transport equation: **a)** if there are no collisions between particles in the system ($\Omega = 0$), the Eq. 2.8 becomes a homogeneous equation sometimes called the Vlasov equation (Bertrand, Sarto, and Ghizzo, 2019), while, **b)** if no external forces are applied to the system ($\boldsymbol{F} = 0$), the Eq. 2.8 is the same as an advective equation, commonly called an inhomogeneous Boltzmann equation (Sukop and Thorne, 2007). Although some can solve both particular cases analytical or numerical method, in the general case, approximations must be made to describe the collision operator Ω, and to $\nabla_{\boldsymbol{p}} f$ as well.

2.5.1 The BGKW model for the collision term

Deriving a mathematical expression for the collision term Ω is highly complex. However, Ω can be approximated by a reasonably simple expression, where the idea is to linearise Ω around the local equilibrium. If we follow the principles of statistical

mechanics, the details of a binary collision do not significantly influence the calculation of the system mean values (Bhatnagar, Gross, and Krook, 1954). Therefore, the main effect of Ω is to bring/keep the distribution function f to/in equilibrium (Welander, 1954). That is, the particle populations tend to a local equilibrium within a relaxation time.

The BGKW model, named after its developers Bhatnagar, Gross, Krook, and Welch, is a simplified kinetic model used in the study of gas dynamics and the Boltzmann equation. It's employed to approximate the collision term in the Boltzmann equation for rarefied gas flows. In the BGKW model, the collision term Ω is approximated using a single relaxation time approximation, and it is typically represented by the following equation:

$$\Omega_{(f)} = -\frac{1}{\tau}\left(f - f^{\text{eq}}\right) \tag{2.10}$$

where τ is the relaxation time, a parameter representing the time it takes for a gas to reach local equilibrium after a collision. $1/\tau$ is the collision frequency and f^{eq} is the particle distribution function at equilibrium that can be derived from the Maxwell-Boltzmann distribution function (Bhatnagar, Gross, and Krook, 1954).

2.5.2 Incorporation of external force fields

Applying an external force field over a system can be simplified using the methodology developed by Martys *et al.* (Martys, Shan, and Chen, 1998). Since Ω is responsible for keeping f near or in equilibrium, f does not differ much from f^{eq}, then the functions with respect to momentum can be approximately equal up to third order. According to Martys *et al.*:

$$\nabla_{\boldsymbol{p}} f \approx \nabla_{\boldsymbol{p}} f^{\text{eq}} = -\frac{1}{m}\frac{(\boldsymbol{c} - \boldsymbol{v})}{c_s^2} f^{\text{eq}} \tag{2.11}$$

where $\boldsymbol{c} = \boldsymbol{p}/m$ is the microscopic velocity of the particles and c_s is the velocity of sound that comes from the isentropic thermodynamic relation $c_s = \partial p/\partial \rho\Big|_s$.

Fluid dynamics equations	
Navier-Stokes equation	**Boltzmann equation**
$\frac{\partial \boldsymbol{v}}{\partial t} + (\boldsymbol{v} \cdot \nabla)\boldsymbol{v} = \frac{\mu}{\rho}\nabla^2 \boldsymbol{v} - \frac{1}{\rho}\nabla p$	$\frac{\partial f}{\partial t} + \boldsymbol{c} \cdot \nabla f = -\frac{1}{\tau}\left(f - f^{\text{eq}}\right)$
Characteristics:	Characteristics:
• Second order PDE, due to: $\nabla^2 \boldsymbol{v}$ • Need to tread the nonlinear convective term: $(\boldsymbol{v} \cdot \nabla)\boldsymbol{v}$ • Need to solve Poisson equation for the pressure • Interfacial tension and wetability are introduced under geometric concepts.	• First order PDE • Avoids term convective, convection becomes simple advection: $\boldsymbol{c} \cdot \nabla f$ • The pressure is obtained from ideal gas equation. • Capillary phenomena are interpreted as fluid-fluid/fluid-solid interactions.

TABLE 2.1: Comparison of continuum and kinetic models expressed by the Navier-Stokes equation and the Boltzmann equation respectively.

2.5.3 The approximate Boltzmann transport equation

As the BGKW collision model is a simple linear equation, and the inclusion of forces is reasonably straightforward, it is possible to derive an approximate version of the Boltzmann equation with a mathematically feasible form for solving by substituting Eq. 2.10 and Eq. 2.11 into Eq. 2.8, as shown below:

$$\frac{\partial f}{\partial t} + \boldsymbol{c} \cdot \nabla f = -\frac{1}{\tau}\left(f - \frac{\tau}{\tau'} f^{\text{eq}}\right) \tag{2.12}$$

$$\frac{1}{\tau'} = \frac{1}{\tau} + \frac{\boldsymbol{F}}{m} \cdot \frac{(\boldsymbol{c} - \boldsymbol{v})}{c_s^2}$$

where $\nabla \equiv \nabla_{\boldsymbol{r}}$ is the common nabla operator. Making $\boldsymbol{F} = 0$, Eq. 2.12 becomes a equation called the Boltzmann equation, as follow:

$$\frac{\partial f}{\partial t} + \boldsymbol{c} \cdot \nabla f = -\frac{1}{\tau}\left(f - f^{\text{eq}}\right) \tag{2.13}$$

Eq. 2.13 is the central equation for developing the LBM methodology applied in various fields, particularly in CFD.

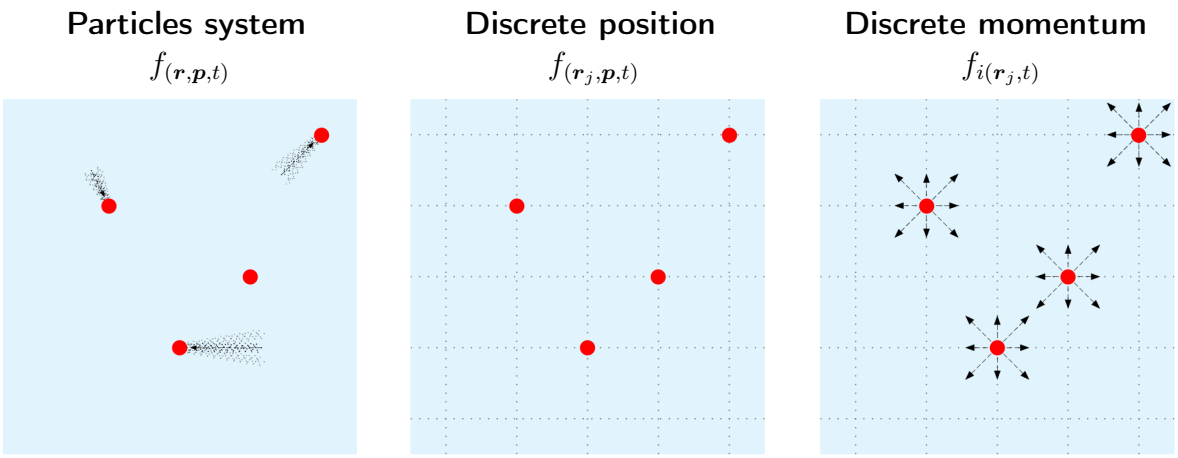

FIGURE 2.4: Phase space discretization process: Position discretization and subsequent momentum discretization.

Mathematically, Eq. 2.13 is a first-order linear PDE but of the advective and inhomogeneous type, where the zero-order term $(\frac{1}{\tau}f)$ indicates the creation/destruction of the dependent variable. In comparison, the inhomogeneous term $(\frac{1}{\tau}f^{\text{eq}})$ suggests the presence of sources/sinks in the system domain (Arfken, Weber, and Harris, 2011). Regarding the solution of PDEs describing fluid dynamics, the Boltzmann equation has convenient characteristics compared to CFD models based on the Navier-Stokes equation (see, Tab. 2.1). Furthermore, since the Navier-Stokes equation can be derived from the Boltzmann equation using the Chapman-Ensokg expansion (Chapman and Cowling, 1970), Eq. 2.13 can replace macroscopic models in CFD simulations.

2.6 Lattice Boltzmann Method

Continuous variables such as the particles' location, direction of motion, and time evolution must be discretised to solve the Boltzmann equation from a numerical approach (see Eq. 2.13). In the discretisation process of $(\boldsymbol{r}, \boldsymbol{p}, t)$, phase space discretisation generates a spatial grid and a lattice formed by the directions of motion (see Fig. 2.4). In contrast, temporal discretisation generates the computational simulation steps. Lattice nodes are mathematical points that represent particles and are often called virtual particles, pseudoparticles or fictive particles.

The lattice generated by the momentum discretisation is called Boltzmann lattice and is the fundamental basis of the LBM methodology. A lattice is formed by $\boldsymbol{c}_i = \boldsymbol{p}_i/m$ called lattice velocities with a certain statistical weight w_i. In contrast, the lattice configuration is determined by the phenomenon nature under study,

such as fluid dynamics, heat transfer, electromagnetism, etc (Mohamad, 2011). The Boltzmann lattices have a nomenclature expressed as $\mathrm{D}_n\mathrm{Q}_\ell$, where n indicates the spatial dimension and ℓ is the number of directions for the particle displacements (see details, App. A). Hence, the momentum discretisation converts the probability distribution function into a set of functions $\{f_0, f_1, f_2, \ldots, f_{\ell-1}\}$, then: $f_{(\boldsymbol{r},\boldsymbol{p},t)} \rightarrow f_{i(\boldsymbol{r},t)}$.

Therefore, the functions $f_i = f_{i(\boldsymbol{r},t)}$ can be discretised in time and space by finite differences using the following approximate derivatives:

$$\left.\begin{aligned} \frac{\partial f_i}{\partial t} &\approx \frac{f_{i(\boldsymbol{r},t+\Delta t)} - f_{i(\boldsymbol{r},t)}}{\Delta t} \\ \nabla f_i &\approx \frac{f_{i(\boldsymbol{r}+\Delta\boldsymbol{r},t+\Delta t)} - f_{i(\boldsymbol{r},t+\Delta t)}}{\Delta \boldsymbol{r}} \end{aligned}\right\} \tag{2.14}$$

where the positional derivative (or gradient) is calculated at the subsequent time $t+\Delta t$.

Substituting the approximate derivatives (Eq. 2.14) in the Boltzmann equation (see Eq. 2.13) and considering the lattice velocities $\boldsymbol{c}_i = \Delta\boldsymbol{r}/\Delta t$, we obtain the fundamental equation of the LBM methodology, as shown below:

$$f_{i(\boldsymbol{r}+\boldsymbol{c}_i\Delta t,t+\Delta t)} - f_{i(\boldsymbol{r},t)} = -\frac{\Delta t}{\tau}\left[f_{i(\boldsymbol{r},t)} - f^{\mathrm{eq}}_{i(\boldsymbol{r},t)}\right] \tag{2.15}$$

$$\Delta f_i = \Omega_i \Delta t$$

where Eq. 2.15 represents a system of linear equations. The left side of Eq. 2.15 expresses the *streaming process*, while the right side the *collision process*.

The streaming process represents the advection or movement of distribution functions from one lattice node to another based on their velocity vectors: $f_{i(\boldsymbol{r},t)} \rightarrow f_{i(\boldsymbol{r}+\boldsymbol{c}_i\Delta t,t+\Delta t)}$, see details in App. B. Suppose the displacement occurs near a boundary condition. In that case, the streaming process requires some modifications depending on the type of boundary, such as Bounce-back, Periodic, Dirichlet, etc. (see App. B). The streaming process enables LBM to approximate the behavior of fluid particles as they move through space and time, capturing the fluid

flow dynamics.

The collision process represents the interaction and relaxation of distribution functions within the lattice nodes: $f_{i(\boldsymbol{r},t)} \rightarrow f^{*}_{i(\boldsymbol{r},t)} \rightarrow f^{\text{eq}}_{i(\boldsymbol{r},t)}$. In this step, the distribution functions are updated at each lattice node to account for particle collisions. A relaxation process gradually brings the distribution functions closer to the local equilibrium state, where the relaxation time τ determines how quickly the distribution functions reach their equilibrium values. Since both processes can be calculated independently and the collision occurs in the same space-time, this approach naturally favours parallel programming in the collision case (Körner et al., 2006).

In fluid dynamics, a driving force acting on a system can be implemented by applying Dirichlet boundary conditions or modifying the collision operator Ω_i. The boundary conditions can be a pressure difference assigned to the inlet/outlet boundary or velocity injection (or flow rate) assigned to the inlet boundary (see App. B). Meanwhile, external field forces or internal capillary forces can be directly incorporated into the collision operator. Martys *et al.* (Shan and Chen, 1993) incorporate internal/external forces by modifying the collision operator Ω through approximations of the momentum gradient $\nabla_{\boldsymbol{p}} f$ (see Sec. 2.5).

Similarly, as the Boltzmann transport equation (Eq. 2.8) of the continuous model satisfies the conservation of mass, momentum and energy (see, Eq. 2.9), the set of Boltzmann equations (Eq. 2.15) must satisfy conservation principles during the collision process (Mohamad, 2011). In incompressible and isothermal fluids, the conservation of mass and momentum can be expressed as follows:

$$\left.\begin{aligned} \rho_{(\boldsymbol{r},t)} &\approx \sum_{i=0}^{\ell-1} f_{i(\boldsymbol{r},t)} \\ \rho_{(\boldsymbol{r},t)}\, \boldsymbol{v}_{(\boldsymbol{r},t)} &\approx \sum_{i=0}^{\ell-1} f_{i(\boldsymbol{r},t)}\, \boldsymbol{c}_i \end{aligned}\right\} \tag{2.16}$$

where ℓ indicates the number of directions for the displacements, and $i = 0$ corresponds to the possibility of no motion (particles remain in the same position).

2.6.1 Equilibrium distribution function

The equilibrium function f^{eq} is a fundamental component of the collision process in the LBM methodology. The type of physical phenomenon under study determines the mathematical form of f^{eq} that depends on the system's macroscopic variables[1]. For example, in a collection of particles represented by a density ρ and moving with a the collective macroscopic velocity $\boldsymbol{v}$ is similar to a fluid, and f^{eq} is computed based on density and velocity. The formula for f^{eq} is usually derived from the Maxwell-Boltzmann distribution function, which describes the statistical distribution of particle velocities in a fluid (Sukop and Thorne, 2007), as shown below:

$$f^{\text{eq}}_{(\boldsymbol{r},\boldsymbol{c})} = \rho \left(\frac{m\beta}{2\pi}\right)^{\frac{1}{2}D} e^{-\frac{1}{2}m\beta(\boldsymbol{c}-\boldsymbol{v})^2} \tag{2.17}$$

where β is the thermodynamic beta constant, $\boldsymbol{c}$ is the microscopic velocity of the particles and $D = 1, 2, 3$ is the dimensional space.

Expanding Eq. 2.17 into a Taylor series: $e^{-x} = 1 - x + \frac{1}{2}x^2 - \frac{1}{6}x^3 \ldots$, the following expression is obtained:

$$f^{\text{eq}}_{(\boldsymbol{r},\boldsymbol{c})} = \rho \left(\frac{m\beta}{2\pi}\right)^{\frac{1}{2}D} e^{-\frac{1}{2}m\beta\, c^2} \left[1 + m\beta(\boldsymbol{c}\cdot\boldsymbol{v}) - \frac{1}{2}m\beta v^2 + m\beta(\boldsymbol{c}\cdot\boldsymbol{v})^2 - \ldots\right] \tag{2.18}$$

The general form of a discrete equilibrium distribution function in a specific direction i (Mohamad, 2011), can be written up in second order as follows:

$$f^{\text{eq}}_{i(\boldsymbol{r},t)} = w_i\, \rho_{(\boldsymbol{r},t)} \left[\mathrm{A} + \mathrm{B}(\boldsymbol{c}_i \cdot \boldsymbol{v}_{(\boldsymbol{r},t)}) + \mathrm{C}(\boldsymbol{c}_i \cdot \boldsymbol{v}_{(\boldsymbol{r},t)})^2 + \mathrm{D}(\boldsymbol{v}_{(\boldsymbol{r},t)} \cdot \boldsymbol{v}_{(\boldsymbol{r},t)})\right] \tag{2.19}$$

$$w_i = \left(\frac{m\beta}{2\pi}\right)^{\frac{1}{2}D} e^{-\frac{1}{2}m\beta\, c_i^2}$$

where A, B, C, and D are constants determined based on the conservation principles (mass, momentum and energy).

[1] LBM was initially applied to fluid dynamics, then to other fields such as diffusion, phase transition, acoustic, electromagnetism, etc.

Lattice	***d***
D_1Q_2	1
D_1Q_3	2
D_2Q_4	2
D_2Q_5	3
D_2Q_9	3
D_3Q_{19}	3
D_3Q_{27}	3

TABLE 2.2: List of lattice dimension values for different lattice configurations in: 1D, 2D and 3D.

The macroscopic quantities $\rho_{(\boldsymbol{r},t)}$ and $\boldsymbol{v}_{(\boldsymbol{r},t)}$ represent some parameters of a particular system, for example, concentration, temperature, electric or magnetic field, etc. Meanwhile, the coefficient w_i represented the statistical weight of the possible velocities $\boldsymbol{c}_i$ for the movement of particles (see Eq. 2.19). The configuration of the possible directions of movement and their respective weight distribution is determined based on the conservation principle of mass and momentum (Mohamad, 2011).

2.6.2 Bridge between micro and macro scales

In the streaming process, the particles flow through the lattice, and then there must be a characteristic transport coefficient between the transported material and the medium. This coefficient is a macroscopic quantity of a physical system that must be related to the system's microscopic quantities (Mohamad, 2011). Therefore, the connection between the macroscale and microscale can be obtained through this coefficient using the Chapman-Enskog expansion (Chapman and Cowling, 1970). In fluid dynamics, there is a relationship between the kinematic viscosity of the fluid ν and the collision frequency between particles or relaxation time τ (see Eq. 2.10), as shown below:

$$\nu = c_s^2 \left(\tau - \frac{\Delta t}{2} \right) \tag{2.20}$$

In order to normalise the velocity of sound as $c_s = 1/\sqrt{3}$, the microscopic velocity $\boldsymbol{c}$ and the flow velocity $\boldsymbol{v}$ of the Maxwell-Boltzmann distribution must be normalised by $\sqrt{RT}$ (Mohamad, 2011). Consequently, the velocity of sound in the Boltzmann

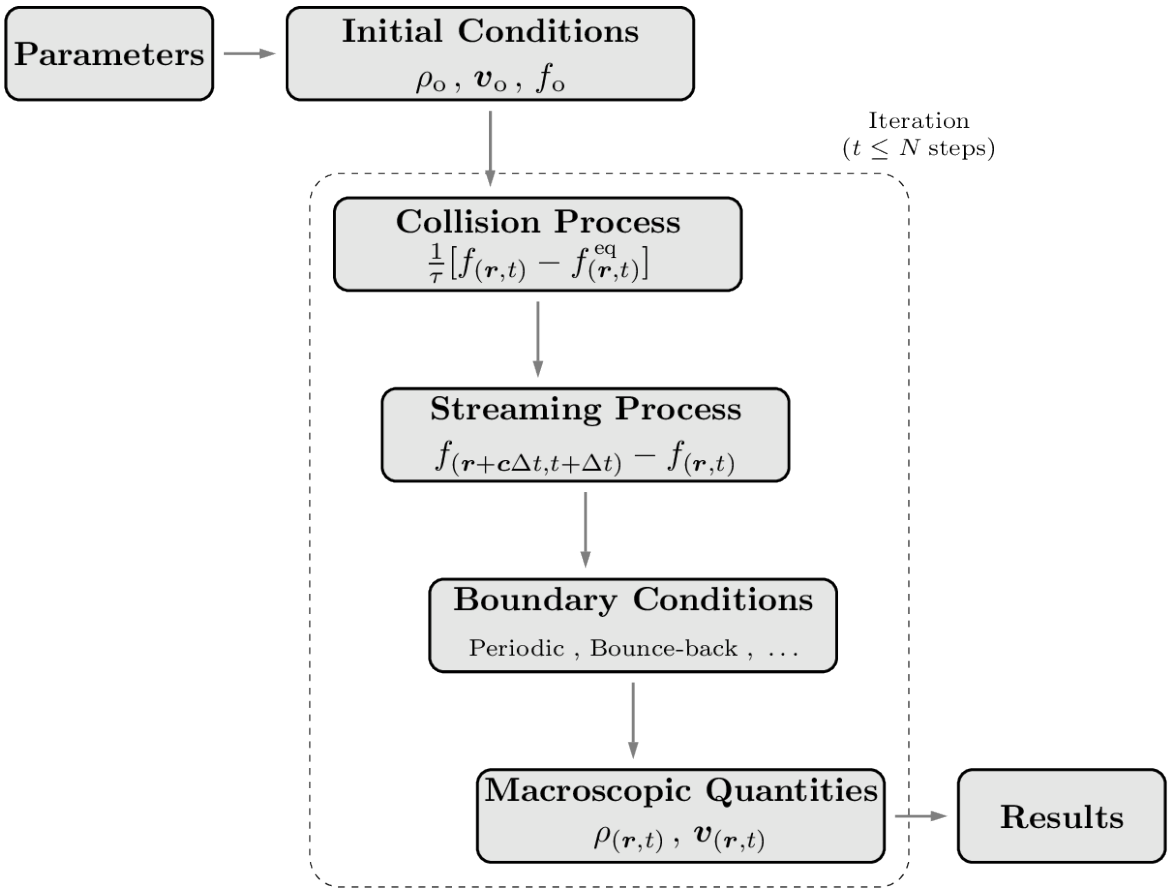

FIGURE 2.5: LBM algorithm: Main steps for the systematic application of the LBM methodology.

model can be written as:

$$c_s = \frac{c}{\sqrt{d}} \tag{2.21}$$

where d is the lattice dimension, dependent on spatial dimension and particularly on the lattice configuration. Tab. 2.2 show the lattice dimension value for different lattice configurations discussed in App. B.

In summary, LBM bridges the microscale, where individual particles behaviour is described, and the macroscale, where collective fluid behaviour is observed. This bridge allows the study and simulation of fluid dynamics across a wide range of length and time scales, making LBM a versatile tool in various scientific and engineering applications.

2.7 LBM implementation in Fluid Dynamics

The application of the LBM to simulate and study fluid flow and related phenomena, such as flows in porous media, multiphase flows, heat transfer, etc. It involves translating the mathematical and algorithmic principles of the LBM into computer code (see Fig. 2.5). Alternatively, software that can simulate the behaviour of fluids. Below is a list (main algorithm) of the key elements necessary for implementing the LBM methodology:

a) Lattice. Due to their links structure and the statistical weight, the lattice configurations applied to the fluid dynamics are D_2Q_9, D_3Q_{19} and D_3Q_{27} (see App. A), preserve the isotropy and the Galilean invariance (Mohamad, 2011).

b) Macroscopic quantities. The conservation equations Eqs. 2.16 with normalised mass ($\Delta m = 1$) describe the density and velocity of the fluid, as shown below:

$$\rho_{(\boldsymbol{r},t)} = \sum_{i=0}^{\ell-1} f_{i(\boldsymbol{r},t)} \tag{2.22}$$

$$\boldsymbol{v}_{(\boldsymbol{r},t)} = \frac{1}{\rho_{(\boldsymbol{r},t)}} \sum_{i=0}^{\ell-1} f_{i(\boldsymbol{r},t)}\, \boldsymbol{c}_i \tag{2.23}$$

where ℓ is the number of links of a given lattice configuration D_nQ_ℓ.

c) Equilibrium distribution function. The constants in Eq. 2.19 are obtained based on conservation principles and are a function of the speed of sound (Mohamad, 2011). Given $A = 1$, $B = (c_s^2)^{-1}$, $C = \frac{1}{2}(c_s^4)^{-1}$ and $D = -\frac{1}{2}(c_s^2)^{-1}$. Then, the equilibrium function Eq. 2.19 is rewritten as shown below:

$$f^{\,\mathrm{eq}}_{i(\boldsymbol{r},t)} = w_i\, \rho \left[1 + \left(\frac{\boldsymbol{c}_i \cdot \boldsymbol{v}}{c_s^2} \right) + \frac{1}{2} \left(\frac{\boldsymbol{c}_i \cdot \boldsymbol{v}}{c_s^2} \right)^2 - \frac{1}{2} \left(\frac{\boldsymbol{v} \cdot \boldsymbol{v}}{c_s^2} \right) \right] \tag{2.24}$$

where the normalised microscopic velocity is $c = \Delta x/\Delta t = 1$ and the lattice dimension for lattice configurations D_2Q_9 is $d = 3$, then the speed of sound on lattice is $c_s = 1/\sqrt{3}$ (see Eq. 2.21).

d) Discretized Boltzmann equation. A fluidic system with no external forces is modeled by Eq. 2.15. Since $c = 1$, Eq. 2.15 is normalised with respect to time ($\Delta t = 1$) and rewritten as follows:

$$f_{i(\boldsymbol{r}+\boldsymbol{c}_i\Delta t, t+\Delta t)} - f_{i(\boldsymbol{r},t)} = -\frac{1}{\tau}\left[f_{i(\boldsymbol{r},t)} - f^{\text{eq}}_{i(\boldsymbol{r},t)}\right] \tag{2.25}$$

where external or internal forces are included in the collision term (right-hand side of Eq. 2.25), the Explicit Force method, described in the next section, was employed in this work.

In order to perform LBM simulations, intrinsic information about the system must be available, including the density and kinematic viscosity of the fluid. It is also important to know the driving force for the flow, whether it be the force of gravity, pressure difference, or fluid injection.

2.8 Explicit Force method

The presented methodology can be easily and quickly implemented for single component fluids flow in the absence of forces or other source terms. However, implementing forces in the LBM methodology is not trivial since some modifications must be made to represent the force terms properly. For example, in multi-component or multiphase pore-scale systems, intermolecular forces between fluids and walls can be easily incorporated by applying an attractive or repulsive force on the particles. So, interparticle forces in LBM represent a more physical than geometric approach than traditional CFD methods.

The Shan-Chen model is one of the most important LBM implementations (Shan and Chen, 1993). Nevertheless, there are drawbacks to accurately studying various multiphase systems, such as large spurious currents near interfaces, equilibrium densities dependent on the viscosity and numerical instabilities for large viscosities. The Explicit Force model proposed by Yu *et al.* (Yu, Yang, and Fan, 2011) and expanded by Porter *et al.* (Porter et al., 2012) helps address these drawbacks. The model can work with viscosity ratios higher than 1000 with lower spurious currents at the fluid-fluid interfaces and allows equilibrium densities independent of the viscosity.

In this context, the description of multicomponent fluids flow can also be represented by a particle distribution function, where, if collisions do not occur between

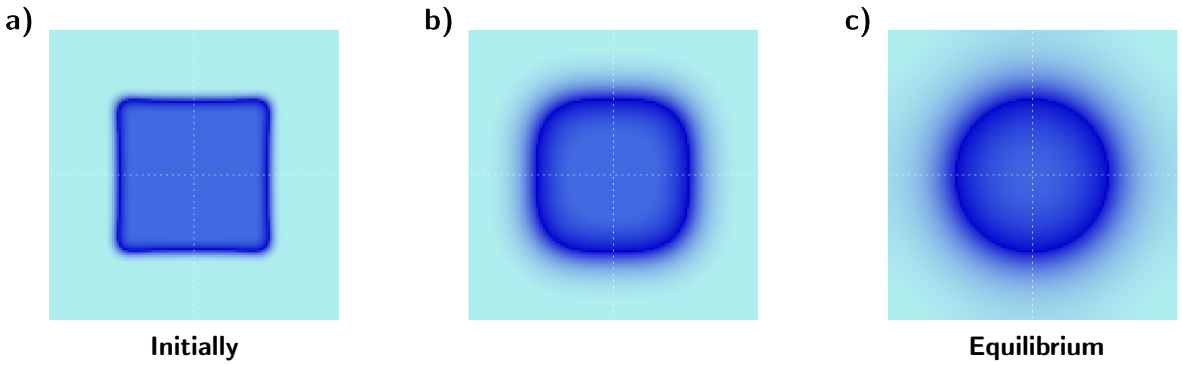

FIGURE 2.6: Schematic representation of a thermodynamic equilibrium process due to *interfacial tension* as a driving force. Case: a water droplet immersed in air that **a)** initially has a square shape and **c)** becomes circular when the system reaches equilibrium.

heterogeneous or homogeneous particles ($\Omega = 0$), the streaming process is modelled by an equation similar to Eq. 2.25, that is:

$$f^k_{i(\boldsymbol{r}+\boldsymbol{c}_i\Delta t, t+\Delta t)} - f^k_{i(\boldsymbol{r},t)} = 0 \tag{2.26}$$

where k represents the k-th fluid component (there are k linear equations).

Nevertheless, if during the streaming process, the particles are subjected to external forces or collisions, Eq. 2.26 is nonzero and can be rewritten as follow:

$$f^k_{i(\boldsymbol{r}+\boldsymbol{c}_i\Delta t, t+\Delta t)} - f^k_{i(\boldsymbol{r},t)} = \Omega^k_{\text{col}} + \Omega^k_{\text{for}} \tag{2.27}$$

where Ω^k_{col} represents momentum changes in the particle distribution arising from collisions between particles of the same type, while Ω^k_{for} denotes momentum alterations attributed to external or internal forces, including collisions between particles of different types at the interface.

The collision term Ω^k_{col} and its respective equilibrium distribution function are defined exactly the same as in the case of single fluids (see Eq. 2.10 and Eq. 2.24), as shown below:

$$\Omega^k_{\text{col}} = -\frac{1}{\tau^k}\left[f^k_{i(\boldsymbol{r},t)} - f^{k\,\text{eq}}_{i(\boldsymbol{r},t)}\right] \tag{2.28}$$

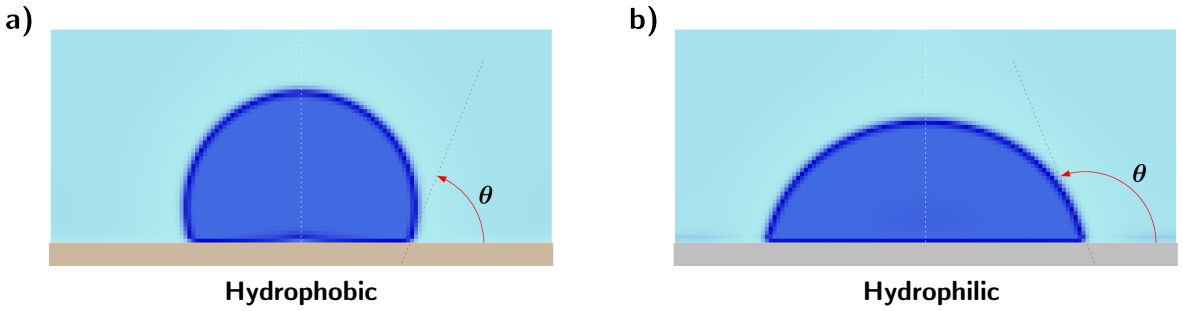

FIGURE 2.7: Schematic representation of the *wettability* phenomenon expressed and quantified through the *contact angle*. Case: a water droplet immersed in air and scattered over a solid horizontal surface with **a)** hydrophobic and **b)** hydrophilic properties.

and

$$f_{i(\boldsymbol{r},t)}^{k\,\mathrm{eq}} = w_i\,\rho^k\left[1+\left(\frac{\boldsymbol{c}_i\cdot\boldsymbol{v}^{\mathrm{eq}}}{c_s^2}\right)+\frac{1}{2}\left(\frac{\boldsymbol{c}_i\cdot\boldsymbol{v}^{\mathrm{eq}}}{c_s^2}\right)^2-\frac{1}{2}\left(\frac{\boldsymbol{v}^{\mathrm{eq}}\cdot\boldsymbol{v}^{\mathrm{eq}}}{c_s^2}\right)\right] \tag{2.29}$$

where τ^k and $\rho^k_{(\boldsymbol{r},t)}$ are the relaxation time and the fluid density k, respectively, and $\boldsymbol{v}^{\mathrm{eq}}_{(\boldsymbol{r},t)}$ is the system equilibrium velocity.

In their original work (Shan and Chen, 1993), Shan and Chen incorporated the force $\boldsymbol{F}^k$ by adjusting momentum $\boldsymbol{p}$. In the Explicit Force of Yu *et al.* (Yu, Yang, and Fan, 2011), the force term is directly included in the fundamental Boltzmann equation via a new collision operator Ω^k_{for} (see Eq. 2.27). The forces operating on the particles are given by:

$$\Omega^k_{\mathrm{for}} = \frac{\Delta t}{2}\left[f_{i(\boldsymbol{r}+\boldsymbol{c}_i\Delta t,t+\Delta t)}^{k\,\mathrm{F}} - f_{i(\boldsymbol{r},t)}^{k\,\mathrm{F}}\right] \tag{2.30}$$

and

$$f_{i(\boldsymbol{r},t)}^{k\,\mathrm{F}} = \frac{\boldsymbol{F}^k\cdot(\boldsymbol{c}_i-\boldsymbol{v}^{\mathrm{eq}})}{\rho^k\,c_s^2}\,f_{i(\boldsymbol{r},t)}^{k\,\mathrm{eq}} \tag{2.31}$$

where $f_i^{k\,\mathrm{F}}$ is the force distribution function, and $\boldsymbol{F}^k$ is a force vector. External forces on the system or other system internal forces can be incorporated into $\boldsymbol{F}^k$.

2.8.1 Incorporation of Forces

To implement external or internal forces in a system using the Explicit Forces model, we must have information on the physical parameters of the applied force at our disposal. For example, body forces, such as the intensity of gravity, capillary forces, such as the interfacial tension between fluids (see Fig. 2.6), and the wall's wettability expressed by the contact angle (see Fig. 2.7).

a) Gravity. External forces acting on the particles, such as the gravity force, are expressed as follows:

$$\boldsymbol{F}^{k} = \rho^{k}_{(\boldsymbol{r})}\, \boldsymbol{g} \tag{2.32}$$

where $\boldsymbol{g}$ is the gravity vector acting on each particle.

b) Interfacial tension. The forces between heterogeneous particles, which give rise to interfacial tension (fluid-fluid interaction), can be included in a similar nearest-neighbour manner, as shown below:

$$\boldsymbol{F}^{k} = -\,\psi^{k}_{(\boldsymbol{r})} \sum_{\bar{k}=1}^{n_k} \sum_{\boldsymbol{r}' \in \mathcal{N}_{\boldsymbol{r}}} g^{k,\bar{k}}\, \mathcal{G}_{(|\boldsymbol{r}'-\boldsymbol{r}|)} \frac{\psi^{\bar{k}}_{(\boldsymbol{r}')} - \psi^{\bar{k}}_{(\boldsymbol{r})}}{|\boldsymbol{r}'-\boldsymbol{r}|} (\boldsymbol{r}'-\boldsymbol{r}) \tag{2.33}$$

where ψ^{k} is the effective mass function, and $\mathcal{N}_{\boldsymbol{r}}$ are the lattice sites that are not walls, whose direct path from $\boldsymbol{r}$ to $\boldsymbol{r}'$ does not include walls. $\mathcal{G}$ is a Green function, and the value of $g^{k,\bar{k}}$ indicates the magnitude of the force.

c) Wettability. The wettability forces are produced between the fluidic particles and a solid wall (fluid-solid interaction). Therefore, the forces that appear in the vicinity of the solid are given by:

$$\boldsymbol{F}^{k} = -\,\rho^{k}_{(\boldsymbol{r})} \sum_{m=1}^{n_m} g^{k,m} \sum_{\boldsymbol{r}' \in \mathcal{W}_m} (\boldsymbol{r}'-\boldsymbol{r}) \tag{2.34}$$

$\mathcal{W}_m$ represents the set of neighbouring wall nodes composed of material m, while $g^{k,m}$ represents the intensity at intermolecular forces between fluid k and material m. The positive forces represent non-wetting forces and vice versa.

The coefficient $\boldsymbol{g}$ represents various body forces (gravitational, electrical or magnetic), while coefficients $g^{k,\bar{k}}$ and $g^{k,m}$ are related to capillary parameters. The relationship between coefficients and parameters is not direct (except for $\boldsymbol{g}$); a process called *parameter mapping* must be performed to obtain the simulation coefficients corresponding to the physical parameters (Coon, Porter, and Kang, 2014; Pereira, Lara, and Miranda, 2016).

2.8.2 Taxila-LBM package

Taxila-LBM software based in Explicit Force method is a powerful parallel implementation of the LBM methodology, tailored to simulate fluid flow in porous and complex geometric environments (Coon, Porter, and Kang, 2014). This feature-rich software offers a versatile array of capabilities. It excels in solving both single and multi-phase systems, handling various mesh dependencies, including D_2Q_9, D_3Q_{19}, and others, on 2D or 3D grids, and easily adapting to different models of connectivity. Leveraging the Shan and Chen Lattice Boltzmann Method, Taxila LBM accommodates multi-phase systems with varying phase viscosities and molecular masses (Porter et al., 2012). Its flexibility extends to utilizing higher-order derivatives or multiple relaxation times to enhance stability, accommodating multiple mineral/wall materials with different wettabilities and contact angles, and supporting arbitrary, heterogeneous boundary conditions.

Furthermore, Taxila-LBM exhibits impressive scalability, performing efficiently on massively parallel systems with tens of thousands of cores while remaining compatible with both multi/single-core desktops and laptops running MacOS or Linux. Its modular, "object-oriented" Fortran-90 design facilitates seamless extension for incorporating new features. In terms of technical components, Taxila-LBM leverages PETSc (Portable, Extensible Toolkit for Scientific Computation) for advanced data structures, communication, and parallel I/O. It can also integrate with PFloTran for micro-scale reactive transport solutions, although complete open-source availability for this coupling may be pending. However, it's important to note that the current version is designed for structured, regular meshes and does not yet support GPU implementation or handle curved geometries or non-bounceback style interior boundary conditions.

Chapter 3

Characterization of Pore Network Models

Abstract

One of the key problems in the dynamics of fluids in porous media is to describe the fluid flow delay when it passes through the internal porous network. A strategy to describe the relationship between the dynamics and the intrinsic pore obstruction structure is to characterise the porous medium by considering its porosity, permeability and tortuosity, among other features. Wettability also plays a significant role in fluid flow phenomena, especially in porous media like rocks and soils, as well as in microfluidic devices and various industrial processes. Where controlling and manipulating the interaction between fluids and solid surfaces can have a significant impact on fluid flow efficiency (accelerate or retard). Several pore network models (PNMs) have been proposed to emulate the porous media of natural reservoirs. Creating a simple model to emulate natural reservoirs involves simplifying the complex geological and fluid flow processes while capturing the essential characteristics. Emulating a natural reservoir using randomly distributed circles is a simplified geometric representation that can provide insights into certain aspects of reservoir behaviour. The primary goal of this chapter is to characterise the degree of randomness of PNMs using Shannon entropy. Since the entropy value can be considered as a petrophysical parameter along with porosity, tortuosity and permeability. In addition, tortuosity and permeability are studied under hydrodynamic concepts, taking into account wettability.

3.1 Introduction

Due to the porous media complexity found in nature, there are no purely analytical solutions for fluid flow, except in artificial structures that emulate a natural porous media designed by objects with regular geometry, for example, the flow through equiradial spheres immersed in a cubic matrix (Sangani and Acrivos, 1982). Preliminary porous media studies were based on simplifications that idealised complex porous structures using models similar to random fractal structures (Balankin and Elizarraraz, 2012) or disordered percolation structures (Andrade et al., 1995). Although these models provided morphological information, such as the topology and interconnectivity of the pore-scale structure, the use of this geometric information in the modelling of structures to emulate real porous media hydraulically was not well established. The main hypothesis was to assume a random distribution of the regions that form the system structure, where the morphological characteristics of the regions do not correlate. However, recent studies from percolation theory and fractal geometry suggest that some porous materials exhibit correlations at different pore scales, where the correlations could affect the porous structure's global properties (Andrade et al., 1995).

In nature, porous media properties such as permeability or tortuosity may vary according to the porous region. For example, there may be highly permeable and practically impermeable regions. In addition, the permeable regions may or may not be connected to the impermeable ones (Dandekar, 2013). The inhomogeneous character of an actual structure is basically due to cavities covering most of the porosity and throats connecting the cavities. The cavities may have different proportions and are generally located in groups and not homogeneously distributed. Even though porous media modelling could contemplate geometric aspects such as heterogeneity and interconnectivity of cavities and throats on a micrometric scale, we must also consider physical aspects such as capillary phenomena within the porous material micropores. Capillary effects become more prominent and significant as the dimensions of a system are reduced to the microscale (Zhou et al., 2017).

In microfluidics, the morphological architecture of porous media and the wettability of the fluid-solid system are crucial factors in fluid flow (Dandekar, 2006). Regardless of the system metric scale, the random porous structure defines the flow path, and the walls act as obstacles to the effective displacement of the fluid. At the microscale, the degree of hydrophobicity or hydrophilicity of the pore walls, together with the

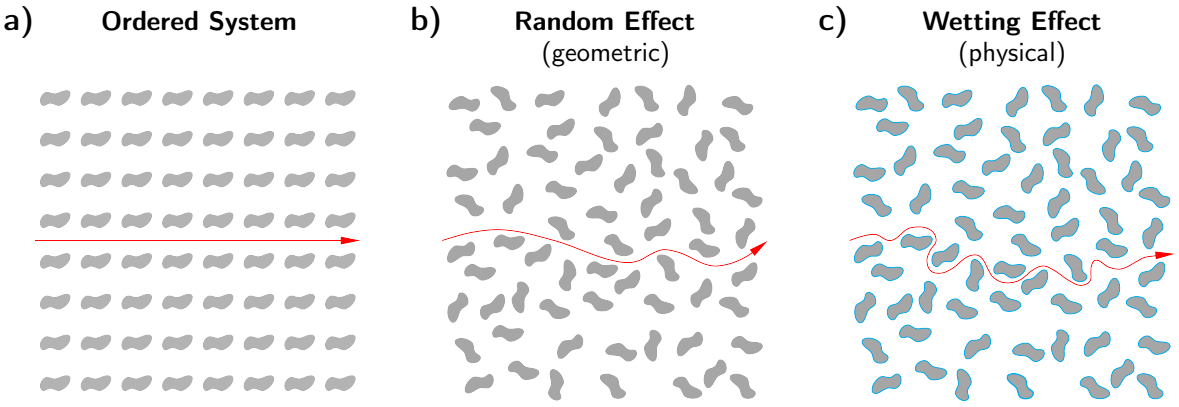

FIGURE 3.1: The illustration shows the effect of *randomness* and *wettability* of porous media on fluid dynamics. Case: flow or streamline (red arrow) in a porous medium that **a)** initially is structurally ordered, **b)** then the streamline is visibly affected by the obstacles randomness and **c)** finally also by the walls wettability.

random distribution of pores, determine flow retardation and fluid entrapment within the channel network (Fagbemi, Tahmasebi, and Piri, 2018).

The main objective of this chapter is to characterise random porous network models (PNMs) using Shannon entropy. A statistical analysis is performed on the Voronoi diagrams generated within the PNMs to quantify randomity. Subsequently, the most relevant petrophysical parameters in fluid dynamics are reviewed: porosity, tortuosity and permeability. The tortuous and permeable parameters are calculated based on hydrodynamic concepts such as hydraulic tortuosity and Darcy permeability. To demonstrate the effectiveness of the hydrodynamic method, our investigation focuses on simple channels with a known analytical solution (Matyka and Koza, 2012; Neuman, 1977).

3.2 Random Pore Network Models (PNMs)

Undoubtedly, the geometric characteristics of the morphological architecture of porous media are determinant and decisive for conducting fluid dynamics studies, regardless of the system metric scale. Concretely, the structure plays a fundamental role in flow obstruction, the path taken by the fluid, and the flow delay time. Since solid parts behave as obstacles to fluid flow, the shape and location of the obstacles must be considered when modelling a porous medium (Suxo and Miranda, 2017). For example, a change in the angular orientation of a polygonal obstacle with respect to the flow direction can significantly impact the velocity field by

distorting the streamlines. Additionally, changing the placement of obstacles can dramatically alter the velocity field by disrupting the path of streamlines (see Fig. 3.1).

Consequently, if the tortuosity or permeability of porous media is calculated according to hydrodynamic concepts such as hydraulic tortuosity and Darcy permeability, the geometric shape and angular orientation of obstacles can modify the tortuous or the permeable characteristics, perturbing the velocity field. Therefore, circular objects instead of polygonal shapes are ideal as obstacles for systematically studying porous media[1] (James and Chatzis, 2004). This is due to the absence of sharp edges and the isotropic orientation with respect to the flow. Furthermore, since objects are defined by only two parameters (centre and radius), the design of PNMs composed of circles are relatively straightforward. Commonly, a PNM is formed by narrow channels interconnecting orderly or randomly distributed points, while in our designed PNMs, the points are the coordinates of circles that act as obstacles to fluid flow (Adloo and Abbasi, 2021).

The placement of obstacles determines the porosity, tortuosity and permeability of porous media (petrophysical parameters) because the group configuration influences more than individual geometry. Notice that if obstacles are placed randomly, there is the possibility of finding different configurations with the same porous, tortuous or permeable value (Merriam, 2012). In Statistical Mechanics, different configurations of energetic molecules in an ideal gas can have the same value of volume, pressure, or temperature (macroscopic parameters). Similarly, in Electromagnetism, different configurations in the orientation of spins within a magnetic material can generate the same magnetization vector (macroscopic parameter). Additionally, the degree of randomness in spin orientation can define or classify the type of magnetic material (diamagnetic, paramagnetic, or ferromagnetic). Therefore, porous media with random configurations with the same petrophysical value must be identified before conducting fluid dynamics simulations. The identification should focus on the entropy of the obstacle distribution because obstacles form the porous medium, and the entropic parameter represents the degree of randomness in any system, whether physical or not (Zhou et al., 2014; Chen et al., 2016).

[1] In the three-dimensional case, spherical objects instead of polyhedral shapes are ideal as obstacles to emulate natural porous media.

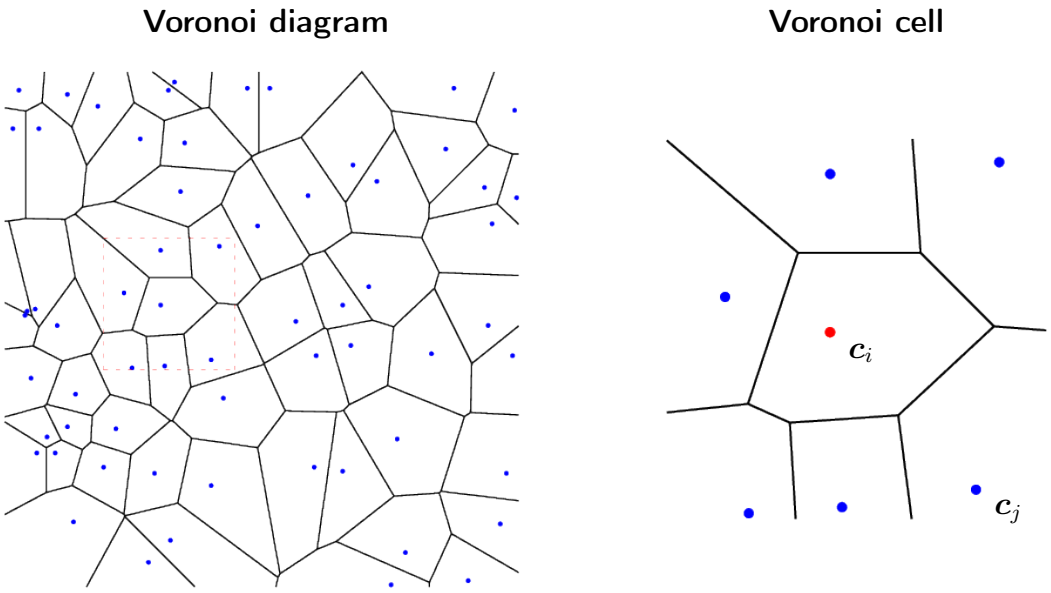

FIGURE 3.2: Schematic of a Voronoi diagram: Voronoi diagram from a set of points called nuclei (blue points) and a Voronoi cell with its respective nucleus $\boldsymbol{c}_i$ (red point) surrounded by neighboring cells $\boldsymbol{c}_j$.

3.2.1 Voronoi diagram

The primary strategy for determining the entropic parameter of porous media is to divide the porous domain into subdomains using Voronoi diagrams (Senechal, 1993). These subdomains are polygonal and have a central nucleus called Thiessen polygons or Voronoi cells (see Fig. 3.2). For example, if the PNMs are designed by circular obstacles, the coordinates of the centers can generate two-dimensional Voronoi diagrams; each circle generates a Voronoi cell, and the centres coincide with the coordinates of the nuclei[2] (Kim, Kim, and Sugihara, 2001).

In a Voronoi diagram, if the set $\boldsymbol{C} = \{\boldsymbol{c}_1, \boldsymbol{c}_2, \boldsymbol{c}_3, \dots\}$ represents the coordinates of the cell nuclei, a Voronoi cell $V_{(\boldsymbol{c}_i)}$ is defined as *"A region where any point* $\boldsymbol{r}$ *is closer to the coordinate* $\boldsymbol{c}_i$ *than to other coordinate* $\boldsymbol{c}_j$*"*. Mathematically, the geometric object $V_{(\boldsymbol{c}_i)}$ is defined as:

$$V_{(\boldsymbol{c}_i)} = \left\{ \boldsymbol{r} \in \mathbb{R} \ \ | : \ \ \|\boldsymbol{r} - \boldsymbol{c}_i\| < \|\boldsymbol{r} - \boldsymbol{c}_j\| \ \ , \ \forall \ \ i \neq j \right\} \tag{3.1}$$

here, the points $\boldsymbol{r}$ form the diagram lines that satisfy the relation $\|\boldsymbol{r} - \boldsymbol{c}_i\| = \|\boldsymbol{r} - \boldsymbol{c}_j\|$.

[2]In the three-dimensional case, the obstacles are spheres that generate polyhedral bodies called Thiessen polyhedrons.

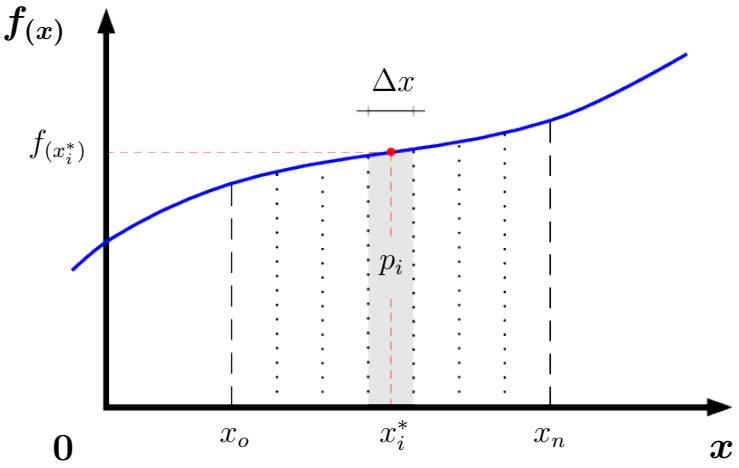

Expected value:

$$\langle x \rangle = \sum_{i=1}^{n} p_i \, x_i$$

$$p_i = f_{(x_i^*)} \Delta x$$

Properties:

1. $f_{(x_i^*)} \geqslant 0$
2. $\sum_{i=1}^{n} f_{(x_i^*)} \Delta x = 1$

FIGURE 3.3: Scheme of a discrete probability distribution function $f_{(x_i^*)}$: Definition of expected value $\langle x \rangle$ and properties of $f_{(x_i^*)}$.

3.3 Shannon entropy

In principle, the degree of randomness of a porous medium (natural, artificial or computational) can be quantified using Shannon entropy (Michalowicz, Nichols, and Bucholtz, 2013). Also known as information entropy or simply entropy, the concept of Information Theory was first introduced by Claude E. Shannon in his 1948 paper *"A Mathematical Theory of Communication."* (Shannon, 1948). The information entropy measures the uncertainty related to the information content; in essence, it quantifies the level of surprise or unpredictability in an information source (Cover and Thomas, 1991). Events with low probability have higher information content, while events with high probability have lower information content. The entropy is highest when all outcomes are equally likely (maximum uncertainty) and lowest when one outcome is certain (minimum uncertainty or predictability).

The information entropy, represented by H for a random variable x and distribution function $f_{(x_i^*)}$ (see Fig. 3.3), measures the average information content associated with the outcomes of that random variable. Mathematically, H is defined as:

$$H = \sum_{i=1}^{n} p_i \, I_i \tag{3.2}$$

$$I_i = \ln\left(\frac{1}{p_i}\right)$$

where p_i is the probability of occurrence i, I_i is the information content of i, and n is

the number of events. Notice that entropy H (Eq. 3.2) has a mathematical structure similar to the expected value $\langle x \rangle$ (see Fig. 3.3), as both express averanges.

In our research, the source of information is the location of the circular obstacles that form the PNMs. Thus, the entropy of PNMs is a purely geometric parameter (just like porosity), as the physical information of PNMs does not intervene in the calculation. Furthermore, since the analysis is stochastic, different configurations can possess the same entropy value. The change in entropy reflected by the variation in configuration can alter the physical parameters: tortuosity and permeability in a fluid flow process (see Fig. 3.1). Therefore, entropy is important for fluid dynamics in random PNMs and becomes another petrophysical parameter alongside porosity, tortuosity and permeability.

3.3.1 Shannon entropy of a Voronoi diagram

Voronoi diagrams can be subjected to a statistical analysis based on some geometric information of the polygonal cells, for example: perimeter, area, number of sides, number of vertices, or the sum of the interior angles of the polygons (Tanemura, 2003; Hinde and Miles, 1980; Crain and Miles, 1976). The chosen geometric information is the random variable denoted by x, which generates the probability distribution function $f_{(x_i^*)}$ (see Fig. 3.3).

To obtain the Shannon entropy of a Voronoi diagram, the following algorithm must be executed:

1. First, define the discretisation value $\Delta x = \ell/n$ by choosing a reference value ℓ (e.g., a multiple of $\langle x \rangle$) and the number of partitions n of the value ℓ.
2. Generate a discrete probability distribution function $f_{(x_i^*)}$ for the random variable x, but normalised concerning $\langle x \rangle$.
3. Obtain the discrete probability set $P = \{p_1, p_2, p_3, \ldots, p_n\}$ using the following relationship: $p_i = f_{(x_i)}\,\Delta x$ (see Fig. 3.3).
4. Finally, calculate the Shannon entropy (H) using the set $P = \{p_i\}$ and Eq. 3.2.

Although the methodology to obtain the Shannon entropy was implemented on Voronoi diagrams in the two-dimensional plane, the implementation in the three-dimensional space is immediate but more complex, where the diagrams are formed by polyhedrons instead of polygons (Koltun and Sharir, 2004).

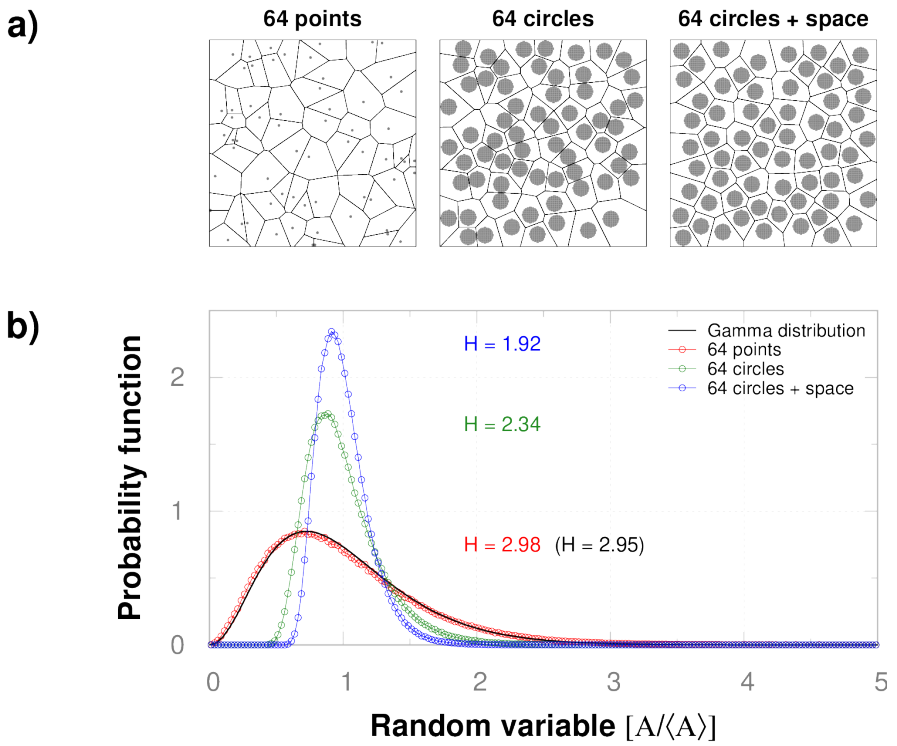

FIGURE 3.4: Design and statistical analysis of PNMs. **a)** Voronoi diagrams generated within a PNM: First, from 64 points distributed randomly without restriction, second, using non-superimposed circles and finally, adding the restriction of a small space between circles. **b)** Distribution functions and their respective entropy compared to the Gamma distribution function. The functions and values are the average of 1000 different random configurations in the three types of PNMs.

3.3.2 Characterization of a PNM using Shannon entropy

Characterising the degree of randomness of a two-dimensional PNM through Shannon entropy is a purely geometric approach, because the analysis is based on the Voronoi diagrams generated within the PNM. Since Voronoi cells collectively cover the entire space of the PNM (pore and wall), the sum of their areas represents the physical dimensions of the PNM. Therefore, the *area* of the Voronoi cells can be chosen as a random variable[3]. If the area is normalized with respect to the average area, the probability distribution function develops around unity and behaves like a Dirac delta function in an ordered case.

To obtain the Shannon entropy of a PNM formed by circular obstacles, the following algorithm must be executed:

[3]In the three-dimensional case, the volume of the Voronoi cells is chosen as a random variable because the sum of their volumes covers the entire PNM.

1. First, implement a periodic update of the computational random seed to generate different random number distributions[4]. The Fortran language has a subroutine that updates the computer's random seed every second (Press, 2007).

2. Design a PNM with non-overlapping circles distributed randomly but separated by a minimum distance more significant than a given circular diameter.

3. Construct a Voronoi diagram within the PNM according to Eq. 3.1 and based on the circle centres as information. The Voro++ package generates the Voronoi diagram (Rycroft, 2009).

4. Generate the function $f_{(x_i^*)}$ by choosing the area of the polygons as a random variable but normalised by the expected value, that is, $x_i = \mathrm{A}_i/\langle \mathrm{A} \rangle$.

5. Finally, using Eq. 3.2, calculate the Shannon entropy of a random PNM formed from circles.

Following the presented algorithm, three types of PNMs were designed consecutively. First, 64 points will be distributed randomly without any restrictions. Non-overlapping circles will be used instead of points, and finally, circles will be separated by a given minimum distance (see Fig. 3.4 a). Due to the stochastic nature of the problem, 1000 different PNMs (various configurations) were designed in each case. Fig. 3.4 b presents only the average curve of function $f_{(x_i^*)}$ and its corresponding entropy H. Furthermore, to compare the proposed methodology with analytical results, Fig. 3.4 b also presents the Gamma distribution function that models the point distribution (Bourguignon et al., 2015; Khodabina and Ahmadabadib, 2010; Stacy et al., 1962). Fig. 3.4 shows a decrease in entropy as design constraints are imposed since a constraint limits the number of configurations. In our work, the PNMs under analysis correspond to the third case because restricting a given minimum distance between circles does not create inaccessible empty space for fluid flow.

3.4 Petrophysical parameters of porous media

In general, a porous medium is a material composed of two phases, a solid matrix and a system of pores that may or may not be interconnected with each other, where the shapes and size of the pores are described geometrically, while the connection of the pores topologically. The most relevant macroscopic quantities are porosity, tortuosity,

[4]Computers generate random numbers from the same random distribution because the random seed is constant. For this reason, the numbers generated are called pseudo-random.

and permeability describes porous media geometrically and topologically independently of other effects (Schön, 2015). However, if the characteristics of the pore scale are micrometric, tortuosity and permeability are affected due to the physical properties of the porous media and the fluid passing through the pores, whereas the porosity is essentially geometric.

3.4.1 Porosity

The most straightforward property of a porous media is the porosity, defined as the fraction of space occupied by the connected pores[5]. However, if there are unconnected or isolated porous regions, these regions are not considered because they do not allow fluid flow (Scheidegger, 2020). The porosity ϕ can vary from 0 to 1 and is expressed as follows:

$$\phi = \frac{S^{\text{pore}}}{S^{\text{total}}} \tag{3.3}$$

S^{total} is the total space of porous medium (solid + pores), and S^{pore} is the space occupied by pores (empty).

3.4.2 Tortuosity and permeability in microfluidics

While the wettability of the porous material is not relevant at the macroscale, the effect of wettability becomes important at the microscale. The structure shape and material wettability are determining factors for the flow of microfluidics. Specifically, wettability is responsible for the surface of the porous medium becoming wet or the liquid being trapped in the micropores. Additionally, the wettability effect may affect the flow, changing the trajectory that the fluid undergoes compared to the trajectory developed without considering the wettability (see Fig. 3.1).

Specifically, there is a change in the velocities field, depending on the degree of hydrophobicity or hydrophilicity of the fluid-solid system. Besides the change with respect to the velocity intensity, there is a modification in its streamlines, mainly in the narrow parts of the porous media, due to capillary and adhesion processes (see Fig. 3.1). Thus, since characteristics that define a porous media, such as tortuosity

[5]If the porous system is two-dimensional or three-dimensional, the space S is equal to the area or volume respectively.

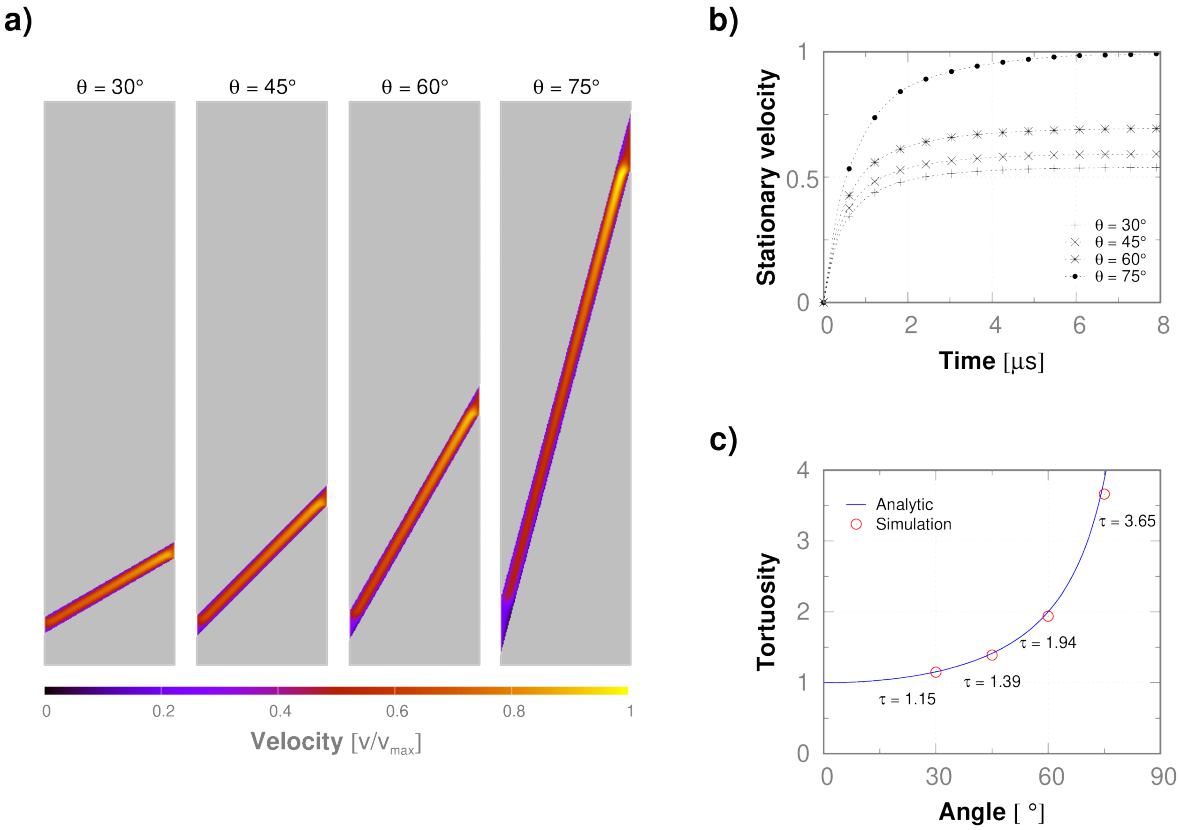

FIGURE 3.5: Tortuosity in a channel of constant narrow width at different angles of inclination. **a)** Fluid velocity field in the inclined channels. **b)** Normalized stationary velocity relative to the case of greater inclination. **c)** Comparison between analytical tortuosity and simulated hydraulic tortuosity.

and permeability, may be in function of the velocities field, these would be strongly affected due to wettability because this one information would reside in the velocities field. Nevertheless, the fluid velocity field must reach a stationary state to obtain the tortuous or permeable characteristics of porous media, taking into account the wettability effect.

3.4.3 Hydraulic tortuosity

In fluid dynamics and porous media, tortuosity, represented by τ, explicitly refers to measuring how much longer and convoluted the flow path is compared to the straight-line distance between two points (Scheidegger, 2020). It quantifies the complexity of the flow path within the medium, from a minimum value equal to unity to high values indicating more sinuous and irregular paths ($\tau \geqslant 1$). However, there is an alternative method called *hydraulic tortuosity* that makes use of the velocities field

rather than determining the streamlines (Duda, Koza, and Matyka, 2011), where this one method simplifies work in cases such as complex geometries or three-dimensional porous media. The fluid flow (velocity field) must reach a steady state to obtain the system's tortuosity, denoted by τ. Mathematically, τ is expressed as:

$$\tau = \frac{\sum_{i}^{N_x}\sum_{j}^{N_y} v_{ij}}{\sum_{i}^{N_x}\sum_{j}^{N_y} v_{ij}^{\text{eff}}} \tag{3.4}$$

v_{ij} is the velocity modulus inside the channel, and v_{ij}^{eff} is a velocity component with a direction parallel to fluid injection (horizontal from right to left).

To verify the method's effectiveness, we calculate the hydraulic tortuosity of simple channels inclined at four different angles with respect to the horizontal line (see Fig. 3.5 a). Previously, we calculated the velocity profile when the system reaches a steady state using LBM simulations, where the injection velocity is the driving force applied as a Dirichlet boundary condition (see details, App. B). Subsequently, from the velocity field and the Eq. 3.4 we calculate the hydraulic tortuosity of the channels. The physical system is multicomponent with brine and oil as the injected and displaced fluids, respectively, within a hydrophilic clay channels (see details, App. C). However, to emulate a single-component system, as an initial condition, the channel starts filled with brine, and the presence of oil is almost negligible at the end of the channel. In order to compare LBM simulations with analytical results, strategically, only the central part of the channel is analyzed, avoiding the ends where boundary conditions for multicomponent systems are applied.

The system reaches a stationary state in approximately $8\mu s$ in each case (see Fig. 3.5 b) and the velocity field at that time are presented in Fig. 3.5 a. While, in Fig. 3.5 c, we can see the results obtained in comparison with analytical results, which come from An entirely geometric analysis whose result is equal to $\tau = 1/\cos\theta$ (Duda, Koza, and Matyka, 2011). In conclusion, comparing results suggests that the hydraulic tortuosity method is valid. However, there is a substantial difference as the inclination angle increases since the tortuosity decreases slightly, perhaps due to the hydrophilic property of the clay channel ($\theta = 69°$).

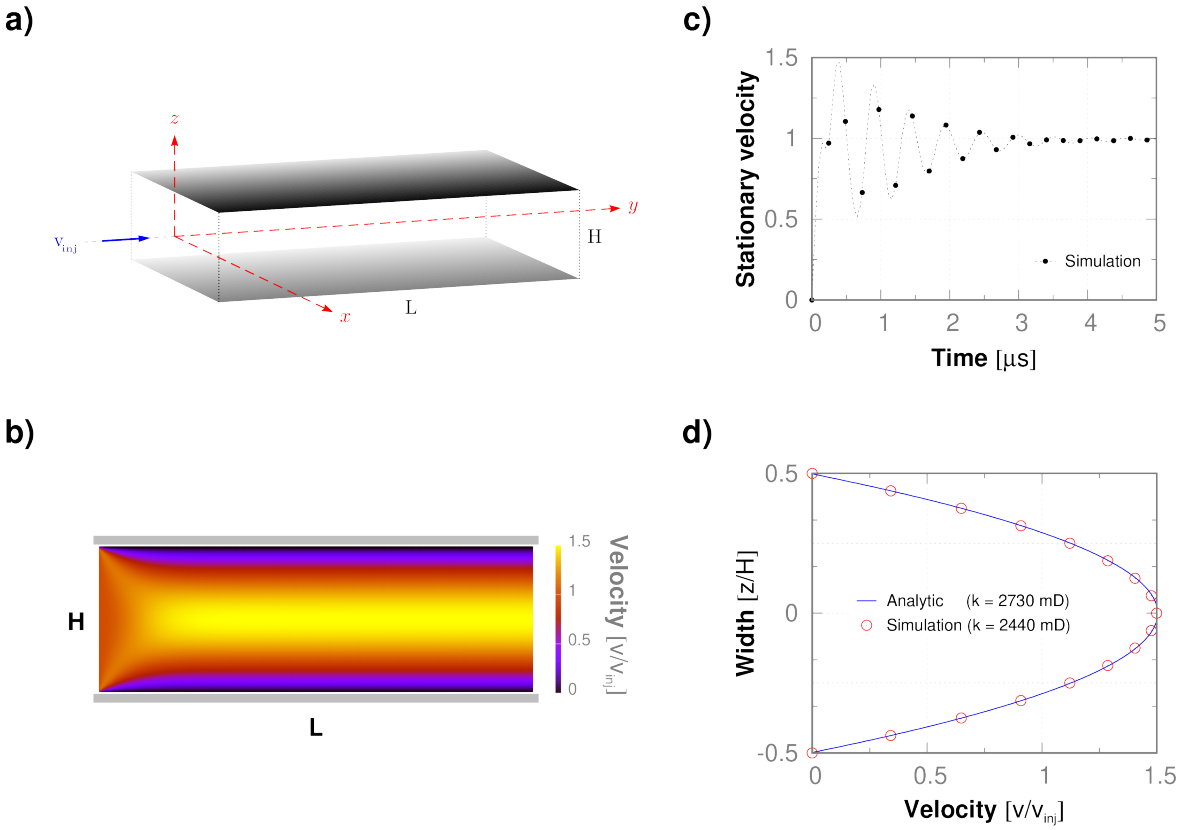

FIGURE 3.6: Hagen-Poiseuille flow by fluid injection. **a)** Scheme of a channel formed by parallel plates. **b)** Fluid velocity field in the channel. **c)** Normalized stationary velocity. **d)** Comparison of results between the analytical and simulated velocity field, where the simulated profile belongs to the channel center ($L/2$).

3.4.4 Darcy permeability

Permeability is a property of materials, especially porous or granular substances that describes their ability to allow fluids (such as liquids or gases) to pass through them (Chapuis and Aubertin, 2003). It measures the ease with which fluids can flow or permeate through a given material under the influence of a pressure difference. It is typically represented by the symbol k and expressed in units of area, such as square meters (m^2) or milidarcies (mD), a standard unit in the oil and gas industry. Specifically, the concept of permeability can be defined by Darcy's empirical law, which uses the velocity field and the pressure profile (Bauer et al., 2019). Just like hydraulic tortuosity, *Darcy permeability* must be calculated when the velocity and pressure of

the flow reach a steady state. Mathematically, k is expressed as:

$$k = \mu \frac{\sum_{i}^{N_x} \sum_{j}^{N_y} v_{ij}}{\sum_{j}^{N_y} \left(p_j^{\text{in}} - p_j^{\text{out}} \right)} \tag{3.5}$$

p_j^{in} and p_j^{out} are the input and output pressures, respectively, μ is dynamic viscosity, and v_{ij} is the velocity modulus inside the channel.

To test the Darcy method, we calculated the permeability of the Hagen-Poiseuille flow, which consists of a fluid that circulates through a channel formed by two parallel plates of length L and separated by a distance H, where $L \gg H$ (see Fig. 3.6 a). In our case, the driving force for fluid flow is generated by fluid injection at the left boundary of the channel or Dirichlet boundary condition (see details, App. B). We performed LBM simulations to calculate the Darcy permeability until we reached a steady state. Thus, we obtain the Darcy permeability by Eq. 3.5 using the steady-state velocity and pressure profiles (see Fig. 3.6 b and Fig. 3.6 c).

Suppose the Hagen-Poiseuille flow is generated by fluid injection. In that case, the analytical solution of the velocity profile has a parabolic shape with a maximum velocity relatively equal to $v/v_{\text{inj}} = 1.5$ as show in Fig. 3.6 d (Mohamad, 2011). Then, the permeability value of the Hagen-Poiseuille flow can be obtained analytically by combining the solution of the Navier-Stokes equation and Darcy empirical law, whose value is equal to $k = H^2/12$ (Zhao et al., 2020). In conclusion, the analytical and simulated velocity fields have the same parabolic character (see Fig. 3.6 d). However, there is a difference in the permeability value; the simulated value ($k = 2440\, mD$) is lower than the analytical one ($k = 2730\, mD$). Analytical permeability, derived from the macroscopic continuum model, does not consider wettability. In contrast, Darcy permeability uses LBM simulations that include wettability information. Therefore, the hydrophilic characteristics of the clay plates ($\theta = 69°$) reduce permeability due to fluid adhesion on the plates.

Chapter 4

Enhanced Oil Recovery in PNMs

Abstract

To estimate the amount of oil that can be extracted from natural reservoirs, understanding capillary phenomena such as wettability and interfacial tension at rock-brine-oil interfaces is decisive. One of the nanotechnological applications in the oil industry are nanoparticles as rock wettability modifiers for Enhanced Oil Recovery (EOR). In addition, we must also consider the characteristics of fluid flow and morphology of porous medi, such as pore connectivity, porosity, tortuosity and permeability, for EOR processes. In this chapter, in order to explore the possible applications of nanoparticles in EOR processes, we apply a multiscalar hierarchical calculation protocol that combines the LBM methodology and data from MD, where MD data is mapped as input parameters in LBM simulations. Our objective is twofold: to study the porous structure effect and the nanoparticles inclusion effect on the oil extraction process. More specifically, we study the brine injection dispersed with or without nanoparticles into clay porous media previously filled with oil. We have considered different functionalized SiO_2 nanoparticles (hydroxylated, sulfonic acid and polyethylene glycol). Regarding the porous structure, we study the oil displacement process by injecting brine into porous media formed by obstacles that have the same porosity value but different geometric considerations, varying the obstacles in: shape (squares, hexagons, octagons and circles), size (circles of four different proportions) and location (four random configurations of small circles). Our results indicate that for constant porosity and the same injected fluid, square obstacles and small circular obstacles displace more oil, while random configurations retain an amount of oil. Furthermore, for the same porous structure, we observe that polyethylene glycol nanoparticles are more effective in displacing oil with respect to the others.

4.1 Introduction

There are still significant research groups focused on the optimization and development of new processes for the oil recovery from natural reservoirs. In an oil extraction process, 5 to 25% of the total can be recovered by natural depletion, while 10 to 20% additional oil can be recovered by water flooding or gas injection (Morrow, 1990). Therefore, the objective of the new methodologies is to recover the remaining fraction of oil trapped in rock structures due to interfacial phenomena and capillary forces. In this context, in order to estimate the amount of oil that could be recovered from natural reservoirs, we must understand the mechanism of wettability at the rock-brine-oil interfaces (Green, Willhite, et al., 1998; Donaldson and Alam, 2013).

The potential use of nanostructures as wettability modifiers for enhanced oil recovery processes is one of the most promising applications in the oil & gas industry (Suleimanov, Ismailov, and Veliyev, 2011). Where, these nanostructures are economically viable to produce on a large scale with a certain degree of control. In addition, their surface and interfacial properties can be adjusted for a given natural reservoir (Munshi et al., 2008). In EOR processes, we must also consider characteristics of the dispersed injected fluid of nanoparticles to extract oil, as well as the mineralogy and morphology of the porous media, such as the rocks wettability, the connectivity of the pores, the porosity, tortuosity and permeability of the system (Tiab and Donaldson, 2015).

From experimental measurements or molecular dynamics simulations, we can obtain data for the system under study, including the densities and viscosities of the injected and displaced fluids, the interfacial tension between the fluids, and the wettability of the porous structure. Then, the information obtained at the macroscale, microscale or nanoscale is introduced into the field of the mesoscale within the LBM methodology, where interfacial tension and wettability are treated as fluid-fluid and fluid-solid interactions, respectively (Porter et al., 2012). The physical observables obtained in the mesoscale, such as the density and velocity of the fluids, can be compared with the macroscopic variables of the fluid dynamics applied to microfluidics (Mohamad, 2011).

To perform simulations in microfluidics, the fluid flow is modelled using the LBM methodology and the Explicit Force method (Porter et al., 2012), which is a multicomponent interparticle potential LBM for immiscible fluids with large

viscosity relationships, where external forces are directly incorporated into the discrete Boltzmann equation. The Taxila-LBM development by Coon *et al.* (Coon, Porter, and Kang, 2014), is an open source to solve the LBM model that incorporates external forces directly and is written in Fortran, C++ and Python. Taxila-LBM uses PETSc to abstract data structures and communications, allowing codes to achieve excellent parallel performance.

Therefore, computational fluid dynamics (CFD) applied to fluid flow on a microscopic scale plays an important role. In particular, the LBM methodology can model fluid dynamics through complex porous structures. In addition, the computational programming of the modelling is easy to use and can be implemented in parallel computing. Initially, the LBM methodology was developed by McNamara *et al.* (McNamara and Zanetti, 1988) and then applied as a powerful alternative method to solve CFD problems, such as: fluids with immiscible components, interfacial problems, fluid flow in penetrable media, fluid simulations of multiples species and flows in fairly complex porous media (Porter et al., 2012). Currently, the LBM methodology has even been extended to apply of semi-classical (Coelho, Ilha, and Doria, 2016) and relativistic fluids (Mendoza et al., 2010). Here, we study the petrophysical properties of the oil extraction process through the porous structure of an artificial rock with controlled geometries using a hierarchical approach that combines LBM simulations and data from MD (Pereira, Lara, and Miranda, 2016).

In this chapter, we study the oil extraction process in porous media through LBM simulations. Still, since the system is multicomponent at micrometer scale, we apply the Explicit Force method to address the interfacial tension and wettability. We study the porous structure effect in the oil extraction and we determined the nanoparticle inclusion effect in the enhanced oil recovery. In particular, we study the injection of dispersed fluids of nanoparticles into clay porous structures filled with oil. We have considered different nanoparticles (hydroxylated, sulfonic acid and polyethylene glycol) dispersed in brine, as well as the case of without nanoparticles. Regarding the porous structure, we study the oil displacement process by injecting brine without nanoparticles into porous media that have the same porosity value, where the pores have different geometric considerations based on the obstacles variation, such as: shape (square, hexagonal, octagonal or circular), circles size in four different proportions and circles distribution for four random configurations. Regarding the nanoparticles inclusion, we verified the power of surfactants for oil recovery in diverse porous media, such as: random structures, dead-end pores and three-dimensional cases.

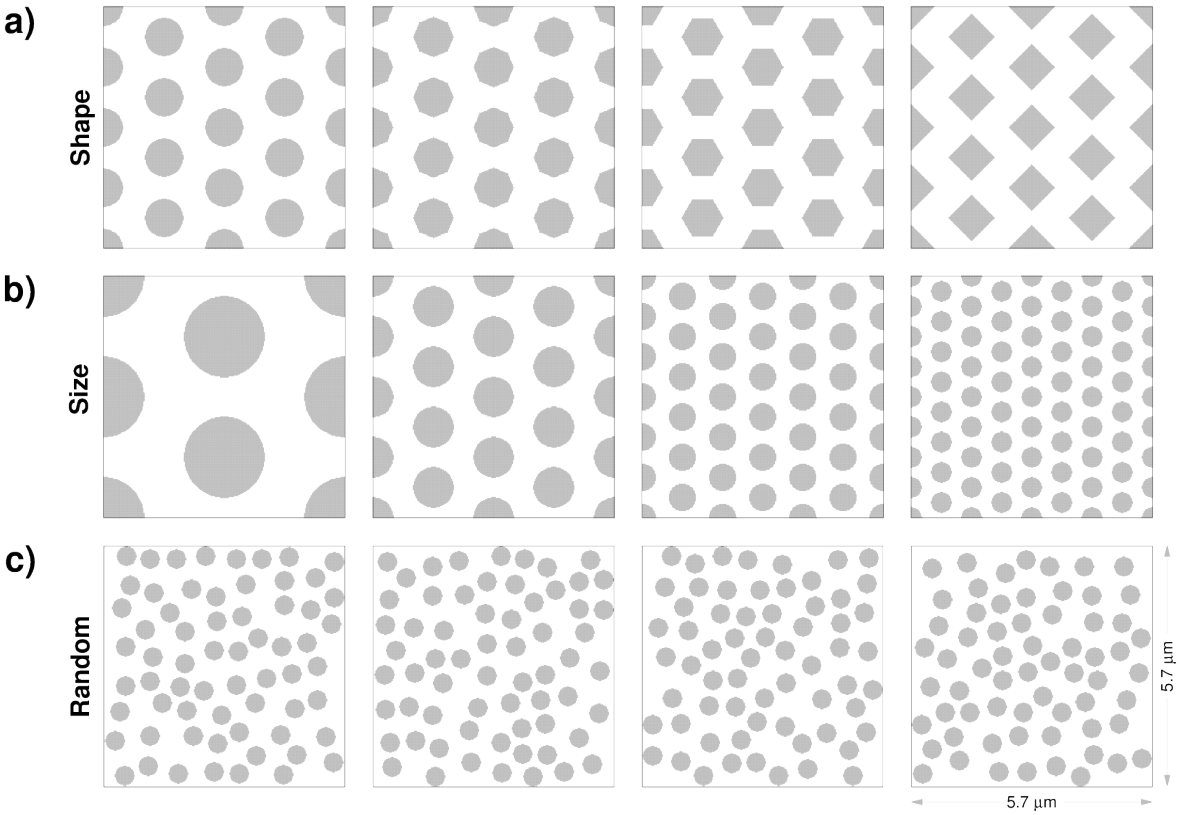

FIGURE 4.1: Basic porous structures formed by geometric objects and designed to have the same porosity value ($\phi = 0.68$), where the gray regions represent a solid area and the white color represents the porous space. Porous structures according to solid objects are classified into: **a)** different shapes, **b)** different sizes and **c)** different random locations.

4.2 Methodology

The methodological approach on oil extraction is divided into two main parts: **(1)** we study the porous structure effect on the oil recovery process and **(2)** we determinate the nanoparticle inclusion effect on enhanced oil recovery. Firstly, in order to explore the possible effects of the porous structure, we consider the role of obstacles in the porous structure design, such as: **(i)** shape, **(j)** size and **(k)** location (see, Fig. 4.1). Secondly, in order to explore the effectiveness of nanoparticles, we have considered different nanoparticles added to the injected fluid, such as: **(a)** without nanoparticles, **(b)** hydroxylated, **(c)** sulfonic acid and **(d)** polyethylene glycol (see, Tab. C.1). The nanoparticles effect is tested in relatively complex porous media such as: **(u)** random structure, **(v)** dead-end pores and **(w)** three-dimensional.

4.2.1 Pore Netwok Models (PNMs)

In particular, because our main objective is to study oil extraction at microscale, the porous systems (PNM) under study have micrometric dimensions. The system global domain has a square shape with a lateral length equal to $L = 5.7\,\mu m$. In order to emulate a porous media, different types of geometric objects are introduced as obstacles to fluid flow within the domain. The porous structures are designed to generate the same porosity equal to $\phi = 0.68$, obtained by the Eq. 3.3. Specifically, we design: **(i)** squares, hexagons, octagons and circles to vary the obstacles shape, **(j)** whereas we use circles of different radius to vary the obstacles size and **(k)** finally we use small circles to vary the obstacles location using random configurations (see, Fig. 4.1).

4.2.2 Oil extraction process in PNMs

Subsequently, from the porous structure under analysis, we proceed to performed oil extraction studies within the PNMs. The physical system is composed of a porous structure and the displaced and injected fluids that pass through the pores, where the PNM structure is montmorillonite clay (MMT), the displaced fluid is light oil, and the injected fluid is API brine (8% NaCl and 2% $CaCl_2$). Where, **(a)** in addition to the pure brine solution (NoNP), there are three types of SiO_2 nanoparticle solutions: **(b)** hydroxylated (NP-H), **(c)** functionalized with sulfonic acid (NP-SA) and **(d)** functionalized with polyethylene glycol (NP-PEG2) (see Tab. C.1). Initially, the confined oil occupies the entire pore space of the PNM. To generate fluid flow from left to right, a brine solution is injected into the left contour of the PNM with an injection velocity of $\boldsymbol{v} = 0.44\,m/s$.

Due to the studies of oil extraction processes are approached completely through LBM simulations (see, Chap. 2), the methodology requires physical information of the fluids under study, such as densities and viscosities. Furthermore, since the physical dimensions of the porous structure under analysis are micrometric, the fluid-fluid and solid-fluid interactions are decisive in the fluids flow and the oil extraction process. Therefore, the methodology also necessitates microscopic physical information, such as the interfacial tension between immiscible fluids and the wettability of the porous media, which is expressed as the contact angle. Specifically, microscopic information is necessary when applying the Explicit Force method (see Sec. 2.8).

The information required for the LBM methodology is based on the work conduced by Pereira *et al.* (Pereira, Lara, and Miranda, 2016), as presented in Tab. C.1. To

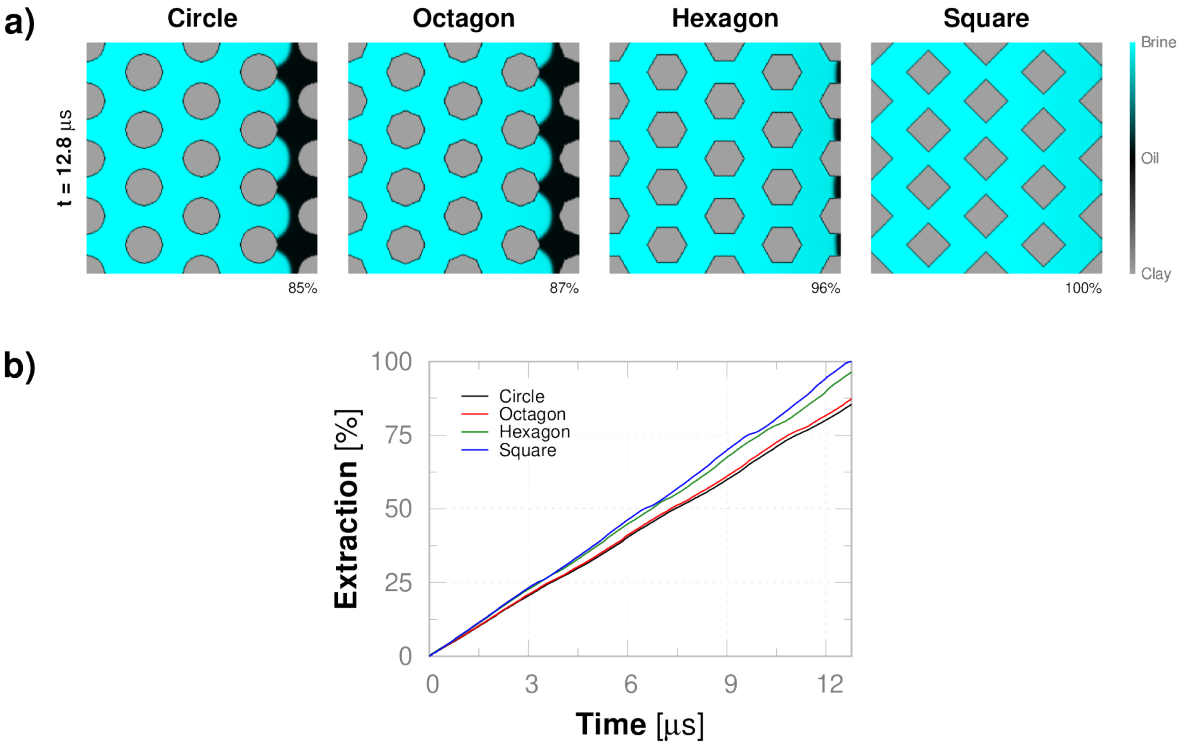

FIGURE 4.2: Oil extraction process in PNMs with obstacles of different form. **a)** Snapshot of oil extraction at time $t = 12.8\,\mu s$. **b)** Percentage of oil extraction during the brine injection time.

study the effect of the porous structure on oil extraction, we use brine without the addition of nanoparticles, where the density and kinematic viscosity of brine and oil are $\rho_{\text{b}} = 997\,kg/m^3$, $\nu_{\text{b}} = 0.791 \times 10^{-6}\,m^2/s$ and $\rho_{\text{o}} = 810\,kg/m^3$, $\nu_{\text{o}} = 4.473 \times 10^{-6}\,m^2/s$, respectively, while the interfacial tension and the contact angle are $\gamma = 0.043\,kg/s^2$ and $\theta = 69^{\text{o}}$, respectively. For studying the effect of nanoparticles on enhanced oil recovery, we use brine without nanoparticles and three types of SiO_2 solutions. The presence of nanoparticles modifies the density and kinematic viscosity of the brine, as well as the interfacial tension and wettability of the system (see details in Tab. C.1).

The methodology developed by Pereira (Pereira, Lara, and Miranda, 2016) applies a multiscale hierarchical calculation protocol that combines LBM simulations and data generated by MD (see Tab. C.1), where the data mapped as LBM input parameters are presented in Tab. C.2 (see details in App. C). Our LBM simulations are performed from the mapped data shown in the Tab. C.2. In each LBM simulation, we obtain as result the velocity field and the pressure profile of the system, as well as the density of the fluid injected and displaced at each time step. Therefore, based on the displaced fluid density, we proceed to study the oil extraction process as a function of time.

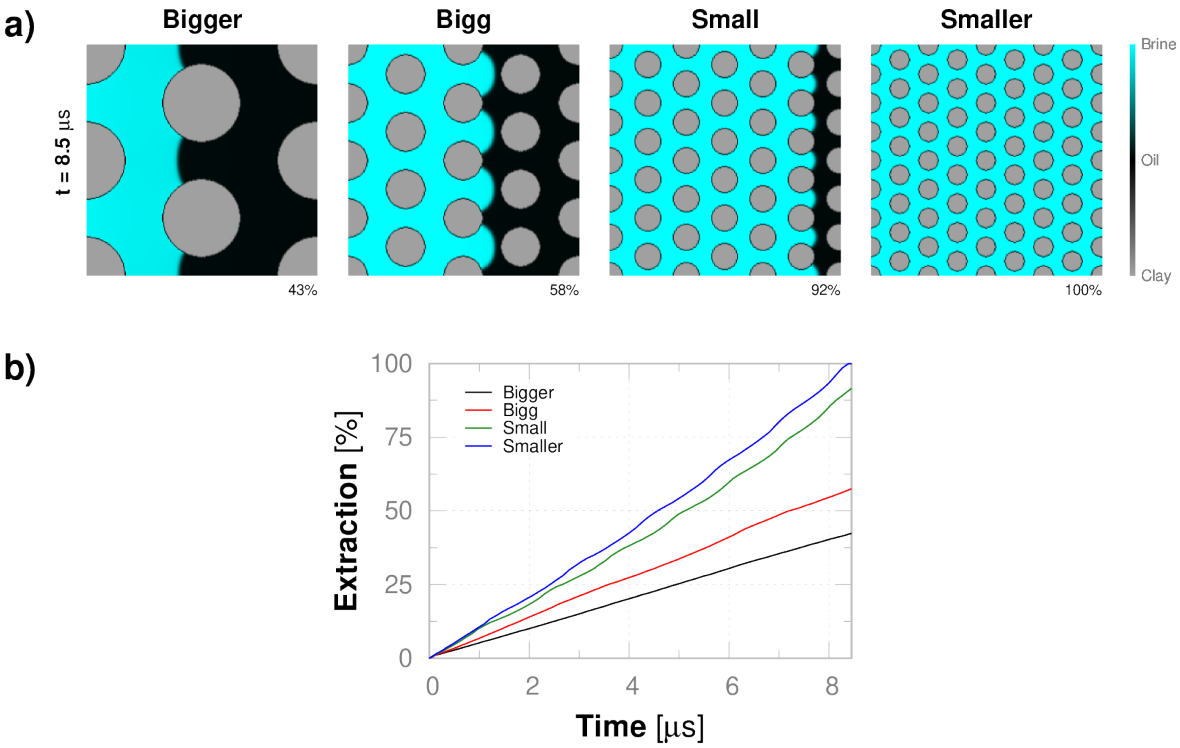

FIGURE 4.3: Oil extraction process in PNMs with circular obstacles of different sizes. **a)** Snapshot of oil extraction at time $t = 8.5\,\mu s$. **b)** Percentage of oil extraction during the brine injection time.

4.3 Results

In microfluidic devices or porous media, the behavior of fluids is often characterized by *Reynolds*, *Mach*, and *Knudsen* criteria, each with its own significance. The Reynolds number ($Re = \boldsymbol{v} \cdot L/\nu_{\mathrm{b}}$) describes the relative importance of inertial forces to viscous forces in microchannels. Low Re values indicate a dominance of viscous forces, leading to predictable laminar flow, while high Re values may result in turbulent flow with chaotic mixing. The Mach number ($Ma = \boldsymbol{v}/\boldsymbol{v}_s$) relates to compressibility effects and is particularly relevant when dealing with gases in microfluidics. At low Ma, incompressible flow assumptions are valid, while at higher Ma, compressibility effects become significant. The Knudsen number ($Kn = Ma/Re$) quantifies the ratio of molecular mean free path to characteristic channel dimensions and is crucial in gas flows at the microscale. When Kn is small, continuum assumptions apply, but as Kn increases, rarefied gas effects become important, leading to deviations from traditional fluid dynamics behavior[1] (Landau and Lifshits, 1959).

[1] In our system under study, $L = 5.7\,\mu m$ represents the lateral length of the PNM, $\boldsymbol{v} = 0.44\,m/s$ denotes the injection velocity, $\nu_{\mathrm{b}} = 0.791 \times 10^{-6}\,m^2/s$ stands for the kinematic viscosity of the injected fluid, and $\boldsymbol{v}_s = 340\,m/s$ is the speed of sound (as mentioned in the physical parameters above).

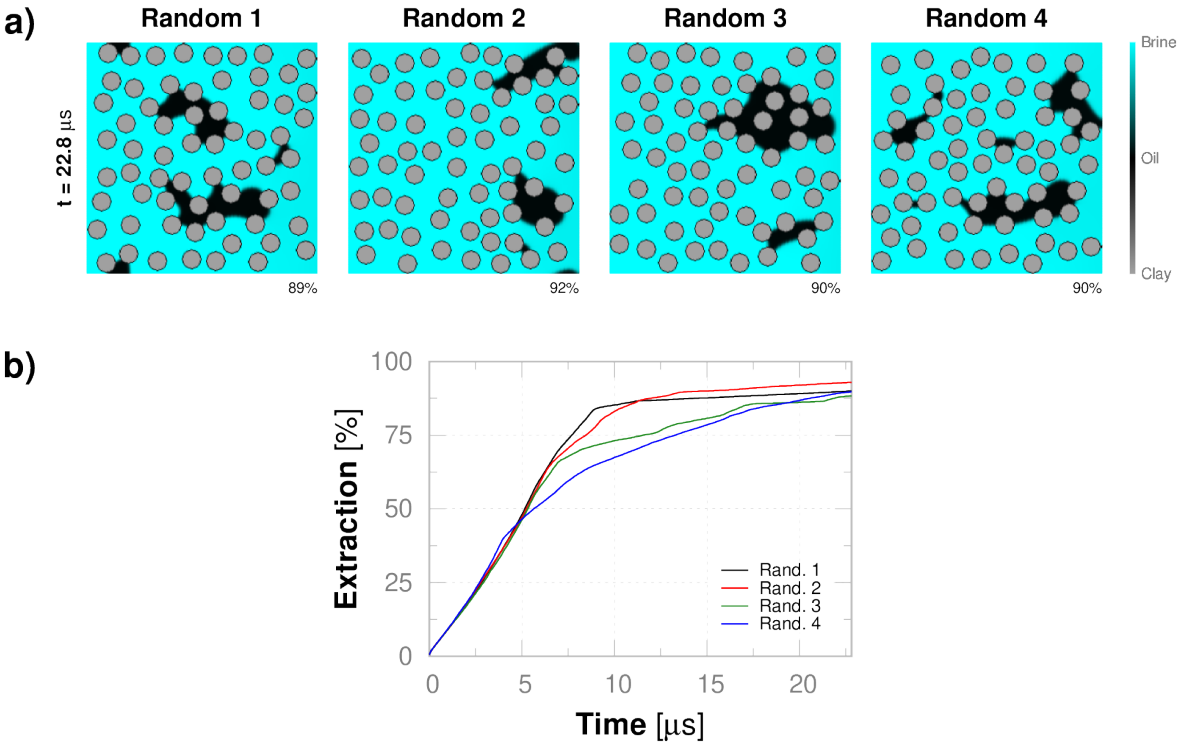

FIGURE 4.4: Oil extraction process in PNMs with small circular obstacles of different random location. **a)** Snapshot of oil extraction at time $t = 22.8\,\mu s$. **b)** Percentage of oil extraction during the brine injection time.

Based on the outlined criteria, the parameters characterizing fluid flow in our LBM simulations are as follows: $Re = 3.17$, $Ma = 1.27 \times 10^{-3}$ and $Kn = 4.03 \times 10^{-4}$. These criteria indicate that the fluid flows fall into the following categories: laminar regime ($Re \ll 2000$), velocities lower than the velocity of sound ($Ma \ll 1$), and slip flow close to the continuous regime ($0.001 < Kn < 0.1$). Therefore, with a Reynolds number of $Re = 3.17$, we derive the main lattice parameters (dimensionless) for LBM simulations: the lateral length is $L^* = 256$, the injection velocity is $v* = 0.003$, and the kinematic viscosity is $\nu_b^* = 0.243$. Subsequently, the space-time scale factors are $\Delta x = L/L^* = 2.22 \times 10^{-8}\,m$ and $\Delta t = (\Delta x)^2 \cdot \nu_b^*/\nu_b = 1.52 \times 10^{-10}\,s$, respectively.

4.3.1 Pore estructure effect in oil extraction

To observe the effect of the porous structure on oil extraction, the porosity ($\phi = 0.68$), injection velocity ($\boldsymbol{v} = 0.44\,m/s$), and other system components (brine-oil-clay) remain unchanged throughout the entire process. The porous structures under investigation

are classified into three cases based on obstacle design: **(i)** different shapes, **(j)** varying sizes, and **(k)** random locations, with the first two cases having a uniform configuration (see Fig. 4.1). In each case, there are four examples of porous structures, and the LBM simulation process ends when one of the examples reaches 100% oil extraction (see Figs. 4.2a–4.4a).

The porous structure effect on oil extraction is based on the geometric characteristics and location of the obstacles, as described below:

a) **Different shape:** (refer to Fig. 4.2) The oil extraction process follows a similar pattern in the four different shapes (square, hexagon, octagon, and circle). In square shape proves to be the most efficient in achieving 100% oil extraction from the PNM in the least amount of time, while the circular shape is the least efficient. The results indicate that, as the number of edges of the polygons (obstacles) decreases or the edges become more pronounced, the velocity field near the surface of the obstacles increases. As analogously, the electric field is more intense on sharp or pointed (metallic) surfaces. Therefore, the polygonal edges of the obstacles facilitate and accelerate the fluids (brine and oil) displacement passing through the PNM (see Fig. 4.2b).

b) **Size variation:** (refer to Fig. 4.3) The oil extraction process exhibits a significant difference between circles of various sizes (bigger, big, small, and smaller). In terms of time, smaller circles prove to be extremely efficient in extracting oil from the PNM compared to bigger circles. The results indicate that as the circle size decreases, the time required to extract 100% of the oil also decreases (see Fig. 4.3b). This is because the velocity field near curved surfaces is greater than that near plane surfaces. Therefore, smaller circles or obstacles with greater curvature facilitate and accelerate fluid flow for oil extraction from PNMs (see Fig. 4.3a).

c) **Random location:** (refer to Fig. 4.4) In contrast to the previous ordered cases, the oil extraction process reveals that a certain percentage of oil remains trapped inside the PNMs (formed by smaller circles), in all four random distributions. The results show that, due to the randomness of the obstacles that form the PNMs, approximately 10% of oil on average remains trapped in the pore network, in all random cases. Fig. 4.4b shows that, all the curves exhibit a horizontal trend when they reach approximately 90% extraction, and even when doubling the extraction time compared to the ordered cases, the horizontal

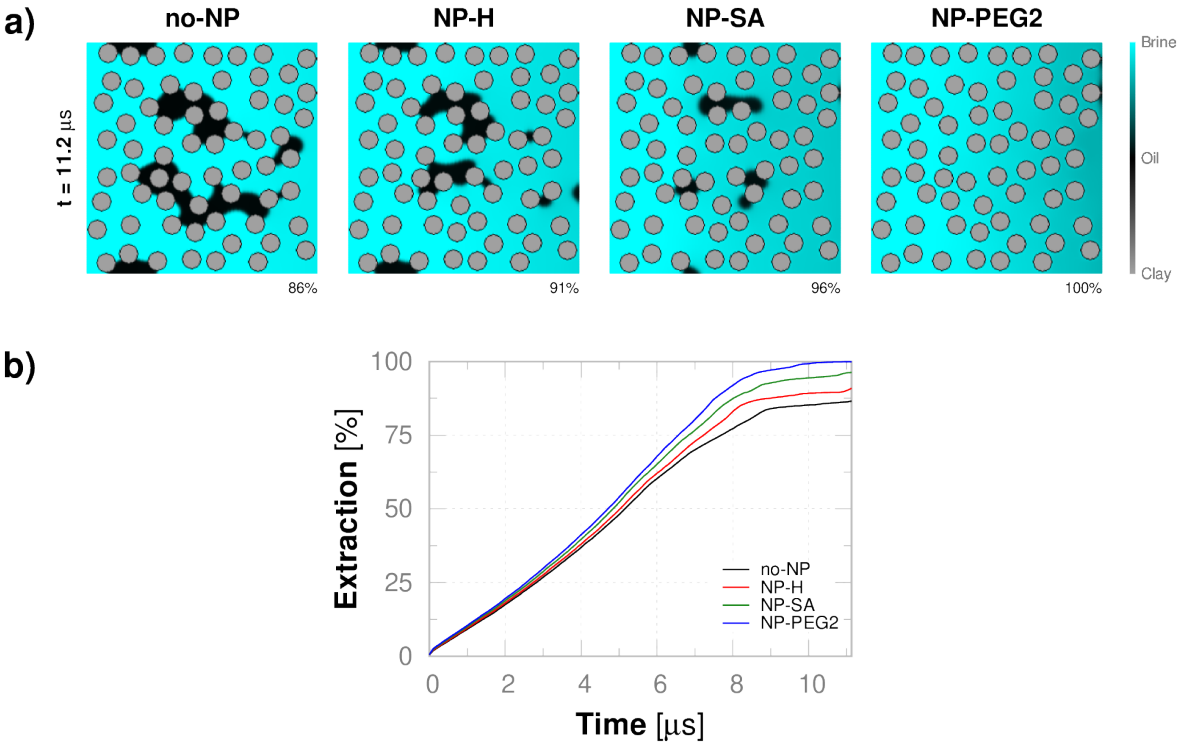

FIGURE 4.5: Enhanced oil recovery by using different nanoparticles in a PNM with small circular obstacles of random configuration. **a)** Snapshot of enhanced oil recovery at time $t = 11.2\,\mu s$. **b)** Percentage of oil extraction during the brine injection time.

trend persists. While the inclination is not perfectly horizontal, indicating the possibility of eventually extracting all the oil, the required injection time would be too long for practical purposes. Therefore, PNMs with random characteristics can retain oil within their internal pores (see Fig. 4.4a).

The quantity of extracted oil and the recovery time are closely related to the arrangement of pores that form a PNM. As PNMs in the first two cases have an ordered pore arrangement, there is the possibility of extracting 100% of the oil by increasing the brine injection time. In contrast, PNMs with a random pore arrangement have the ability to permanently retain a certain quantity of oil within their pores, regardless of the injection time. While the PNM under study is hydrophilic clay, which facilitates oil recovery, the narrow pores can confine oil due to the combined action of brine-oil-clay interfacial forces. Therefore, random PNMs provide the ideal scenario for testing the effectiveness of surfactants, sucha as nanoparticles, in oil recovery processes (EOR). Surfactant techniques are typically employed as a tertiary recovery method after primary and secondary recovery methods have been exhausted.

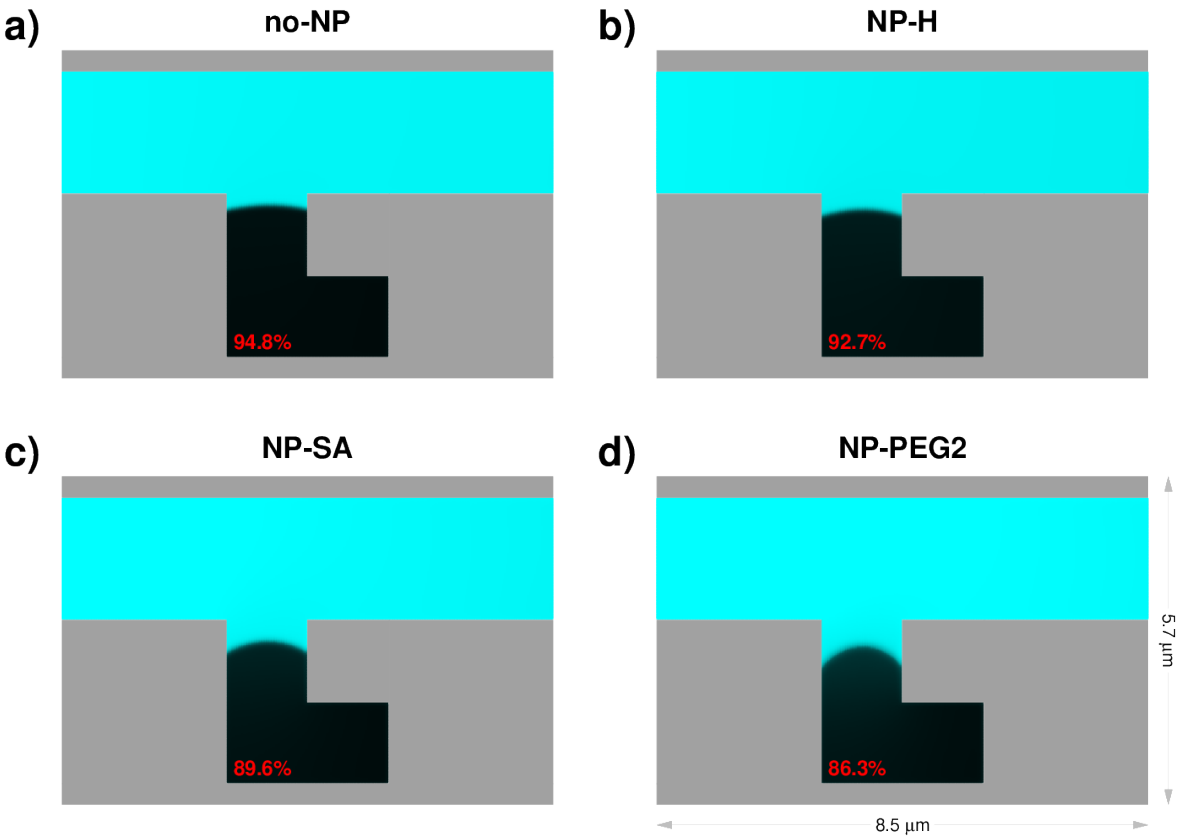

FIGURE 4.6: Enhanced oil recovery in dead-end porous media, where the figures show snapshot when fluid flow reaches stationary state $t > 12\,\mu s$ (oil: black region, brine: cyan region and clay: gray region). The oil recovery amount using **a)** brine without NPs, **b)** brine with NP-H, **c)** brine with NP-SA and **d)** brine with NP-PEG2 are 5.2, 7.3, 10.4 and 13.7% respectively.

4.3.2 Nanoparticles effect in EOR process

Using surfactants in EOR process refers to the application of surfactant chemicals in oil reservoirs to improve the extraction of oil. Surfactants, have the property of reducing the interfacial tension between oil and brine, making it easier to displace and recover trapped oil in the PNM. Surfactants work by modifying the wettability of the PNM's surface and altering the capillary forces that trap oil in narrow channels, small pores, and/or fractures. They also help in emulsifying and mobilizing oil droplets, allowing them to flow more easily through the PNM's channels. The EOR techniques aims to recover additional oil that would otherwise remain permanently trapped in the PNM's pores.

To observe and verify the importance of using surfactants, various nanoparticles are added to the injected brine solution. However, in order to isolate the effects of

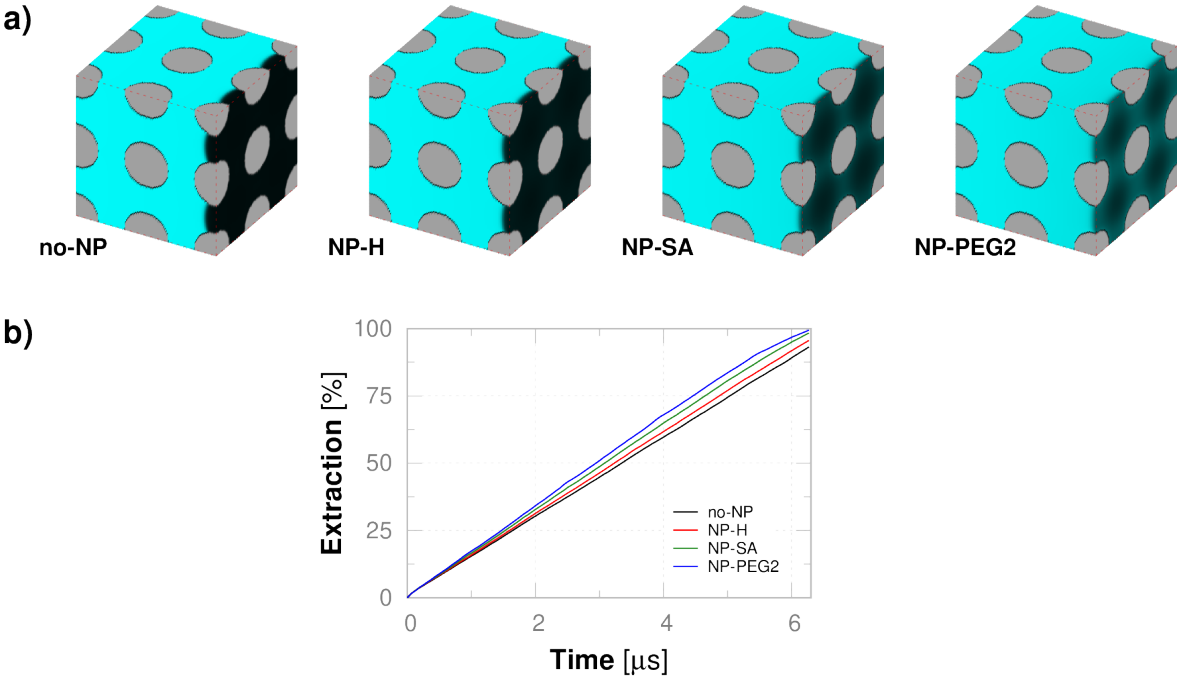

FIGURE 4.7: Enhanced oil recovery in a three-dimensional PNM formed by orderedly located spheres (oil: black region, brine: cyan region and clay: gray region), cases: brine without nanoparticles and with three types of nanoparticle, NP-H, NP-SA and NP-PEG2. **a)** Snapshot of enhanced oil recovery. **b)** Oil extraction as a function of time.

the injection of nanoparticle-dispersed fluid, the system porosity, injection velocity, and other system variables remain unchanged throughout the entire study process. The random PNM that retains the highest quantity of oil in Fig. 4.4a is used as the porous medium under study to improve oil recovery. The first random PNM retains approximately 11% of the oil after a brine injection without the use of nanoparticles for a duration of $22.8\,\mu s$. Then, LBM simulations based on the data from Tab. C.1 are presented in Fig. 4.5, where the chosen random PNM as a test field is subjected to four types of injection, a brine solution without nanoparticles (noNP) compared to three types of nanoparticles added to the brine solution: NP-H, NP-SA, and NP-PEG2 (refer to Tab. C.1).

The results in Fig. 4.5 demonstrate that the use of nanoparticles provides the opportunity to extract 100% of oil from random PNMs, without the possibility of any percentage of oil being permanently retained due to the randomness of the pores. The brine solution without nanoparticles (noNP) is the least efficient for oil recovery, whereas the inclusion of nanoparticles increases the recovery percentage. Among the three types of nanoparticles, NP-PEG2 proves to be the most efficient, displacing

100% of the oil. Next is NP-SA that displaces 96%, and finally, the least efficient is NP-H, which manages to extract 91% (Alvim et al., 2017). The oil recovery time is equal to 11.2 μs, which is similar to the cases of PNMs with an ordered structure and approximately half the time that was simulated in random PNMs.

Additionally, the same recovery process is studied, but applied to a dead-end type porous medium (refer to Fig. 4.6). Dead-end pores are a type of pore structure within a porous medium that lacks an outlet or connection to other neighboring pores or conduits. Fluids trapped within these dead-end pores have limited mobility and are more challenging to displace or extract during various processes, such as fluid flow in porous media or enhanced oil recovery. The results exhibit a similar behavior to that of random PNMs, where NP-PGE2 proves to be the most efficient, displacing approximately 8.5% more oil than the case without nanoparticles (noNP). Specifically, the NP-PEG2 displaces $\approx$ 14% of the oil, followed by NP-SA which displaces $\approx$ 10%, then NP-H which displaces $\approx$ 8%, and finally, the noHP that only manages to extract $\approx$ 5% (Kirch et al., 2020).

Finally, a simple three-dimensional PNM formed by ordered spheres is used as a test field (see Fig. 4.7) and two cases are studied: the injection of brine without nanoparticles and with the addition of NP-PEG2. Because, the use 3D porous media in oil recovery simulations allows for a more accurate, comprehensive, and realistic modeling of fluid behavior in porous media, contributing to improved strategies for oil extraction and reservoir management. These models also facilitate the identification of flow patterns and bottlenecks that can affect the efficiency of oil recovery. The results indicate that in both cases, whether with or without nanoparticles, it is possible to extract 100% of the oil. However, the case with NP-PEG-2 is the most efficient because it requires less injection time, although the difference is minimal. If the porous surface area is increased, such as by using larger spheres, the difference in extraction times would also amplify because the surface is hydrophilic.

4.4 Conclusions

In this chapter, to simulate the (enhanced) oil recovery through the injection of brine with or without dispersed nanoparticles, a hierarchical multiscale computational protocol was applied based on the combination of the Lattice Boltzmann method and Molecular Dynamics data. The displacement of oil was studied using various simple

two-dimensional PNMs (ordered and random), while keeping the system's porosity and injection velocity constant.

First, regarding the effect of the hydrophilic porous structure on the amount of displaced oil, it is observed that porous structures composed of circles are the least efficient compared to other shapes, with the circular shape being the most commonly used computationally to emulate natural porous media. For the same geometric shape but different sizes, the hydrophilic porous structure formed by small circles is more effective compared to the larger ones. Therefore, since the physical reduction of porous media is related to the increase in the simulation network, the expansion of the network does not contribute to the oil extraction process. For hydrophilic porous structures formed by small circles randomly placed, it can be concluded that randomly porous structures better emulate the porous network found in oil reservoirs because a certain amount of oil remains trapped even after brine injection that includes surfactants. In our study, it was observed that the four random porous structures retained an average of 10% of the oil.

Finally, the effect of nanoparticles on oil displacement in hydrophilic porous media is analyzed under three different scenarios: random PNM, dead-end porous medium, and three-dimensional PNM. In the first case, the injection of brine with nanoparticles improved oil recovery. It was even possible to extract 100% of the oil from PNMs that retained $\approx$ 10% after brine injection without nanoparticles. In the second case, the same previous pattern is repeated, demonstrating the importance of using nanoparticles in extreme cases like dead-end pores. The addition of nanoparticles improves recovery by up to $\approx$ 11% compared to an brine injection without nanoparticles. In the last case, the efficiency of using nanoparticles is confirmed, as the injection of brine without nanoparticles takes longer to recover oil compared to the use of nanoparticles.

Chapter 5

Randomness Effect of the PNMs on Fluid Dynamics

Abstract

One of the key problems on fluid dynamics in porous media is to describe the fluid flow delay when it passes through the internal porous network. A strategy to describe the relationship between the dynamics and the intrinsic obstruction porous structure is to characterize the porous medium considering its porosity, permeability and tortuosity among others features. Several PNMs have been proposed to emulate the porous media of the natural reservoirs. These models are usually constructed from obstacles with circular shapes distributed randomly. Our main objective is to characterize random PNMs through the Shannon entropy. For this purpose, we performed a statistical analysis of the Voronoi diagrams generated within a PNM. Based on the assumption that entropic information is a unique feature of the PNMs, we determine: the tortuosity and the permeability using a hierarchical approach that combines LBM simulations and data from MD. In our case study, we consider the fluid-solid interface taking brine for the injected fluid and clay as the porous structure material, respectively. Here, the fluid-solid internal forces are fully considered through the wettability phenomenon. Regarding, the porous structure, we have designed circles based PNMs ranging from perfect ordered model (zero entropy) to a fully disordered ones ($H = 1.92$). Additionally, we have studied the effects of size and porosity by varing the radius and number of the circles, respectively, in PNMs with the same entropy value. Our simulations show that the entropic information is directly related to the degree of tortuosity and permeability, where the randomness of the PNM can lead to the fluid flow delay. In conclusion, the entropy can be characterized essentially as a geometric parameter. From the fluid dynamics perspective, this allows one to determine how tortuous or permeable a random PNM may be based on its entropy.

5.1 Introduction

Fluids flow through porous media has been extensively studied and is common practice in civil engineering, petroleum industry or applications of Lab-on-Chip technology (Mark et al., 2010). In particular, the microfluids study is a multidisciplinary research area that includes parts of the Physics, Chemistry, Biochemistry, Biotechnology, and Electronics among others. Specifically, microfluidics is the science and technology that involves the fluids behavior study, the controllled manipulation of fluids and the design of devices or systems that can reliably and efficiently perform tasks in microchannels with typical dimensions of tens to hundreds of micrometers (Bruus, 2008). Where the velocities field, pressures and temperatura describe the fluid flow that crosses the microchannels that form the system or porous media.

While a combination of Newton's second law and Navier-Stokes hydrodynamics can describe fluid displacement through porous media, the resulting differential equations are often too complex to be applied to real-world problems. Since the modeling is approximate because the analysis is performed at the macroscale, neglecting the capillary effects that become predominant at the microscale (Zhao, MacMinn, and Juanes, 2016). To study microfluidic systems repeatedly but under the same physical-geometric conditions and input parameters, computational numerical simulation is the best option instead of performing experimental measurements. Due to the development of techniques for the geometric visualization-quantification of porous media, as well as, due to the increase in computational capacity-velocity. Furthermore, there is systematic progress in modeling fluid flow at the pore-scale without the need for geometric idealizations in porous media design, while also incorporating relevant physical information into the model.

An ideal numerical method for simulating fluid flows through complex geometries or particularised structures is the Lattice Boltzmann Method (Mohamad, 2011; Sukop and Thorne, 2007; Succi, 2001). The effectiveness and reliability of the method has been confirmed and tested by analytical results in various studies that model flows around solid obstacles with regular and irregular geometry at different scales (Sangtani Lakhwani, Nicolleau, and Brevis, 2019). Furthermore, Boltzmann's methodological approach is very appropriate for conducting studies in the micrometric domain, since microscopic capillary phenomena such as wettability can be easily incorporated into the method (Porter et al., 2012). Hence, studies on the tortuous or permeable characteristics of porous media using the LBM method are more realistic

than studies focused solely on geometry. This is because the method incorporates the information arising from the physical interactions within the fluid-solid system.

In this chapter, our focus is on the study of fluid dynamics within two-dimensional PNMs. These PNMs are constructed using randomly distributed circular objects to mimic natural porous media. Our primary aim in this chapter is to provide a characterization that goes beyond traditional factors like porosity, tortuosity, or permeability. Instead, we focus on the geometric characterization of random PNMs using Shannon entropy. To obtain the entropic value based on Shannon stochastic theory, we perform a statistical analysis from the Voronoi diagrams previously generated within the PNM (see, Chap. 3). Subsequently, assuming that entropic information is a unique feature of a random PNM, we proceed to study the randomness effect on petrophysical parameters such as tortuosity and permeability, using a single fluid described through a hierarchical approach that combines LBM simulations and data from MD (see, Chap. 2). Concretely, we study the petrophysical parameters of random PNMs made of clay filled with brine and injected the same fluid as the driving force of the fluid flow.

5.2 Fluid dynamics in multiscale

Since a fluid at the macroscopic level is considered like a continuous material, this ones are completely determined by parameters such as velocity and density at each point of the material, where the Navier-Stokes equations obtained from a strictly theoretical point of view, are responsible for modeling the system (Chung et al., 2002). Whereas, from a microscopic perspective, a fluid may be represented by atomistic particles and be described through Molecular Dynamics (Leach, 2001), where each discrete entity is defined by its position and velocity governed through Newton laws and interatomic potentials, that are the key point of the methodology. Therefore, between these ones two levels of extreme scales, the Lattice Boltzmann Method operates in the microscale and is constituted as a bridge between the macro and nano scales (Mohamad, 2011), where the ends of its own domain are not well defined.

From MD simulations, we can study phenomena such as wettability that involves the fluids with the porous matrix (porous media). Furthermore, wettability's infomation obtained in the nanoscale (contact angle), we may introduce in the microscale within the LBM methodology as microscopic forces or fluid-solid interactions (Pereira, Lara,

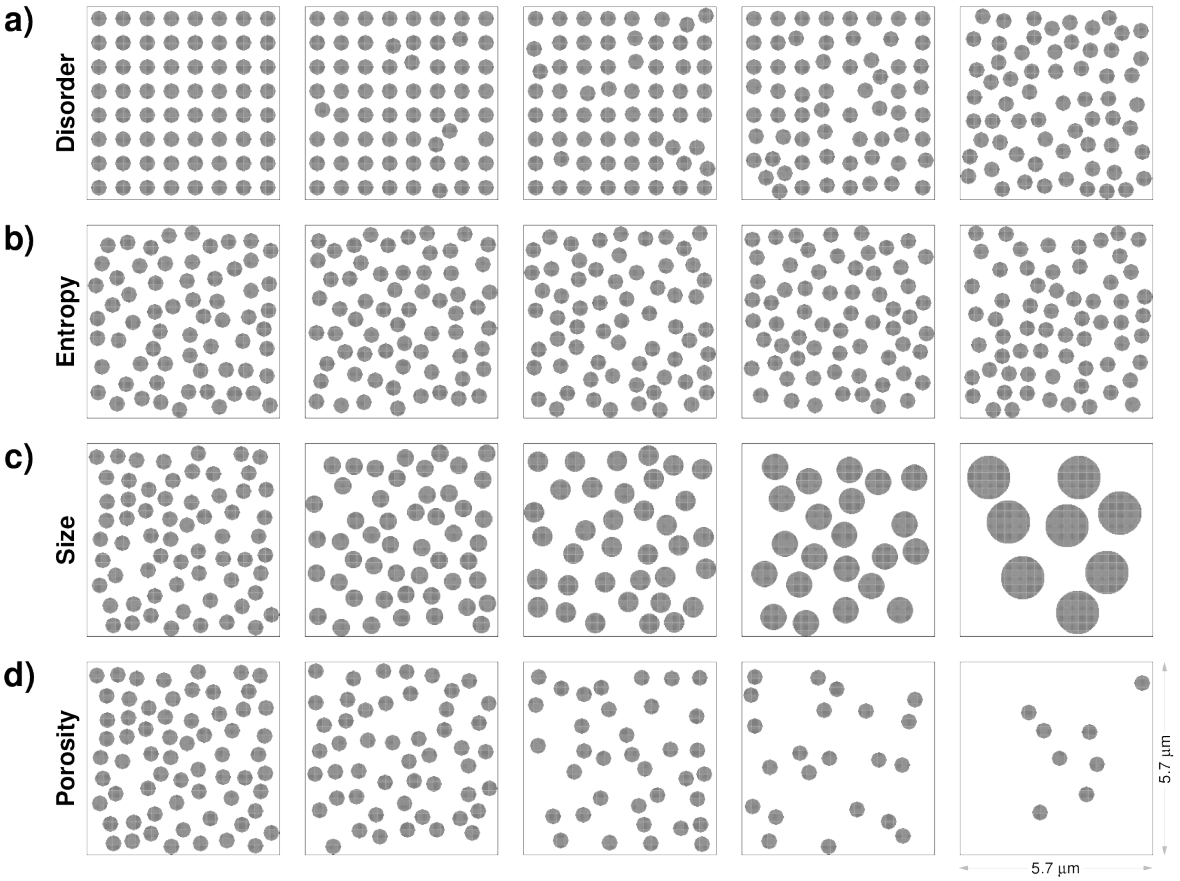

FIGURE 5.1: Designs of two-dimensional PNMs formed by a random distribution of circular geometric objects (obstacles) but without overlapping objects, where the gray regions represent the solid structure and the rest is the pore space (white region). The random PNMs are classified as: **a)** Obstacle disorder variation, **b)** System entropic variation, **c)** Obstacle size variation and **d)** System porosity variation.

and Miranda, 2016). Therefore, physical observables calculated in the microscale using LBM (density, velocity and pressure), may be compared with the macroscopic variables of the Navier-Stokes equations applied to microfluids.

5.3 Methodology

In general, the methodological approach is divided into two stages: **(1)** mathematical-geometric and **(2)** physical-hydrodynamic; both stages are independent topics but correlated with each other according to the main objective of the chapter. Initially, to characterises the randomness of a PNM through Shannon entropy, we performed a statistical analysis on the Voronoi diagram previously generated within the PNM (see Sec. 3.3). Subsequently, we performed a fluid dynamics study to

determine the randomness effect on petrophysical parameters such as tortuosity and permeability of random PNM (see Sec. 3.4). In addition, as an application of the entropic characterisation, we study the variation effect of both the system porosity and the obstacles size on the tortuosity and permeability in PNMs with the same entropic value. The first stage corresponds to the methodology developed in Chap. 3, while the second corresponds to Chap. 2.

5.3.1 Design of PNMs under study

Since our general objective is to study the fluid flow over artificial porous media at the microscale, all designed PNMs have micrometer dimensions. The global domain of the porous system is two-dimensional and has a square shape with a lateral length equal to $L = 5.68\,\mu m$. We introduce circles within the domain as obstacles to fluid flow to emulate a natural porous medium. However, in order not to generate unconnected or isolated regions, the obstacles must have a minimum separation distance equal to or greater than $\Delta \geq 0.09\,\mu m$. That is, for the purposes of our study, the fluid must invade the entire pore network and there should be not empty spaces inaccessible to the fluid. Therefore, the circles size defines the number of obstacles present in the domain, only $N = 64$ circles of radius equal to $r = 0.22\,\mu m$ can be introduced inside the porous domain (see Fig. 3.4a).

For a systematic study of randomness (consequences and applications), we design four different groups of PNMs with five successive cases in each group, as shown in Fig. 5.1. Where, we perform the variation of a parameter without modifying the other system variables: **(a)** obstacles disorder variation, from a perfectly ordered case to a totally disordered case, **(b)** system entropic variation in the totally disordered case, **(c)** obstacles size variation and **(d)** system porosity variation. The first two groups provide ideal environments for characterising and studying the effects of randomness, while the remaining groups are intended for studying other effects in models with a constant entropic value (applications).

The structural design of the PNMs are based mainly on the configuration and geometric characteristics of the obstacles, as described below:

(a) Obstacles disorder variation: The PNMs are designed using $N = 64$ circular obstacles of radius equal to $r = 0.22\,\mu m$, that is, the system porosity and the obstacles size are constant throughout the study process. The system porosity is calculated using the Eq. 3.3 and has a value equal to $\phi = 0.68$ (see

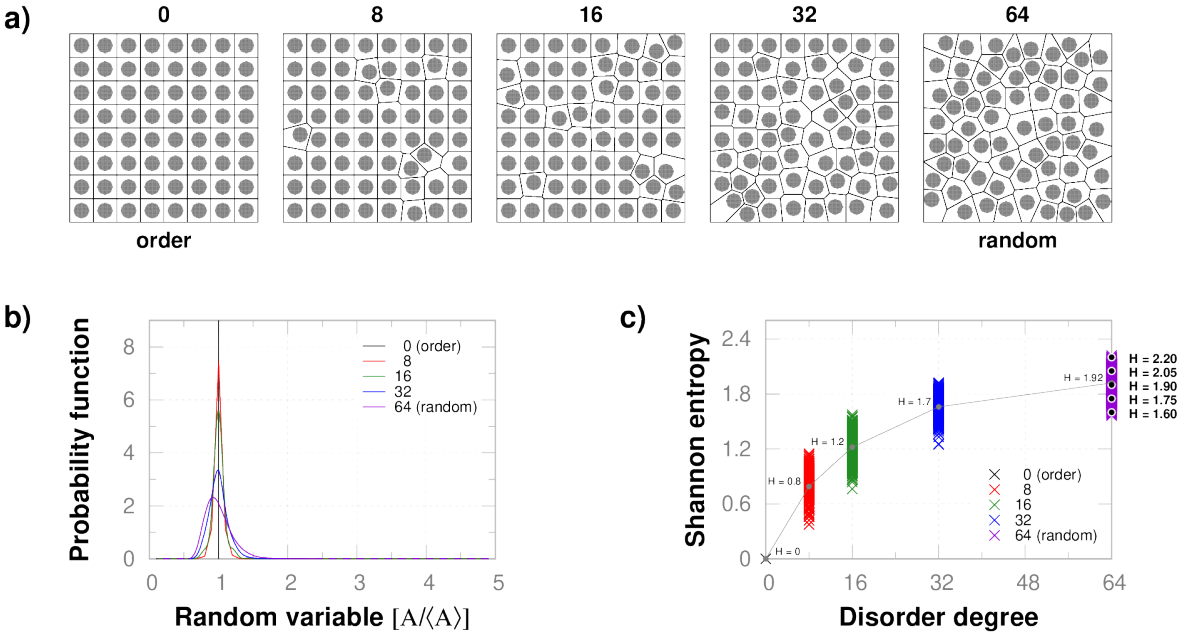

FIGURE 5.2: *Obstacle disorder variation*: Design and statistical analysis of PNMs that present an obstacle disorder in five successive steps. **a)** Voronoi diagrams generated within a PNM. **b)** Probability functions for each disorder degree. **c)** The (averange) Shannon entropy for each disorder degree and its respective spectrum or possible entropy values.

Sec. 3.4). Five types of PNM were designed according to the disorder degree of the obstacles location, where we progressively disorganize an ordered system by randomly locating 0, 8, 16, 32 and 64 obstacles (see, Fig. 5.2a). That is, the ordered system evolves towards a totally random system.

(b) **System entropic variation:** The system under study is the same as the previous case, but focused only on totally random PNMs (see, Fig. 5.2a). We design five random systems with different entropy values $H = 1.60$, 1.75, 1.90, 2.05 and 2.20 following the methodology developed for the characterisation of PNMs (see Sec. 3.3). The possible entropic values of a random PNM formed by 64 circles are between $1.55 < H < 2.25$ approximately, the average value obtained is equal to $H = 1.92$. Therefore the five chosen entropic values cover the possible spectrum (see Fig. 5.2c).

(c) **Obstacles size variation:** To vary the size of the obstacles but without modifying the system porosity and entropy, we designed five different PNMs using $N = 64$, 50, 36, 22 and 8 circular obstacles that are located randomly, where the circles radius are $r = 0.22$, 0.25, 0.30, 0.38 and 0.64 μm, respectively (see Fig. 5.3a). The system porosity has a value equal to $\phi = 0.68$ calculated

using Eq. 3.3 (see Sec. 3.4), while the system entropic value is equal to $H = 1.90$ obtained following the methodology of Sec. 3.3. The segmented horizontal black line in Fig. 5.3c indicates the possibility of designing PNMs varying the obstacles size but keeping the *entropy* and porosity of the system constant.

(d) System porosity variation: Similar to the previous case, in order to vary the system porosity but without modifying the obstacles size and the system entropy, we design PNMs using $N = 64$, 50, 36, 22 and 8 circular obstacles that are randomly located, where the system porosity is $\phi = 0.68$, 0.75, 0.82, 0.89 and 0.96, respectively (see Fig. 5.4a), calculated using Eq. 3.3 (see Sec. 3.4). The circles radius is equal to $r = 0.22\,\mu m$, while the system entropic value is equal to $H = 1.90$ obtained following the methodology of Sec. 3.3. As in the previous case, the segmented horizontal black line in Fig. 5.4c indicates the possibility of designing PNMs varying the system porosity but keeping the system *entropy* and obstacles size constant.

Due to the stochastic definition of Shannon entropy (see Sec. 3.3), we perform 1000 different random configurations for each PNM design, which generates a spectrum or possible entropic values of PNM (crosses in Figs. 5.2c−5.4c), where the average represents the entropy of PNM (gray dots in Figs. 5.2c−5.4c). However, if we require a PNM with a certain entropy value, there are the possibility of finding several PNMs that have different random configurations but with the same entropy value (black dots in Figs. 5.2c−5.4c).

5.3.2 Fluid dynamics in PNMs

Having previously defined the PNMs structural configuration, we proceed to performed fluid dynamics studies within the PNMs. The physical system is conformed of a porous structure and a single fluid flowing through the pores, where the PNM structure is montmorillonite clay (MMT) and the fluid is API brine (8% NaCl and 2% $CaCl_2$). Initially, the fluid covers the PNM entire pore space, then, to generate a fluid flow from left to right, the same fluid is injected as a driving force along the PNM left contour, with an injection velocity equal to $v = 0.44\,m/s$.

Since the study of fluid dynamics is at a micrometer scale, we apply LBM simulations based on the Explicit Force method (see Sec. 2.8). Therefore, the methodology requires system physical information such as: density, viscosity and wettability. The required data are presented in Tab. C.1 (see details in App. C) that

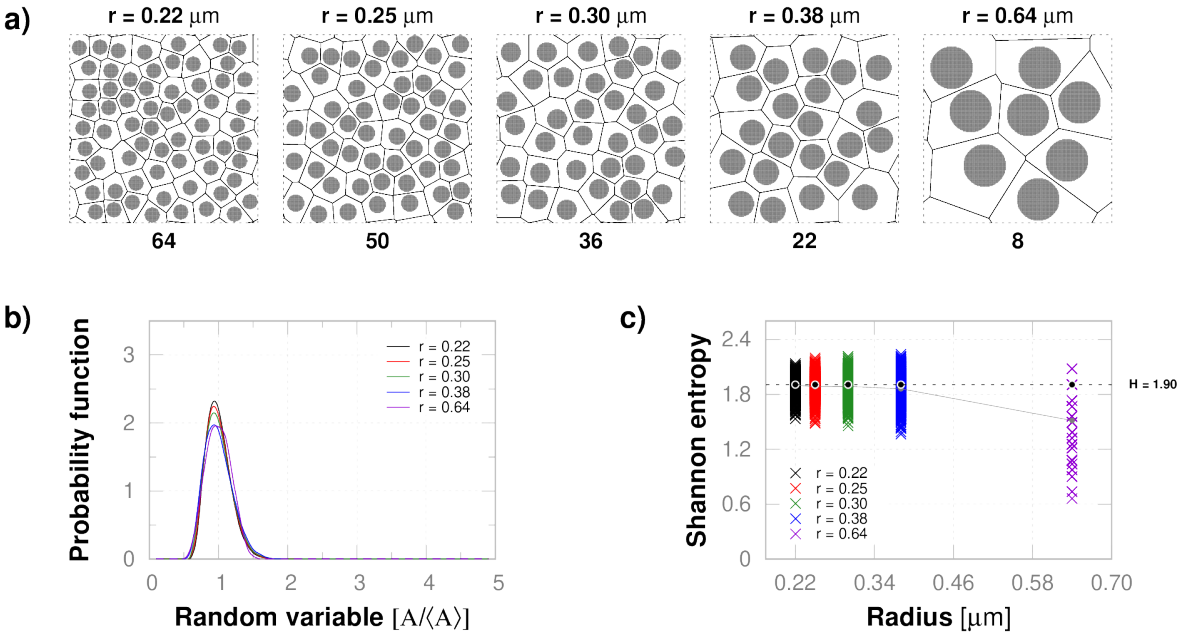

FIGURE 5.3: *Obstacle size variation*: Design and statistical analysis of PNMs formed by obstacles of five different sizes. **a)** Voronoi diagrams generated within a PNM. **b)** Probability functions for each size. **c)** The Shannon entropy of constant value $H = 1.90$ for each size and its respective spectrum or possible entropy values.

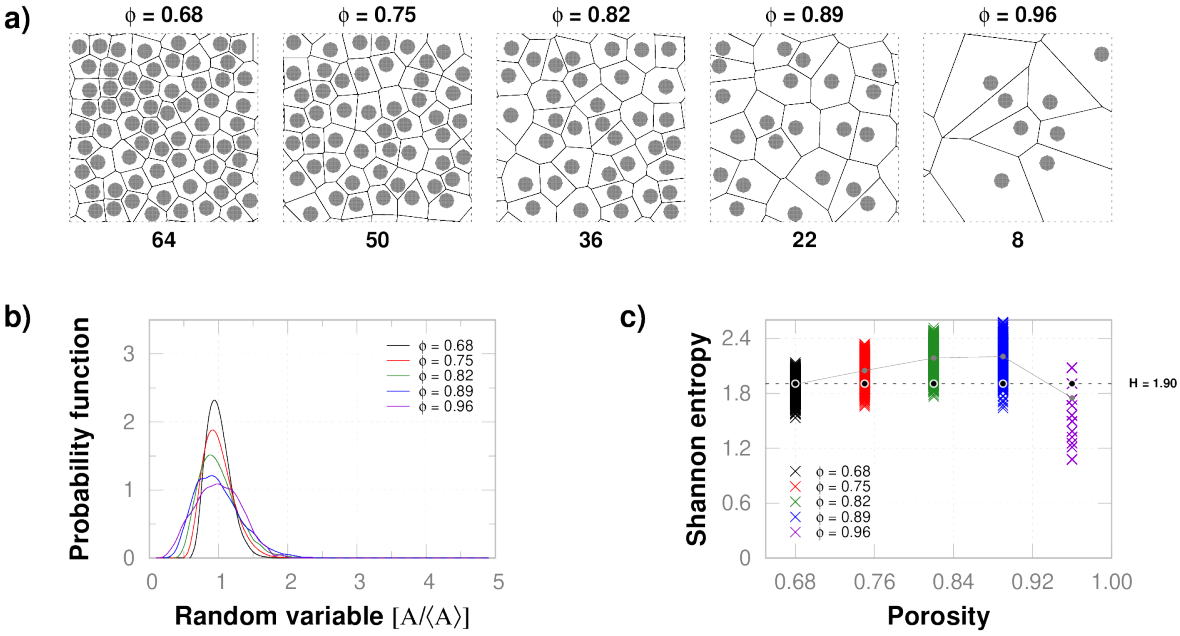

FIGURE 5.4: *System porosity variation*: Design and statistical analysis of PNMs that have five different porosities based on the obstacle number. **a)** Voronoi diagrams generated within a PNM. **b)** Probability functions for each porosity. **c)** The Shannon entropy of constant value $H = 1.90$ for each porosity and its respective spectrum or possible entropy values.

come from the work performed by Pereira (Pereira, Lara, and Miranda, 2016), where the density and viscosity of the fluid are $\rho = 997\,kg/m^3$ and $\nu = 0.791 \times 10^{-6}\,m^2/s$, respectively, while the wettability of the system brine-clay expressed by the contact angle is $\theta = 69^o$. In addition, we also apply the methodology developed by Pereira, which consists of a multiscale hierarchical calculation protocol that combines LBM simulations and data from MD, where the data are mapped as LBM input parameters that are presented in the Tab. C.2 (see details in App. C).

In each fluid dynamics simulation through LBM methodology, we obtain as results the velocity field and the pressure profile of the fluid that are necessary to determine the hydraulic tortuosity and the Darcy permeability of the PNMs, using Eq. 3.4 and Eq. 3.5, respectively. However, since LBM simulations are applied to PNMs designed through stochastic processes (randomly located obstacles), we performed 10 LBM simulations on the same PNM under study that maintains the same parameters but of different random configuration. Therefore, the petrophysical parameters of a PNM come from the average of 10 LBM simulations[1] (see Figs. 5.5–5.8).

5.4 Results

In the geometric part, based on the Voronoi diagram that subdivides a random PNM formed by circles into Voronoi cells (polygons), a statistical analysis is conducted on the area of the polygons to calculate Shannon entropy (refer to Sec. 3.3). To generate the *entropy spectrum*, representing all possible entropy values of the random PNM under study, 1000 configurations of randomly distributed circles were designed while keeping all geometric variables constant. In fact, within the entropy spectrum domain, several different configurations can be generated that share the same entropy value. This phenomenon is analogous to what occurs in Statistical Mechanics, where different molecular kinetic energy configurations of an ideal gas can yield the same temperature value (Pathria and Beale, 2011). In Electromagnetism, different arrangements of spin orientations in a magnetic material can give rise to an identical magnetization vector, a macroscopic parameter. Moreover, the degree of randomness in spin orientation serves to characterize the nature of the magnetic material, distinguishing between diamagnetic, paramagnetic, or ferromagnetic types (Jackson, 2007).

[1] Although there is the possibility of finding more than 10 PNMs of different random configuration but with the same entropic value, the high computational cost of LBM simulations limits us to choosing only 10 PNMs.

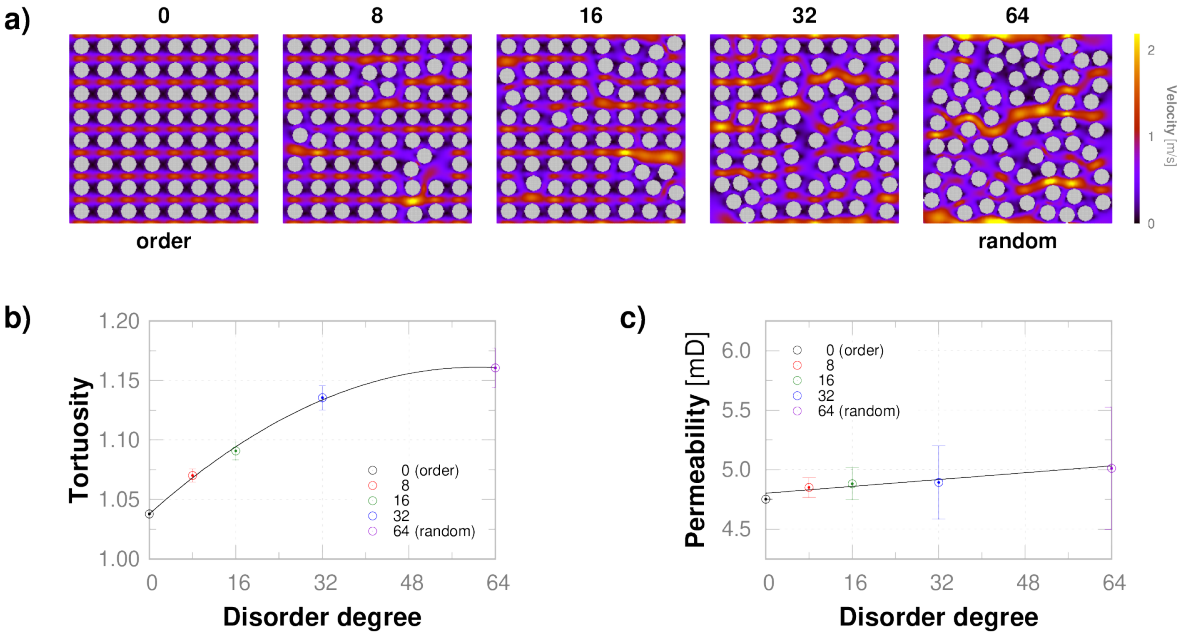

FIGURE 5.5: *Obstacle disorder effect*: Disorder degree effect on fluid dynamics. **a)** Snapshot of the velocity field of the fluid flow at steady state. **b)** Disorder degree effect on the tortuosity of PNMs. **c)** Disorder degree effect on the permeability of PNMs.

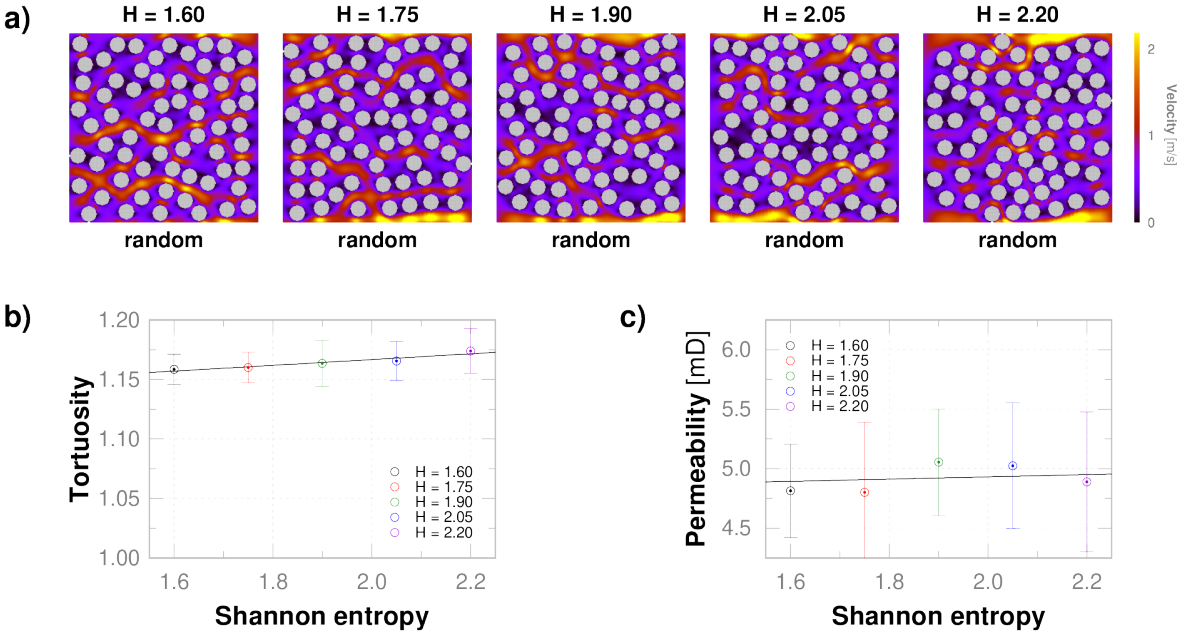

FIGURE 5.6: *System entropy effect*: Entropy variation effect on fluid dynamics. **a)** Snapshot of the velocity field of the fluid flow at steady state. **b)** Entropy variation effect on the tortuosity of PNMs. **c)** Entropy variation effect on the permeability of PNMs.

In the dynamic part, fluid dynamics simulations were conducted using the LBM methodology on random PNMs characterized by a specific entropy value (refer to Sec. 3.3). From the entropy spectrum, 10 random PNMs with different configurations that share the same entropy value were selected. In other words, for each random PNM identified by its entropy value, 10 fluid dynamics simulations were conducted. Consequently, since the velocity field and pressure profile describe fluid dynamics, the hydraulic tortuosity and Darcy permeability of a random PNM represent the average values obtained from 10 different random configurations (refer to Sec. 3.4).

The results obtained in this chapter can be categorized into two main parts. Initially, the random effect on fluid dynamics is verified in two successive stages: first by increasing the degree of disorder among the obstacles, and then by varying the system's entropy when the obstacles are completely disordered (refer to Fig. 5.5 and Fig. 5.6 respectively). Secondly, to evaluate the influence of other parameters such as obstacle size and system porosity, random PNMs with identical entropy values are employed (refer to Fig. 5.7 and Fig. 5.8 respectively).

a) **Obstacles disorder effect:** The effects of the degree of disorder on tortuosity and permeability are studied in PNMs with identical porosity ($\phi = 0.68$) and obstacles of the same size ($r = 0.22\,\mu m$). With regard to the porous structure, an increase in the disorder of the obstacles from 0, 8, 16, 32 to 64 predictably results in an increase in the entropy value of the PNM under study, from $H = 0$, 0.81, 1.22, 1.65 to 1.92 respectively. This implies that the perfectly ordered case has an entropy value of zero, whereas the completely disordered case has a value equal to 1.92, as show Fig. 5.2. Regarding fluid dynamics, the velocity field demonstrates that increasing the disorder among the obstacles leads to the generation of more intense regions (see Fig. 5.5a). This implies that disorder leads to greater tortuosity in the flow, owing to the disordered collision between the fluid and obstacles (see Fig. 5.5c). However, disorder leads to higher permeability because the velocity is greater when the flow circumvents disordered obstacles compared to ordered ones (see Fig. 5.5b).

b) **System entropy effect:** The system under study is the same as in the previous case but focused solely on the completely random PNM. Five random PNMs was designed with uniformly spaced entropy diferent values covering the entire entropy spectrum, where the central value ($H = 1.90$) is close to the average value ($H = 1.92$), as shown in Fig. 5.2 c. Then, the effects of increasing entropy on tortuosity and permeability are analyzed in random PNMs. Regarding

tortuosity, Fig. 5.6b shows a tendency to increase as observed in the previous case, but to a lesser extent. Conversely, permeability does not exhibit significant changes with increasing entropy, as show Fig. 5.6c.

c) **Obstacles size effect:** The effects of altering obstacle size on tortuosity and permeability are studied in PNMs with the same porosity value ($\phi = 0.68$) and identical entropy values ($H = 1.90$). To maintain constant porosity and increase the size of the obstacles from $r = 0.22$, 0.25, 0.30, 0.38 to $0.64\,\mu m$, $N = 64$, 50, 36, 22, and 8 obstacles are used in the design, respectively (refer to Fig. 5.3a). Meanwhile, for entropy, configurations with the same entropy value are selected from the spectrum. Fig. 5.7 represents tortuosity and permeability as a function of size (circle radius), and the results indicate that as the size of the obstacles increases, the PNM becomes more tortuous and permeable, as show Fig. 5.7b and Fig. 5.7c, respectively. However, the permeability is more affected compared to the previous cases.

d) **System porosity effect:** The effects of varying the system's porosity on tortuosity and permeability are studied in PNMs with obstacles of the same size ($r = 0.22\,\mu m$) and identical entropy values ($H = 1.90$). To increase the system's porosity from $\phi = 0.68$, 0.75, 0.82, 0.89 to 0.96, $N = 64$, 50, 36, 22, and 8 obstacles of the same size are used in the design, respectively (see Fig. 5.4a). Meanwhile, for constant entropy, configurations with the same entropy value are selected. Regarding the results, tortuosity demonstrates a tendency to decrease towards its minimum value ($\tau = 1$) as the system's porosity increases towards its maximum value ($\phi = 1$), as illustrated in Fig. 5.8b. Meanwhile, permeability increases dramatically and is more affected than in all previous cases, as shown in Fig. 5.8c.

In summary, the quantification the randomness of the circles comprising a PNM using a geometric parameter as Shannon entropy, allows for the study of the variation in other physical parameters such as tortuosity and permeability that are related to fluid dynamics. In other words, Shannon entropy can infer how tortuous or permeable a random PNM can be. However, the most significant result is that Shannon entropy can be considered as a parameter that characterizes the randomness of a PNM, at the same level as porosity, tortuosity, and permeability parameters, which define the PNM. In this context, different random configurations of obstacles can yield the same values for porosity, tortuosity, permeability, and entropy. Analogously to what occurs within an ideal gas in Statistical Mechanics, different molecular configurations related to

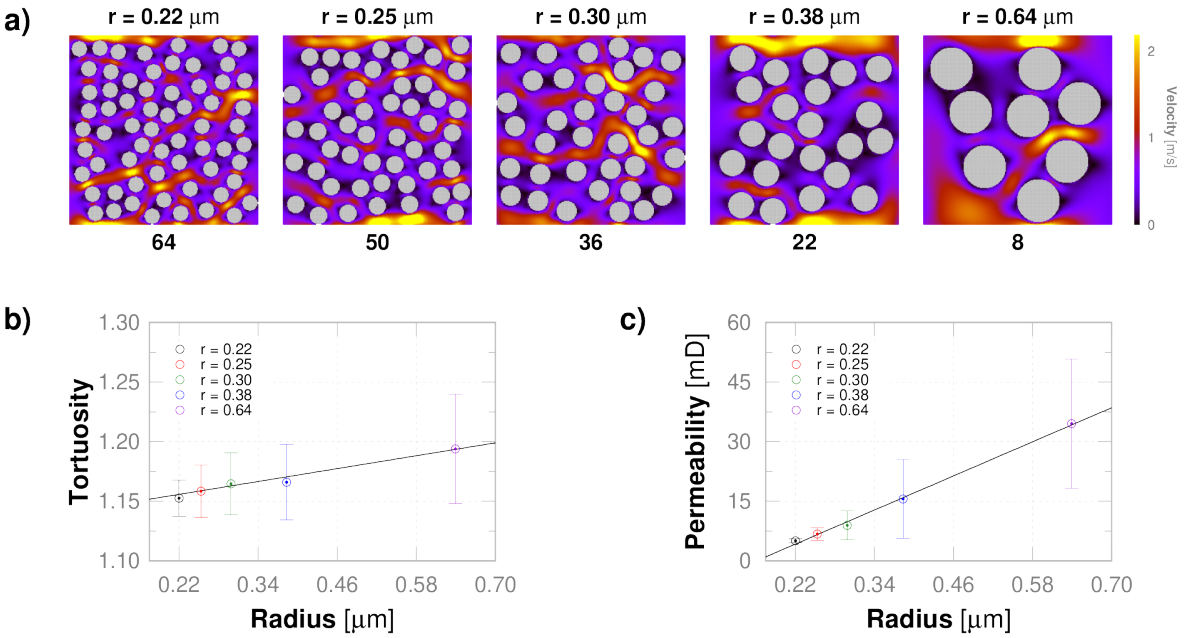

FIGURE 5.7: *Ostacle size effect*: Size variation effect on fluid dynamics. **a)** Snapshot of the velocity field of the fluid flow at steady state. **b)** Size variation effect on the tortuosity of PNMs. **c)** Size variation effect on the permeability of PNMs.

kinetic energy can yield the same values of temperature, pressure, volume, and entropy, which are macroscopic variables defining the ideal gas. Similarly, in Electromagnetism, various configurations of spin orientations within a magnetic material can generate the same magnetization vector.

5.5 Conclusions

In this chapter, with objetive to investigate the effect of randomness in hydrophilic porous media on fluid flow, computationally designed PNMs consisting of small circles were created. Then, to obtain the Shannon entropy of a PNM, a strictly geometric-statistical analysis was conducted on the Voronoi diagrams generated within the PNMs. The obtained entropy value is unique and contains essential information about the randomness of the pores, which is decisive in fluid dynamics studies. The study determined that the degree of tortuosity and the level of permeability of a PNM is closely related to the entropic information. Specifically, an essentially geometric feature like Shannon entropy can infer (or predict) how tortuous or permeable a hydrophilic PNM can be for fluid flow. Moreover, the study concludes that the Shannon entropy of a random PNM can be equally significant as the petrophysical parameters of porosity,

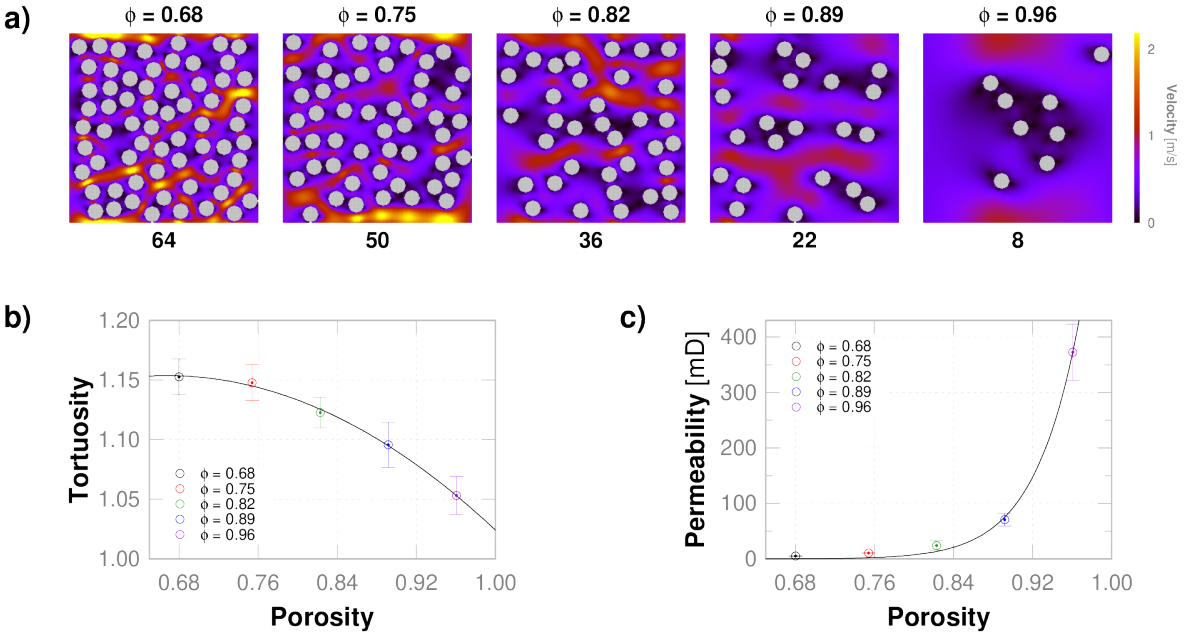

FIGURE 5.8: *System porosity effect*: Porosity variation effect on fluid dynamics. **a)** Snapshot of the velocity field of the fluid flow at steady state. **b)** Porosity variation effect on the tortuosity of PNMs. **c)** Porosity variation effect on the permeability of PNMs.

tortuosity, and permeability. This significance arises from the fact that the entropy parameter is the sole quantifier of the degree of randomness in a PNM.

Chapter 6

Randomness Effect of the PNMs on Oil Recovery

Abstract

Here, our primary goal is to determine the relationship between the morphology-topology of the porous media at the micrometer-scale and the oil-trapped quantity in rocks after fluid injection. The physical properties such as interfacial tension and wettability at the water-petroleum-rock interfaces, should be understood to estimate the amount of crude petroleum that could be extracted from natural deposits. Additionally, petrophysical information of the porous media is crucial, especially the shape, porosity, and pore distribution and their effects on the oil displacement due to the brine injection process. In the previous chapter (see Chap. 5), we desinged and characterised two-dimensional random PNMs through Shannon entropy to study the random effect on fluid dynamics (single fluid). In this chapter, starting from the PNMs designed in the previous chapter, we investigate the correlations between the oil displacement process and the entropic information of the random PNMs, using a hierarchical protocol that combines the LBM simulations and data from MD (two fluids). We consider the brine-oil-clay interfaces, where brine and oil are the injected and extracted fluid, respectively, while clay constitutes the PNMs structure. Thus, in this work we explore oil recovery in four cases: varying circles order, system entropy, circles size, and system porosity, while keeping the other parameters constant. Our results show that entropic information is directly related to the oil-trapped quantity; that is, a high degree of randomness can capture more oil, while size variation does not produce significant changes, and a reduction in porosity means more oil capture. In conclusion, a purely physical process such as the oil-trapped quantity can be inferred from an essentially geometric characteristic, such as the morphology-topology of the porous media quantified by Shannon entropy.

6.1 Introduction

The first petroleum global crisis in 1973 (and the second in 1979) sparked a significant research effort to develop new efficient methods/studies for oil recovery from natural reservoirs. On average, 5 to 25% of the total existing oil in the reservoir can be recovered by natural depletion (pressure gradients), whereas 10 to 20% more oil can be extracted by water flooding, gas injection or thermal processes (Kemper, 2020). The remaining fraction is the target of the new methods/studies and is mainly associated with the residual petroleum adsorbed on the rocky surface or trapped in the microchannels of the reservoir (Amirpour et al., 2015). In this context, understanding rock material's wettability mechanism and porous structural morphology is paramount to estimating the amount of crude petroleum in underground resources (Morrow, 1990).

The capillary phenomena, interfacial tension and wettability are determining factors in diverse natural processes, microfluidics technology or petroleum industries, such as, atmospheric carbon sequestration, Lab-on-a-chip design or enhanced oil recovery, respectively (Robin, M., 2001). Specifically, the degree of wettability of the porous material has a significant and dramatic impact on the displacement of fluids over the porous structure channels, such as oil extraction by water invasion, where the wetting characteristics of the walls and the interfacial tension of the fluids involved play a crucial role (Du Plessis and Masliyah, 1988). Although the quantification and efficiency of petroleum extraction are closely related to wettability, the physics involved at pore-scale of immiscible fluids moving within porous media is not fully understood (Iglauer et al., 2012).

Another critical problem in the physics of porous media is to understand/describe the delay experienced by the fluids flow when going through the internal pores network, that is, the obstruction to the flow due to the porous structure (Liang et al., 2018). There is a need to understand/describe the extraction process of the captured petroleum, mainly due to the geometric shape of the porous structure, which is beyond wettable physical properties (Liu et al., 2023). To describe the properties of a porous structure related to its ability to delay flow or capture fluids, an alternative commonly used in the literature is to characterise the porous medium through petrophysical parameters such as porosity, permeability or tortuosity among others (Rao, Kuznetsov, and Jin, 2020). However, since there is an inherent randomness in the pore network structure of a natural porous medium, the mentioned parameters cannot explain the delay/capture due to the complex structure.

Natural reservoirs can be computationally emulated using PNMs, which are commonly constructed through a random distribution of circular or spherical geometric obstacles. These PNMs are used to study the petroleum extraction process from underground resources. In Chap. 4, we performed studies on PNMs designed by diverse types of obstacles located in an orderly and randomly but keeping the porosity constant. In the first case, the results showed that circular obstacles and circles with a larger radius delay the fluids flow, but all ordered PNMs showed 100% petroleum extraction. However, random PNMs constructed by smaller circles showed an average recovery of only 90% with the remaining 10% permanently trapped within the porous medium (Suxo and Miranda, 2017). The last result motivates the study of Chap. 5 that characterises random PNMs through Shannon Entropy, then adresses the flow delay (a single fluid) through tortuosity/permeability in random PNMs designed with the same entropic value.

In this chapter, we study the petroleum extraction process on random PNMs characterized in the previous chapter using entropy-based design (see, Chap. 5). Specifically, we determined the relationship between the degree of randomness of the PNMs (quantified by Shannon entropy) and the amount of petroleum that can be extracted or the percentage of petroleum trapped inside the PNM. Subsequently, we study the extraction of petroleum as a function of the system porosity and obstacles size, but we keep the system entropy (and other parameters) constant in both cases. For this objective, we apply a multiscale hierarchical protocol that simulates multicomponent fluids at the micrometer scale using the LBM methodology, in combination with data or physical parameters that come from nanometer dimensions of the MD (see Chap. 2). The physical system contemplates the brine-oil-clay interfaces, where brine and oil are the injected fluid and extracted fluid, respectively, while clay constitutes the PNMs.

6.2 Methodology

In general, this study was motivated by the results obtained in Suxo's *et al.* work (Suxo and Miranda, 2017), and is based on the previous two chapters, Chap. 4 and Chap. 5. The first chapter qualitatively demonstrated that random PNMs tend to trap oil in oil recovery processes, while the second chapter quantified the randomness of various types of PNMs using an entropic value. Therefore, in this chapter, our primary focus is on examining the relationship between the system's entropic value

and the quantity of oil trapped in the pores. All the PNMs studied in this chapter were introduced in Chap. 5 (refer to Fig. 5.1).

According to the entropic value of the PNMs, the study is divided into two parts: **(1)** PNMs with diverse entropic values and **(2)** PNMs that maintain the constant entropic value. The first part has two cases: **(a)** progressive disordering of the obstacles from an ordered state to a totally disordered state and **(b)** system entropic variation in a totally disordered state; in both cases the obstacles size and the system porosity are constants. The second part also has two cases: **(c)** obstacles size variation but keeping the system porosity and entropy constant and **(d)** system porosity variation but keeping the obstacles size and the system entropy constant (see details, Fig. 5.1).

Once the geometric structural configuration of the PNMs has been defined, the global system formed by the brine-clay-oil interfaces is subjected to the following mathematical conditions. As an initial condition, the oil covers the entire pore space of the PNM at steady state (zero velocity). As a primary boundary condition, the brine velocity has a constant value in the left boundary, emulating a brine injection or driving force for displace oil from PNM. Meanwhile, the upper-lower contours are modelled as periodic boundary conditions, and the right boundary is free concerning the velocity.

6.3 Oil recovery from random PNMs

When the oil recovery process is on a micrometer scale like the rock pore dimensions of a natural reservoir, LBM simulations are ideal for addressing interfacial tension between fluids and wall wettability. Because both capillary properties are modelled as fluid-fluid and fluid-solid microscopic interactions within the Explicit Force method exposed in Sec. 2.8 (Porter et al., 2012). In addition, the method has specific free software called Taxila-LBM (Coon, Porter, and Kang, 2014). Thus, we apply the multiscale hierarchical calculation protocol developed by Pereira that combines LBM simulations and input data from MD (Pereira, Lara, and Miranda, 2016).

Random PNMs of clay form the physical system that emulates a natural reservoir (MMT: Montmorillonite), with brine (API: 8% NaCl and 2% $CaCl_2$) as injected fluid and oil (light model) as displaced fluid. The data of the physical system are presented

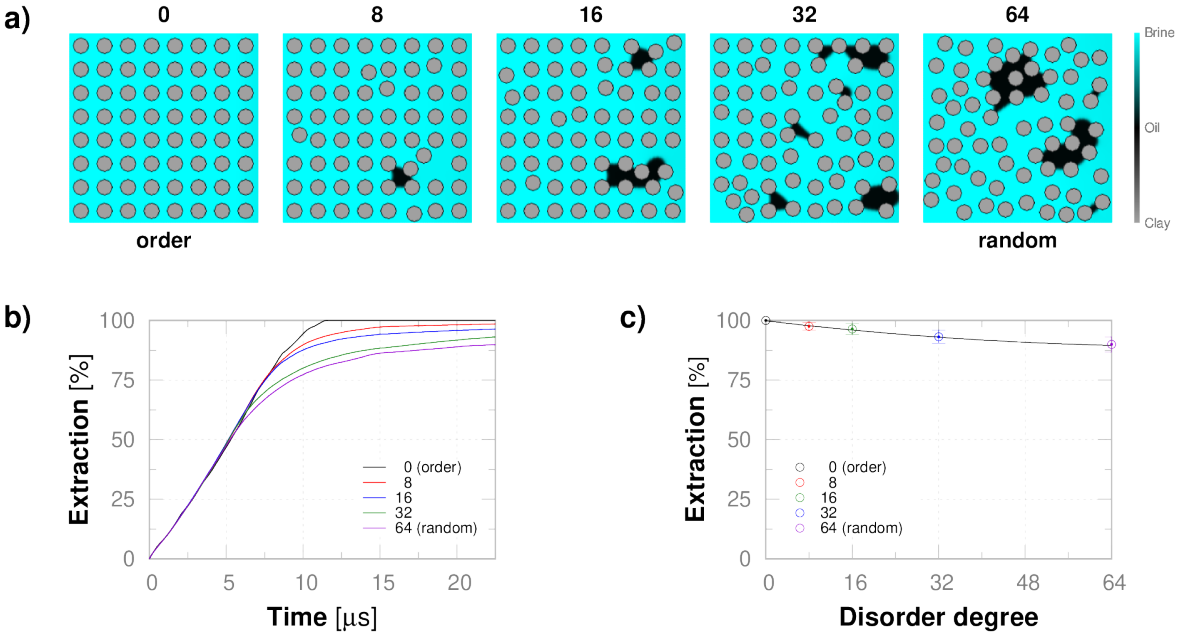

FIGURE 6.1: *Obstacle disorder effect*: Disorder degree effect on oil recovery process. **a)** Final snapshot of the oil recovery process. **b)** Percentage of oil extracted as a function of time. **c)** Relationship between the percentage of oil extracted and the disorder degree.

in Tab. C.1 that come from Pereira's *et al.* work (Pereira, Lara, and Miranda, 2016), where the densities and viscosities of brine and oil are: $\rho_b = 997\,kg/m^3$, $\rho_o = 810\,kg/m^3$ and $\nu_b = 0.791 \times 10^{-6} m^2/s$, $\nu_o = 4.473 \times 10^{-6} m^2/s$, respectively, while the interfacial tension and wettability (contact angle) are: $\gamma = 0.043\,kg/s^2$ and $\theta = 69°$, respectively. In the simulations, an injection velocity equal to $v = 0.44\,m/s$ is applied to the system and the physical data mapped as input simulation parameters are presented in Tab. C.2 (see details in App. C).

In a fluid flow simulation using LBM, we obtain the density of the injected and displaced fluid, the flow velocity field and the system pressure profile. From the density data of the fluids in the PNM, we perform calculations of the percentage of oil recovered or the percentage of oil captured by the PNM. Nevertheless, since the scenario of the LBM simulations is PNMs designed through stochastic processes (randomly located obstacles), we necessarily perform several LBM simulations but in different configurations of the same PNM under study. The percentage of recovered oil is calculated using the average of several LBM simulations. Although there is the possibility of finding many configurations of the same PNM model, the high computational cost of LBM simulations limits us to choose only ten.

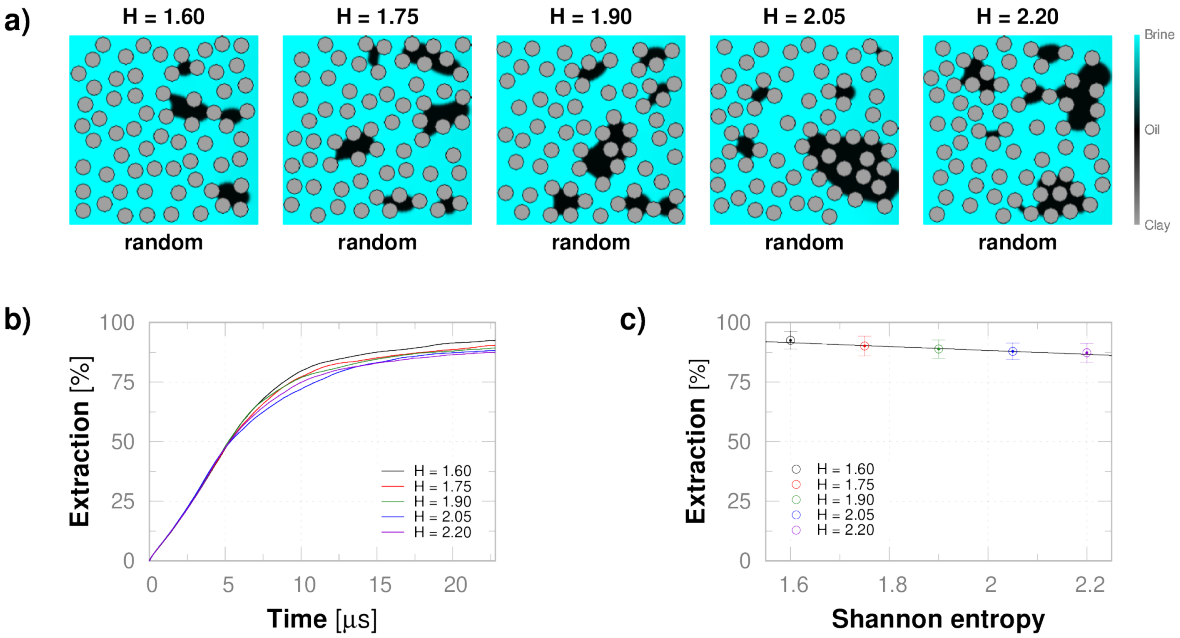

FIGURE 6.2: *System entropy effect*: Entropy variation effect on oil recovery process. **a)** Final snapshot of the oil recovery process. **b)** Percentage of oil extracted as a function of time. **c)** Relationship between the percentage of oil extracted and the system entropy.

6.4 Results

The results of the oil recovery process applied to a random PNM are divided into two parts, depending on whether the entropy of the PNM is variable or constant. All the random PNMs under investigation were introduced in Chap. 5 to study the effect of randomness on fluid dynamics (refer to Fig. 5.1). At first, the influence of randomness on oil recovery is examined in two consecutive stages: **a)** increasing the disorder of the obstacles from perfect order to complete disorder, and then **b)** varying the system's entropy in the fully disordered scenario (refer to Fig. 6.1 and Fig. 6.2 respectively). Secondly, to evaluate the influence of other parameters such as **c)** obstacle sizes and **d)** system's porosity, random PNMs with identical entropy values are employed (refer to Fig. 6.3 and Fig. 6.4 respectively).

(a) Obstacles disorder effect: The effect of disorder on the oil recovery process is verified, in PNMs with identical porosity ($\phi = 0.68$) and composed of circular obstacles of the same size ($r = 0.22\,\mu m$). The results from Fig. 6.1 show a decrease in the percentage of recovered oil as the obstacles in the PNM become disordered. Fig. 6.1c indicates that in the perfectly ordered PNM, 100% of the oil is recovered, while in the completely disordered PNM, approximately 90% is recovered. In other words, approximately 10% of the oil

remains permanently trapped in fully disordered cases. Fig. 6.1b confirms the permanent confinement of a certain percentage of oil, in PNMs with obstacles exhibiting some degree of disorder. Only the curve of the perfectly ordered PNM reaches 100%, while the other curves follow a horizontal trend before reaching 100% (see Fig. 6.1b). Although the almost-horizontal curves could eventually reach 100%, the time required for practical purposes is infinite.

(b) System entropy effect: In this stage, the study focuses on examining the effect of entropy variation on oil recovery processes, in completely disordered PNMs from the previous stage. The results from Fig. 6.2 show a decrease in the percentage of recovered oil as the entropy of the PNM increases. Fig. 6.2c indicates that in the PNM with lower entropy, approximately 93% of the oil is recovered, while in the PNM with higher entropy, approximately 88% is recovered. This implies that within a fully disordered PNM with maximum entropy, the quantity of trapped oil can potentially reach around 15%. Fig. 6.2b shows oil confinement in all cases, where all the curves become horizontal before reaching 100%, as in the previous stage.

(c) Obstacles size effect: The effect of varying the size (circular obstacles) on the oil recovery process is studied in PNMs with the same porosity ($\phi = 0.68$) and identical entropy ($H = 1.90$). The results from Fig. 6.3 show that the percentage of recovered oil is not significantly affected by the variation in the size of the obstacles comprising the PNM. The recovery of 89% of oil remains nearly constant in all five cases (see Fig. 6.3c). Similar to the previous cases, Fig. 6.3b shows oil confinement in random PNMs, which in this case confines approximately 11% of oil.

(d) System porosity effect: The effect of varying porosity on the oil recovery process is studied, in PNMs with obstacles of the same size ($r = 0.22\,\mu m$) and identical entropy value ($H = 1.90$). Overall, the results from Fig. 6.4 show a slight increase in the percentage of oil recovery as the porosity of the PNM increases. However, the extraction percentage increases dramatically when the porosity is approximately 0.85, similar to the behavior of a step function that divides the results into two nearly horizontal regions: 89% and 97%, respectively (see Fig. 6.4c). This unique behavior in Fig. 6.4c is due to the maximum entropy value occurring when the porosity is approximately 0.85 (refer to Fig. 5.4).

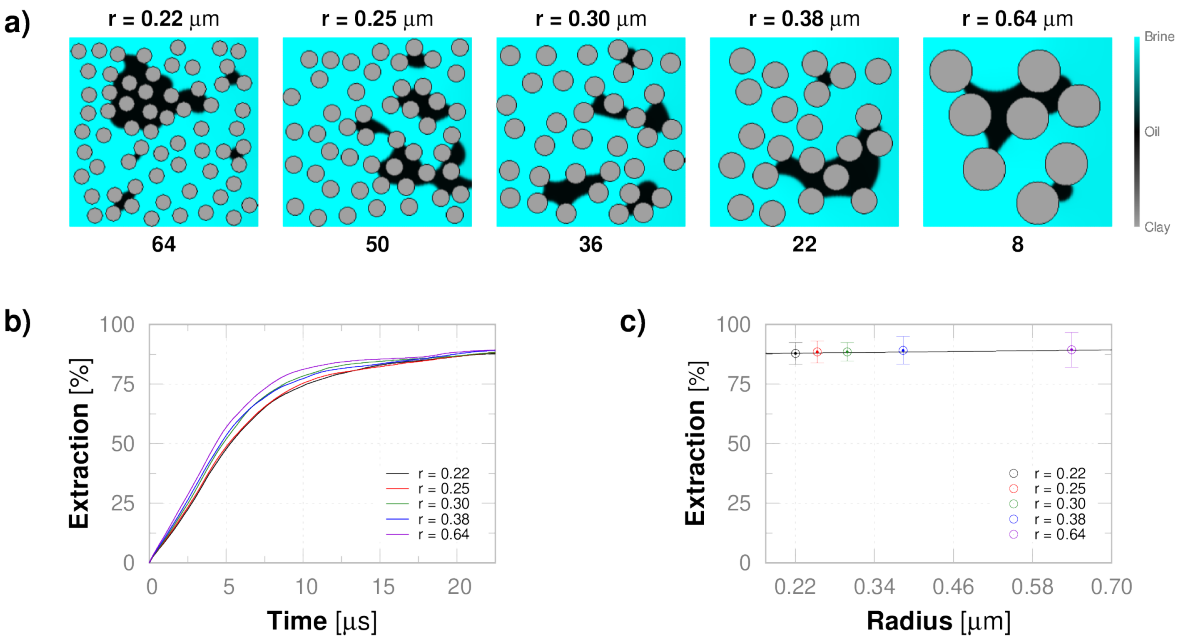

FIGURE 6.3: *Ostacle size effect*: Size variation effect on oil recovery process. **a)** Final snapshot of the oil recovery process. **b)** Percentage of oil extracted as a function of time. **c)** Relationship between the percentage of oil extracted and the obstacle size.

The confinement of oil within random PNMs is primarily a consequence of the complex and unpredictable nature of the pore structure. In these media, pore sizes, shapes, and connectivity vary randomly, leading to irregular fluid pathways. Capillary forces, driven by the interplay between fluid surface tension, wettability of the surfaces, and the size of the pores, play a crucial role in this entrapment. When oil encounters such a porous environment, capillary forces can become dominant. If the capillary forces are strong enough, they can prevent oil from moving freely through the pores. This can occur when the pore sizes are on the order of the capillary length scale, causing oil to be retained within smaller pores or isolated pockets. While the material of the random PNMs under investigation is hydrophilic, which facilitates the extraction of oil, the randomness of the PNM combined with the brine-oil-clay interfacial forces can permanently confine oil.

6.5 Conclusions

In Chap. 5, it was determined that the Shannon entropy value of a PNM is unique and contains information about the randomness of the pores, which is crucial in fluid dynamics studies. In this chapter, it was observed that the oil recovery process is also closely related to entropic information. Specifically, a fundamentally geometric

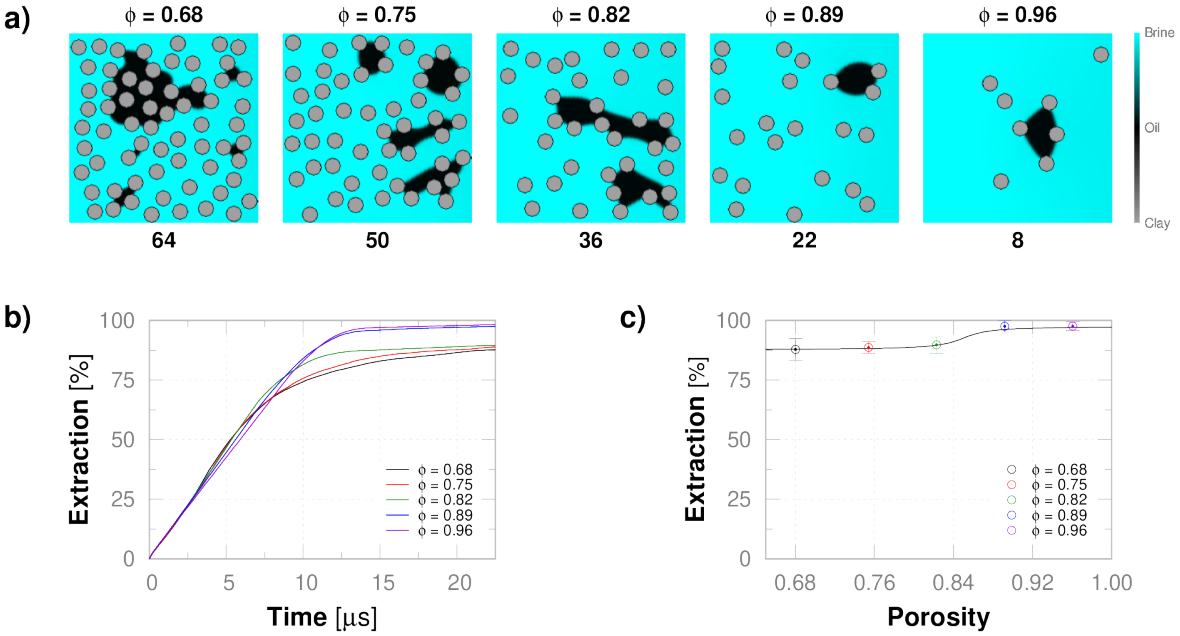

FIGURE 6.4: *System porosity effect*: Porosity variation effect on oil recovery process. **a)** Final snapshot of the oil recovery process. **b)** Percentage of oil extracted as a function of time. **c)** Relationship between the percentage of oil extracted and the system porosity.

characteristic like the entropy of a PNM can infer or predict the amount of oil that remains permanently trapped within the PNM. In our study, the randomness of a hydrophilic PNM formed by 64 small circles randomly distributed has the capacity to trap oil in the range of approximately 7.5% and 12.5%.

Chapter 7

Effects of Heterogeneity Porous Media on Oil Extraction

Abstract

Capillary phenomena become predominant at the micrometer scale and have a dramatic impact on the displacement of fluids in porous media, such as fluid dynamics studies (single fluid) or petroleum recovery processes (multicomponent). Especially, in porous rocks or artificial devices formed by heterogeneous microchannels of different wettability. Depending on the degree of wettability and heterogeneity of the walls, the fluids flow can be retarded and/or confined in the micropores. The LBM methodology in combination with the Explicit Force method is ideal for addressing multicomponent flows in heterogeneous porous media. Because physical parameters such as the interfacial tension between fluids and the wettability of the porous surface can be incorporated as microscopic interaction mechanisms. In this chapter, LBM simulations are performed to study the tortuosity, permeability and oil recovery of heterogeneous PNMs that possess extreme wettable characteristics: hydrophobic and hydrophilic. The physical data of the system under study, such as: density, viscosity, interfacial tension and wettability, come from a previous experimental work that are mapped as input parameters in our LBM simulations. The results show that PNMs with hydrophilic surfaces are more tortuous and less permeable than hydrophobic ones. In relation to oil recovery, hydrophilic PNMs facilitate extraction, while hydrophobic ones tend to obstruct the process.

7.1 Introduction

The wettability phenomenon is critical factor in numerous natural processes and industrial operations, encompassing oil extraction, carbon dioxide sequestration, PDMS microfluidic chip, biomedical devices, chemical manufacturing, oil & gas pipelines, mineral processing, soil mechanics, environmental cleanup and various other applications (Zhang, Liu, and Jiang, 2019). Specifically, when dealing with the immiscible liquid displacement within porous materials, significantly influences the effectiveness of the displacement process (Anderson, 1987). For example, the wettability of reservoir rocks affects how easily oil can be displaced by water or other fluids. Rocks with favorable wettability for oil (oil-wet) tend to retain oil, making it difficult to recover. Adjusting the wettability can improve oil recovery rates (Jadhunandan and Morrow, 1995).

The effect of wettability on immiscible fluids flow within porous media arises directly from the complex pore-scale physics. The progressive infiltration of the pores is a direct function of the viscosity ratio between the displaced and invading phases, the interfacial tension between the fluids and the degree of wettability of the walls (Berg, 1993). Fluid flow is within the laminar regime similar to an infinitesimally driven piston, where one phase is pushed completely by the other and the displaced liquid can leave a thin film on the wall (wall-wet). When capillary forces are stronger than viscous, the thin film adhered to the wall forms a fluidic ring that interrupts the flow, the event is called rupture (Sarr, 1983). In addition to the complexity of oil displacement via water injection, the non-uniform nature of reservoir wettability properties further complicates the analysis (Robin, M., 2001).

Experimental results about immiscible fluids flow within simple microfluidic devices indicate that porous media with hydrophilic characteristics can improve oil recovery. The quantity of the displaced fluid increases when the porous medium is wetted by the invading fluid. Wu *et al.* designed a random network of micrometric straight channels to analyze the effect of wettability and homogeneity of the pores (Wu et al., 2012). The report indicates that oil displacement was greater in hydrophilic devices. Lee *et al.* implemented the fabrication of microfluidic devices with heterogeneous wetting characteristics. The report shows that heterogeneity generates trapped oil ganglia. If the percentage of hydrophilic surface is increased, the quantity of trapped oil is lower (Lee, Lee, and Doyle, 2015). Trojer *et al.* demonstrated that increasing the wettability of the porous medium leads to a more effective displacement (Trojer,

Szulczewski, and Juanes, 2015).

Incorporating wettability into LBM involves introducing modifications to the traditional LBM algorithm to consider fluid-solid interactions within porous media. Models should describe how different wetting properties affect the interaction between particles (homogeneous or heterogeneous) and solid surfaces (Tian and Qiu, 2022). Just as interfacial tension should be described as fluid-fluid interactions that occur between heterogeneous particles at the fluidic interface (Ansarinasab and Jamialahmadi, 2016). Some models can introduces wettability by specifying appropriate boundary conditions at the solid-fluid interfaces. For example, if a surface is hydrophobic, you might use a slip boundary condition to mimic the reduced interaction between the fluid and the solid (Akai, Bijeljic, and Blunt, 2018). Others can modify the collision operator to account for wettability effects. This might involve introducing additional terms in the collision step that account for the interaction between the fluid and solid surfaces, which depends on the wetting properties (Yang et al., 2022).

In contrast to the previous chapters that use computational simulations data in the LBM, this chapter employs experimental measurements data (Avendaño et al., 2019). The data consist of water and oil as the invading and displaced phases respectively, in porous media with extreme wettability characteristics: *hydrophobic* and *hydrophilic*. In general, the oil recovery process in hydrophobic, hydrophilic, and heterogeneous PNMs is studied, using LBM simulations following the methodology developed in Chap. 2. Specifically, the effect of heterogeneity on oil recovery is studied, in heterogeneous PNMs composed of hydrophobic and hydrophilic fractional parts.

7.2 Methodology

Wettability refers to the interaction mechanism of fluids in contact with solid surfaces, which can significantly affect flow displacement and interfacial tension in narrow channels. Its incorporation into the LBM can add complexity to the simulations depending on the nature of the problem being modeled. The Explicit Force model presented in Sec. 2.8, considers capillary effects to address multicomponent or multiphase flows in heterogeneous porous media (Porter et al., 2012). The model has its own software called Taxila-LBM to computationally emulate oil recovery from reservoirs (Coon, Porter, and Kang, 2014).

EXPERIMENTAL MEASUREMENTS DATA[a]						
Glass	**Water**		**Oil**		**Water-Oil-Glass**	
	ρ_{w} $(\frac{kg}{m^3})$	ν_{w} $(10^{-6}\ \frac{m^2}{s})$	ρ_{o} $(\frac{kg}{m^3})$	ν_{o} $(10^{-6}\ \frac{m^2}{s})$	$\gamma_{\text{w-o}}$ $(\frac{kg}{s^2})$	$\theta_{\text{w-g}}$ $(^\circ)$
Hydrophilic	997	0.903	845	21.065	33.8×10^{-3}	29
Hydrophobic						149

[a]Conducted by *LMMP PUC-Rio* (Avendaño et al., 2019).

TABLE 7.1: Summary of data from experimental measurements of oil recovery processes by water injection, into glass porous media with walls covered by a thin hydrophilic or hydrophobic layer.

7.2.1 Experimental data

In the continuum model, the Navier-Stokes equation requires the fluid density and viscosity as input data, which typically come from experimental measurements at the macroscale. However, at the mesoscale where capillary phenomena arise, the LBM additionally requires the interfacial tension between fluids and wettability of the porous medium as input data. In this chapter, experimental data from the *Laboratory of Microhydrodynamics and Flow in Porous Media* (*LMMP-PUC-Rio*) are used as input data. Avendaño *et al.* have all the necessary information for our LBM simulations, as shown in Tab. 7.1 (Avendaño et al., 2019).

The experimental setup consists of glass micromodels (porous media) produced by Dolomite Microfluidics (Dolomite, 2023). They have the same chemical composition and structural geometry but differ in the treatment of the porous surface to create hydrophobic and hydrophilic micromodels ($\theta = 149°$ and $\theta = 29°$ respectively). Concerning the fluids, the invading phase comprises food-grade deionized water, whereas the displaced phase consists of silicone oil (Drakeol 7, Agecom). The Tab.

MAPPING EXPERIMENTAL DATA								
Glass	**Water**		**Oil**		**Water-Oil-Glass**			
	ρ^*_{w}	τ_{w}	ρ^*_{o}	τ_{o}	$\gamma^*_{\text{w-o}}$	$g^{\text{w-o}}$	$g^{\text{w-g}}$	$g^{\text{o-g}}$
Hydrophobic	1.000	1.200	0.847	16.847	0.050	0.150	$+0.049$	-0.049
Hydrophilic							$+0.065$	-0.065

TABLE 7.2: Summary of the input parameters for the LBM simulations that come from the mapping of experimental data (see Tab. 7.1).

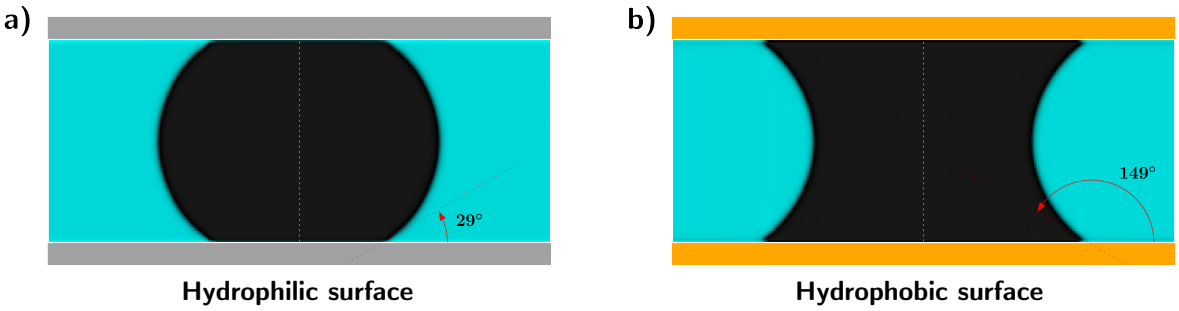

FIGURE 7.1: Experimental data mapping that generates input parameters for LBM simulations. Final snapshot of LBM simulations for an oil bubble in the middle of water and confined by two parallel plates, cases: **a)** hydrophilic and **b)** hydrophobic surface.

7.1 provides a summary of experimental measurements for the involved fluids, where the density (ρ), kinematic viscosity (ν) and interfacial tension (γ) are the same in both types of micromodels.

7.2.2 Mapping experimental data to LBM simulations

In numerical analysis, the physical units are usually transformed into dimensionless units to facilitate numerical computation and discretization process (Scheid, 1968). In LBM applied to fluid dynamics, discretization and transformation sets the density equal to unity for the mass discretization, and the temporal discretization is subject to the kinematic viscosity, while the spatial discretization is similar to traditional numerical methods (see details in App. C). The fluid-fluid and fluid-solid interactions related to interfacial tension and wettability respectively, must be calculated through a process known as data mapping (Huang, Sukop, and Lu, 2015).

In Explicit Force method, data mapping generates the fluid-fluid interaction parameter $g^{\text{k-k'}}$ and two fluid-solid interaction parameters $g^{\text{k-m}}$ and $g^{\text{k'-m}}$, related to the invading and displaced phases respectively. The Taxila-LBM package can support multiple immiscible fluids and a porous medium composed of different materials. In our research, we have experimental data from a biphasic system in two extreme and antagonistic scenarios, hydrophobic and hydrophilic case (see Tab. 7.1). The Tab. 7.2 shows the data mapping results from Tab. 7.1 expressed in dimensionless units and calculated with reference to water. Meanwhile, Fig. 7.1 demostrates that the experimental data can be reproduced using Tab. 7.1 as input data in the Taxila-LBM software. Therefore, Tab. 7.1 can be used to study oil recovery by LBM simulations.

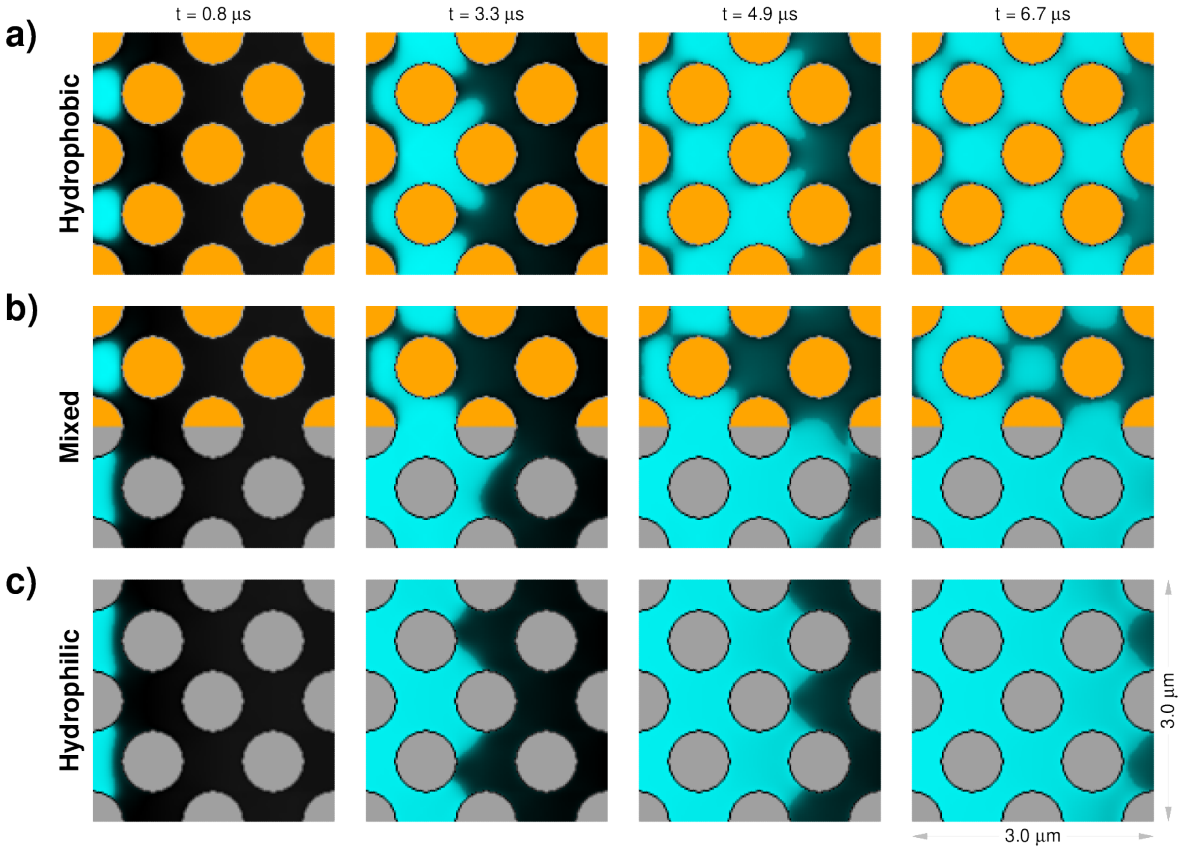

FIGURE 7.2: Oil recovery by water injection on the left side into PNMs with varied wettability for 4 time steps (oil: black region, water: cyan region, hydrophobic: orange region and hydrophilic: gray region), cases: **a)** Hydrophobic, **c)** Hydrophilic and **b)** Mixed.

7.3 Oil recovery in heterogeneous PNMs

7.3.1 Case study

In general, the oil recovery process is explored in three different scenarios based on the wettability of the PNM: **i)** hydrophobic, **ii)** hydrophilic and **iii)** mixed or heterogeneous, formed by a combination of the first two. Initially, the effect of heterogeneity on oil recovery is assessed, using a PNM designed with one half being hydrophobic and the other hydrophilic, referred to as mixed (see Fig. 7.2). Finally, the effect of heterogeneity on the amount of extracted (or trapped) oil is studied, using five heterogeneous PNMs designed with a random mixture of hydrophilic and hydrophobic components in different proportions (see Fig. 7.3).

The PNM is square-shaped with sides measuring $3.00\,\mu m$ and consists of orderly arranged circles, as show in Figs. 7.2-7.3. The petrophysical parameters: porosity ($\phi =$

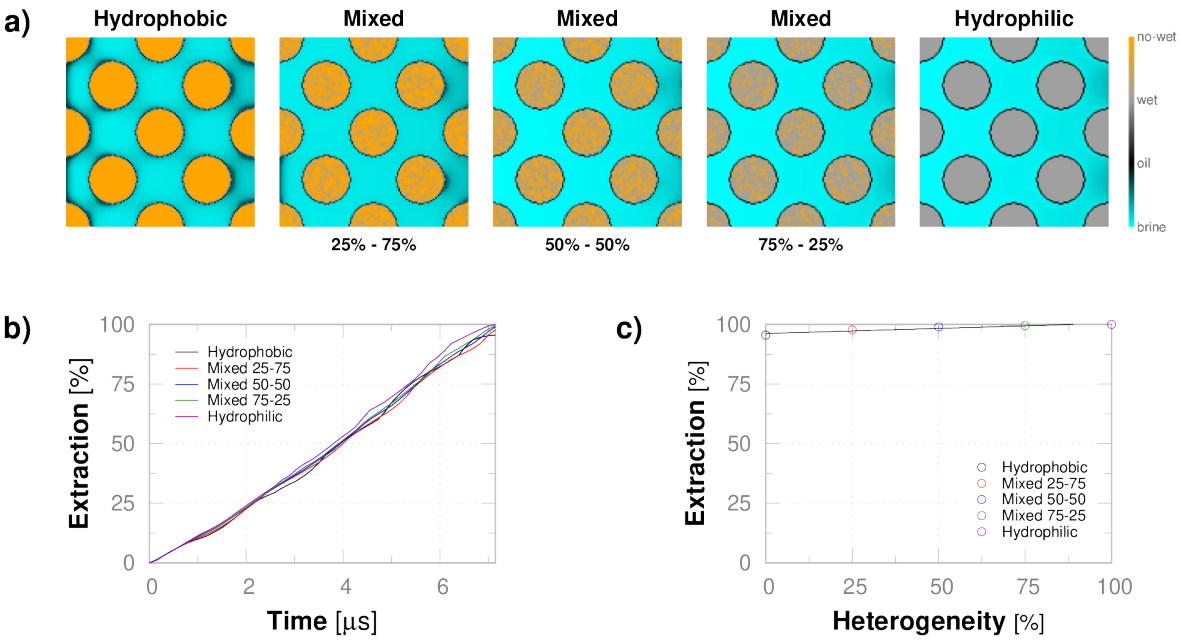

FIGURE 7.3: *Heterogeneity effect*: Heterogeneity variation effect on oil recovery process. **a)** Final snapshot of the oil recovery. **b)** Percentage of oil extracted as a function of time. **c)** Relationship between the percentage of oil extracted and percentage of heterogeneity.

0.60), tortuosity ($\tau = 1.23$), and permeability ($k = 20\,mD$) are calculated according to Sec. 3.4 and indicate that they do not vary significantly. The boundary conditions at the top and bottom of the PNM are periodic, whereas a Dirichlet boundary condition is applied on the left side as a driving force for the flow. A constant velocity of $0.45\,m/s$ is assigned to the left boundary to emulate an injection velocity. Except for the wettability of the PNM, all other variables are held constant.

7.3.2 Results

The process of recovering oil from reservoirs exhibiting heterogeneity in wettability refers to the fact that the surfaces of pores or channels may have varying degrees of wettability with respect to oil (or injected fluids such as water). In other words, some parts of the surface are more oil-wet (hydrophobic), while others are less so (hydrophilic), which can impact the way oil moves through the porous structure and its ultimate recoverability. In our research, we possess experimental data from a biphasic system in two opposing and extreme scenarios, the hydrophobic ($\theta = 149°$) and hydrophilic ($\theta = 29°$) cases, as show in Tab. 7.1.

After performing the mapping of the experimental data (refer to Fig. 7.1 and Tab. 7.2), the oil recovery process applied to heterogeneous PNM is studied using LBM simulations. The Fig. 7.2 illustrates the oil recovery process in hydrophobic, hydrophilic and mixed PNMs at four different time instants. The results obtained indicate that hydrophilic surfaces enhance oil recovery, as shown in the bottom part of Fig. 7.2. The mixed case demonstrates that the hydrophilic part promotes oil displacement, in contrast to the hydrophobic part, which delays oil displacement (see Fig. 7.2 b). The water injection appears to displace oil from hydrophilic surfaces, while the oil tends to adhere on hydrophobic surfaces.

On the other hand, the Fig. 7.3 illustrates the oil recovery process from PNMs with various degrees of heterogeneity, where the recovery curves over time follow a similar pattern in all cases (see Fig. 7.3 b). In general, the results indicate that the amount of oil recovered by water injection is affected by the degree of hydrophobicity of the PNM, as a portion of the oil remains adhered to the hydrophobic surfaces (see Fig. 7.3 a). Meanwhile, in hydrophilic PNMs invaded by water, 100% of the oil is successfully recovered (see Fig. 7.3 c). This implies that the hydrophobic nature of a PNM has the capacity to effectively trap oil, with the potential to retain as much as approximately 5%, depending on the amount of hydrophilic material present within the PNM (see Fig. 7.3 c).

7.4 Conclusions

Recovering oil from natural porous media that exhibit heterogeneity in wettability can be a complex challenge and multidisciplinary that requires a combination of geological, engineering, and chemical expertise. Heterogeneity in wettability means that different regions of the reservoir rock have varying degrees of oil-wet or water-wet characteristics. This heterogeneity can significantly impact the efficiency of oil recovery processes. The choice of recovery method should be based on a thorough understanding of reservoir characteristics and continual monitoring and adaptation of strategies as the reservoir's behavior evolves. Advanced reservoir simulation models can help predict the behavior of fluids in reservoirs with wettability heterogeneity. These computational models can optimize well placement, injection rates, and fluid properties for maximum recovery.

The results generated via LBM simulations confirm the experimental observations that report: *a better oil displacement in hydrophilic porous media* (see Sec. 7.1). The experimental data used in this chapter correspond to oil recovery in either hydrophobic or hydrophilic micromodels, as manufacturing micromodels with both hydrophobic and hydrophilic properties simultaneously is challenging. Meanwhile, the LBM simulations were conducted on PNMs designed of hydrophobic and hydrophilic components to emulate natural porous media, which are typically heterogeneous. Therefore, our results obtained from a complex system like heterogeneous PNMs can reinforce the experimental findings.

Chapter 8

Conclusions and Perspectives

8.1 Conclusions

In Chap. 4, the effect of **a)** shape, **b)** size and **c)** distribution of (flow-obstructing) solid objects on oil recovery was studied. The first two cases are ordered and the last one is entirely random, in hydrophilic PNMs with constant porosity and identical injection velocity. In the ordered cases, the results indicate that PNMs with square objects displace all the oil in less time than PNMs with other geometries (hexagons, octagons, and circles). While PNMs are formed by circular objects of different sizes, PNMs with smaller radius circles displace all the oil before the others. However, the four configurations of random PNMs formed by the smaller circles permanently retain approximately 7% and 12% of the oil.

Despite significantly extending the injection time (up to $\approx 23\mu s$), random PNMs can permanently capture oil, whereas ordered PNMs can extract 100% of the oil in relatively short injection times ($\approx 10\mu s$). Therefore, random PNMs are the ideal scenario to test the effectiveness of different types of nanoparticles and study the effect of nanoparticle inclusion on oil recovery (EOR process). The results show that the nanoparticle NP-PEG2 dispersed in the injection fluid is more effective at displacing the oil from random PNMs than the case without nanoparticles and the other two nanoparticles (NP-H and NP-SA). Similar results were also found in dead-end type PNMs and ordered three-dimensional PNMs.

The findings concerning trapped oil in random PNMs served as motivation for investigating the impact of randomness on tortuosity, permeability and oil recovery. In Chap. 3, a methodology is proposed to quantify the degree of randomness of PNMs using Shannon entropy. Just like porosity, tortuosity and permeability, Shannon entropy can be considered a petrophysical parameter that characterizes a random

PNM. Analogously, the macroscopic variables volume, pressure, temperature and entropy define an ideal gas in Statistical Mechanics. Therefore, Shannon entropy (and porosity) is a purely geometric parameter but closely related to physical parameters such as hydraulic tortuosity, Darcy permeability, and physical processes like oil recovery (topics studied in Chap. 5 and 6).

In Chap. 5, randomly distributed circles are used to design random PNMs. The study determines how the tortuosity and permeability of a hydrophilic PNM are affected when: **a)** circles disorder, **b)** PNM entropy, **c)** circles size and **d)** PNM porosity vary while keeping the other variables constant. The first study's results indicate that as the circles are disordered from an perfect order case to a completely disordered case, tortuosity and permeability increase. The second study also shows a slight increase in tortuosity and permeability as the entropy of the completely disordered case increases. In the third study, there was also an observed rise in tortuosity, with a more pronounced increase in permeability as the size of the circles increased. Finally, the results of the fourth study indicate a decrease in tortuosity and a dramatic increase in permeability as the porosity increases.

In Chap. 6, the same random PNMs introduced in Chap. 5 are employed for a similar study. This chapter investigates the effect of the four variations on oil recovery. The first study show a greater quantity of trapped oil as the circles become disordered. In the perfect order case, 100% of the oil is recovered, while in the fully disordered case, $\approx$10% remains trapped. The second study centred on the fully disordered case, reveals a trapped oil rise as entropy increase. In the fully disordered case with higher entropy, as much as around $\approx$ 13% of the oil can be retained. In the third study, varying the size of the circles does not generate significant changes in oil recovery. The quantity of trapped oil remains nearly constant, at $\approx$ 12%. Finally, the results of the fourth study reveal a unique behavior as porosity increases. For porosities less than 0.85, the quatity of trapped oil remains nearly constant at $\approx$ 12%, conversely, for higher porosities, the amount of oil remains nearly constant at $\approx$3%. This ocurrs because the entropy as a function of porosity is maximal at the point 0.85.

Natural porous media display random characteristics within their porous structure, which can be heterogeneous and composed of various materials possessing diverse physical properties. The studies in Chap. 4 to 6 focused on the randomness of the porous structure of hydrophilic PNMs, whereas Chap. 7 addresses heterogeneous PNMs. The Chap. 7 studies the effect of heterogeneity on oil recovery, where ordered

heterogeneous PNMs were designed, composed of hydrophobic and hydrophilic portions in different percentage proportions. The results show that approximately 5% of oil remains trapped in the completely hydrophobic PNM, and this percentage decreases as the proportion of hydrophilic material increases. In the fully hydrophilic PNM, oil recovery reaches 100%. Investigating oil recovery in both random and heterogeneous PNMs may offer an improved model for extracting oil from natural reservoirs.

8.2 Perspectives

In the study of oil recovery, we observe that the disorder of obstacles in a PMN is capable of permanently retaining a certain quantity of oil, similar to what occurs in a natural reservoir. While PMNs designed with randomly distributed circular obstacles manage to describe some real-world characteristics, the design has two significant constraints: obstacles are only in circular shape and it avoids obstacle overlap. Therefore, for a more realistic study, complex porous media. Porous media with complex geometry plays a significant role in the oil recovery process, especially in enhanced oil recovery (EOR) techniques. These complex geometries can include naturally occurring formations with irregular shapes, as well as artificially created structures to improve oil extraction efficiency.

To computationally emulate complex three-dimensional porous media, digital rocks are often used to understand and optimize fluid flow in reservoir rocks. It involves creating high-resolution 3D models that replicate the microscopic structure and properties of real rock samples. These digital rock models allow fluid flow, permeability and other critical factors to be simulated within the rock matrix, helping to make informed decisions about reservoir management and enhanced oil recovery (EOR) techniques. Digital rock technology enables a deeper understanding of reservoir behavior, reduces the need for physical core analysis, and ultimately contributes to more efficient and cost-effective oil recovery strategies in the petroleum industry.

Another important aspect of fluid dynamics in porous media involves fluid-fluid or fluid-solid interactions with chemical reactions. When dealing with reactive fluids in LBM, the method is extended to account for chemical reactions. This involves incorporating additional rules and variables into the lattice model, so that the simulation can capture not only the fluid's flow dynamics but also the chemical transformations that may occur within the fluid. These reactions could include

processes like combustion, dissolution, precipitation, and other chemical interactions. Simulating reactive fluids with LBM can be useful in various scientific and engineering fields, such as combustion modeling, environmental remediation, chemical engineering, and more. It allows researchers and engineers to gain insights into the interplay between fluid flow and chemical reactions, helping them design and optimize systems in a virtual environment before implementing them in the real world.

Validation of Darcy's Law using Lattice Boltzmann Method (LBM) simulations is a crucial step in confirming the accuracy and reliability of this computational approach in modeling fluid flow through porous media. Darcy's Law, a fundamental principle in fluid dynamics, describes the flow of a fluid through porous media and is based on the proportionality between flow rate, permeability, and pressure gradient. To validate Darcy's Law through LBM simulations, one must ensure that the simulated flow rates and pressure gradients in a porous medium align with the theoretical predictions of Darcy's Law. This involves comparing the LBM results with analytical solutions for specific cases and verifying that the simulated permeability and hydraulic conductivity values match those expected from the physical properties of the porous medium. Successful validation serves as a strong endorsement of the LBM's ability to accurately model fluid flow in porous media and, by extension, its applicability in various engineering and scientific fields.

Appendix A

Boltzmann Lattice

In the LBM implementation, the phase space (position and momentum) and time must be discretized (see, Fig. 2.4). On the one hand, the position discretization generates the nodes where the particles are located. On the other hand, the velocity discretization generates the possible directions or links towards the neighboring nodes (Sukop and Thorne, 2007). Thus, the particles flow with lattice velocity $\boldsymbol{c}_i$ from the central node to the neighboring nodes through the links (streaming process).

In particular, the velocity discretization in value and direction designs a structure called Boltzmann lattice, where each velocity value has a weighting factor w_i according to the direction i and the lattice configuration (see, Fig. A.1, A.2 and A.3). In fact, the common terminology used to refer to a lattice configuration is $\mathrm{D}_n\mathrm{Q}_\ell$, where n represents the dimensional space and ℓ is the number of links (Succi, 2001).

A.1 One dimensional

The lattice configuration $\mathrm{D}_1\mathrm{Q}_3$ has three lattice velocities $\{c_0, c_1, c_2\}$ which belongs to the distribution functions $\{f_0, f_1, f_2\}$ and each one has its respective weight $\{w_0, w_1, w_2\}$, as show in Fig. A.1. For this arrangement, the total number of particles may not exceed three. In the central node resides a stagnant particle f_0, while, the other two particles (f_1 and f_2) move either to the left or right of this node in the streaming process.

We can also use an even simpler configuration called $\mathrm{D}_1\mathrm{Q}_2$ as it can be seen in Fig. A.1. Different from the previous one, this configuration does not have stationary particle in the center of lattice. For that reason, the weighting factors are changed in number and value (see, Fig. A.1).

FIGURE A.1: One-dimensional configuration of Boltzmann lattices and their respective statistical weights, cases: D_1Q_2 and D_1Q_3.

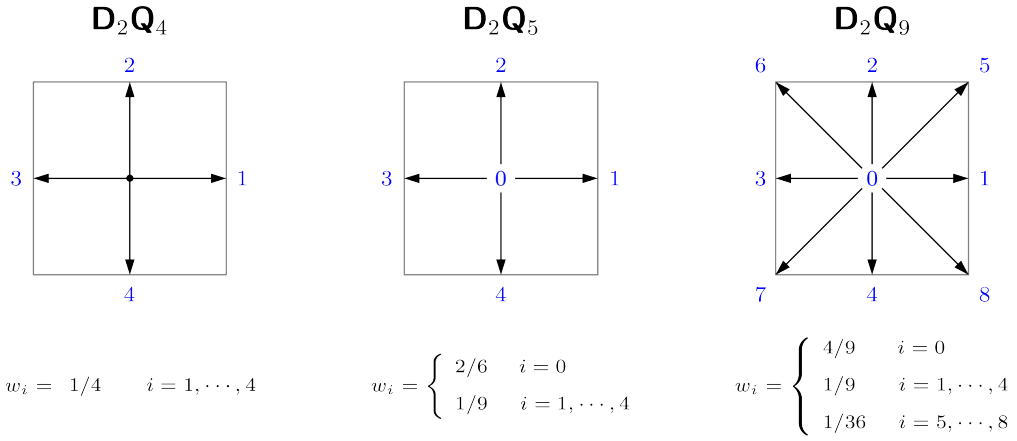

FIGURE A.2: Two-dimensional configuration of Boltzmann lattices and their respective statistical weights, cases: D_2Q_4, D_2Q_5 and D_2Q_9.

A.2 Two dimensional

The Fig. A.2 shows that the description of two-dimensional lattice configurations is similar to one-dimensional ones but more structurally complex. The D_2Q_5 model has five lattice velocities $\{c_0, c_1, c_2, c_3, c_4\}$, where four particles ($f_1, f_2, f_3$ and f_4) are emitted from the central node and one particle resides in the central node f_0. Whereas, the D_2Q_4 model has four lattice velocities and there are no particles in the central node.

Although the D_2Q_4 and D_2Q_5 models are used to describe phenomena such as diffusion or advection, these models cannot describe fluids flow (Mohamad, 2011). A commonly used alternative is the D_2Q_9 model, because the structure is specially designed to address fluid dynamics. This model has the same particles as the D_2Q_5 model, with the addition of four particles (f_5, f_6, f_7, and f_8) that move along the diagonals of the planar lattice (see, Fig. A.2).

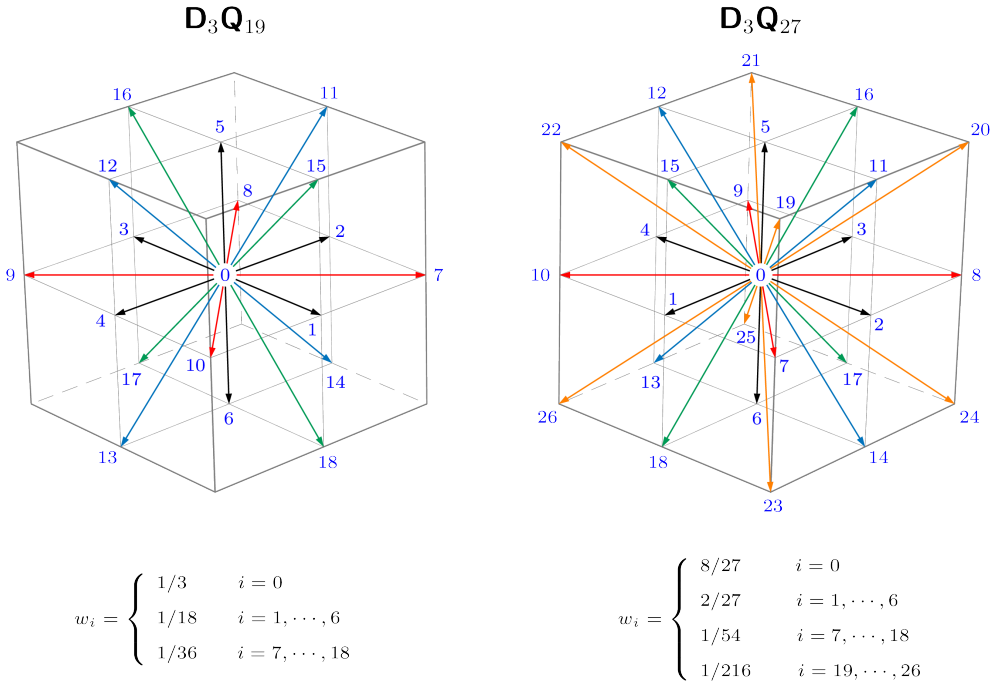

FIGURE A.3: Three-dimensional configuration of Boltzmann lattices and their respective statistical weights, cases: D_3Q_{19} and D_3Q_{27}.

A.3 Three dimensional

In general, two models are used to address problems in three dimensions: D_3Q_{19} and D_3Q_{27} (see, Fig. A.3). Both models have a particle in the center of the lattice and differ in 8 particles. The eight difference particles $(f_{19}, f_{20}, \ldots, f_{26})$ move along the diagonals of the cubic lattice, while the other particles $(f_1, f_2, \ldots, f_{18})$ move identically in both models.

The three-dimensional approach is more complex but more realistic than the two-dimensional and one-dimensional cases (see, Fig. A.3). Nevertheless, both three-dimensional models can address various physical phenomena including fluid dynamics (Mohamad, 2011).

Appendix B

Boundary Conditions

In the streaming process through any lattice Boltzmann configuration, if a central node and its neighbors are within the system domain, the tracking particles displecement from the central node to neighboring nodes is relatively simple (see, Fig. B.1). Nevertheless, if a central node is close to a domain boundary, the particles interaction flowing towards the boundary strongly depends on the type of boundary conditions (Krüger et al., 2016). In Fig. B.2, B.3 and B.4 we can see a domain under different boundary conditions.

In LBM simulations, a crucial and important issue is the accurate and appropriate modeling of boundary conditions (Mohamad, 2011). Because, in order to recover the desired macroscopic boundary conditions that satisfy the conservation principle, the discrete distribution functions must be obtained from the boundary conditions. If the microscopic rules are correctly defined, we can reach the boundary conditions within the macroscopic structure (Sukop and Thorne, 2007).

B.1 Boundary periodic

The periodic boundary conditions are responsible for the connectivity between the boundaries of the simulation domain. In many cases, it is not necessary to impose a boundary condition on the system boundary, such as a solid wall that bounds the region of space by imitating a closed box (Mohamad, 2011). Periodic conditions are particularly useful when you want to isolate an observed phenomenon or when you want to simulate conditions where external effects are negligible (Succi, 2001).

Then, in order to implement periodic conditions, we must connect the boundary from right to left and/or from top to bottom. The result is an infinite system composed of repetitions of this domain. One way to impose such a condition is to make the

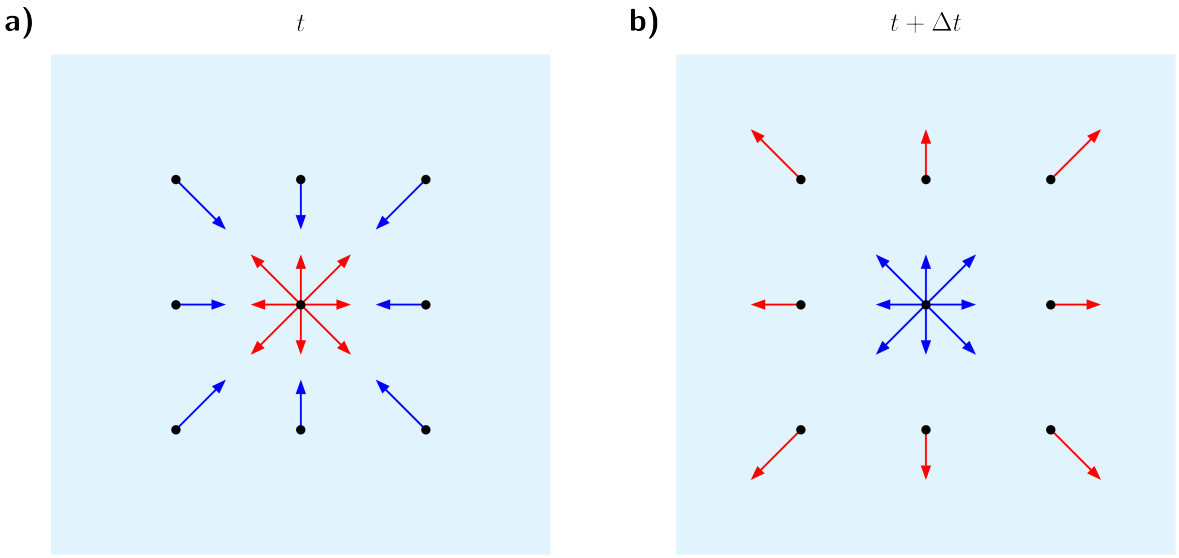

FIGURE B.1: Streaming process between nodes far from the system boundary. **a)** Central node (red arrows) that interacts with its neighbors (blue arrows) at time t. **b)** End of the interaction process between the central node and its neighbors at time $t + \Delta t$.

particles (or particle distribution) leaving the dominion are reinjected on the opposite border, as shown in Fig B.2.

B.2 Bounce-back boundary

The mirror boundary condition has the function to prevent any interference from the border over the system. This is particularly useful when there is a solid wall the opposite border. For example, to prevent the mass transfer across the border where the periodic conditions are being used, the system can be equivalent to a parallel plate system (Sukop and Thorne, 2007). The mirror boundary condition, along the border can be imposed from a specular reflection process, wich mimics the opposite effect to the Bounce-Back condition.

In the Bounce-Back boundary condition, the particles are reflected back in order to ensure a non-slip condition on the wall with zero velocity. This method is commonly used to consider walls and obstacles, where certain nodes in the network are marked as walls, and therefore, are not part of the fluid (Mohamad, 2011). The particle distribution functions in the nodes of the wall do not relax to equilibrium and do not behave according to the evolution equation of Lattice Boltzmann (Eq. 2.15). But

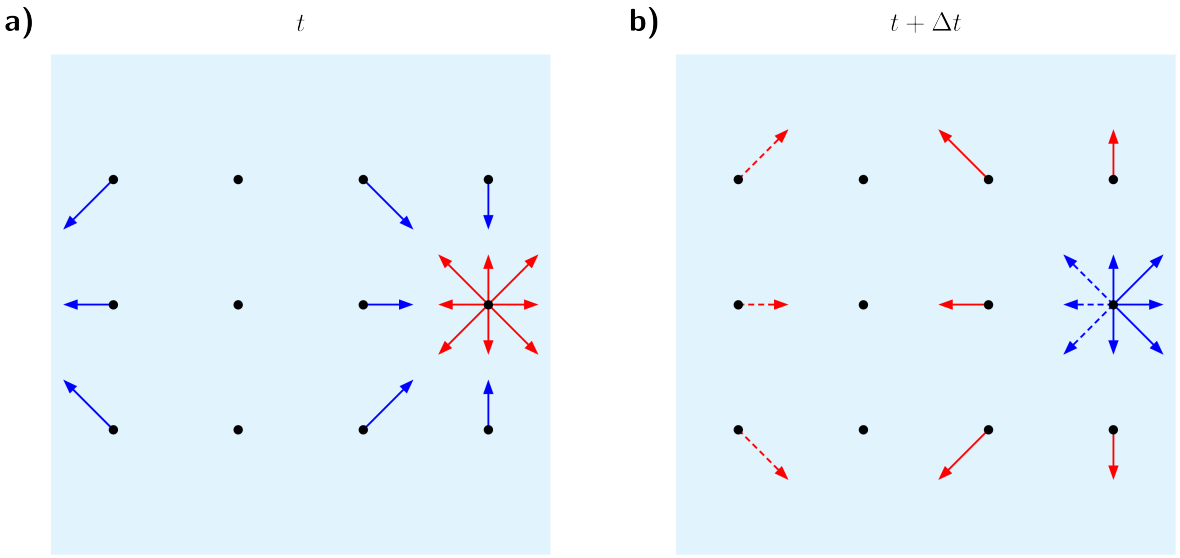

FIGURE B.2: Streaming process in the presence of periodic boundary condition. **a)** A node (red arrows) that interacts with its neighbors (blue arrows) through the periodic boundary (located on the right) at time t. **b)** End of interaction process between the node and its neighbors ($t+\Delta t$).

even so, the non-slip condition is ensured.

The basic idea is very simple and states that the unknown distributions functions assume the values of the functions that have opposite directions. For this purpose two steps occur before in the wall (impact and rebound), as shown in Fig B.3.

B.3 Dirichlet boundary

The velocity boundary condition is more sophisticated than previous ones. This condition introduces a macroscopic velocity ($\boldsymbol{v}_o = v_x\hat{\imath} + v_y\hat{\jmath}$) at the periphery of the domain to be transmitted to the microscopic model. The macroscopic quantities are defined through microscopic distribution functions (see, Sec. 2.6), then it is possible to use Eq. 2.16 to consider the velocity boundary condition (Mohamad, 2011).

In contrast to the case of boundary conditions Bounce-Back, here it is assumed that the edge of the domain and the lattice boundary, are satisfied in the periphery as shown in Fig. B.4. The linkage of the macroscopic velocity to the microscopic distribution is done by the current macroscopic density. The distribution functions having a direction opposite to the velocity boundary and the density are unknown quantity (Mohamad, 2011). The solution of these quantities must be related to the

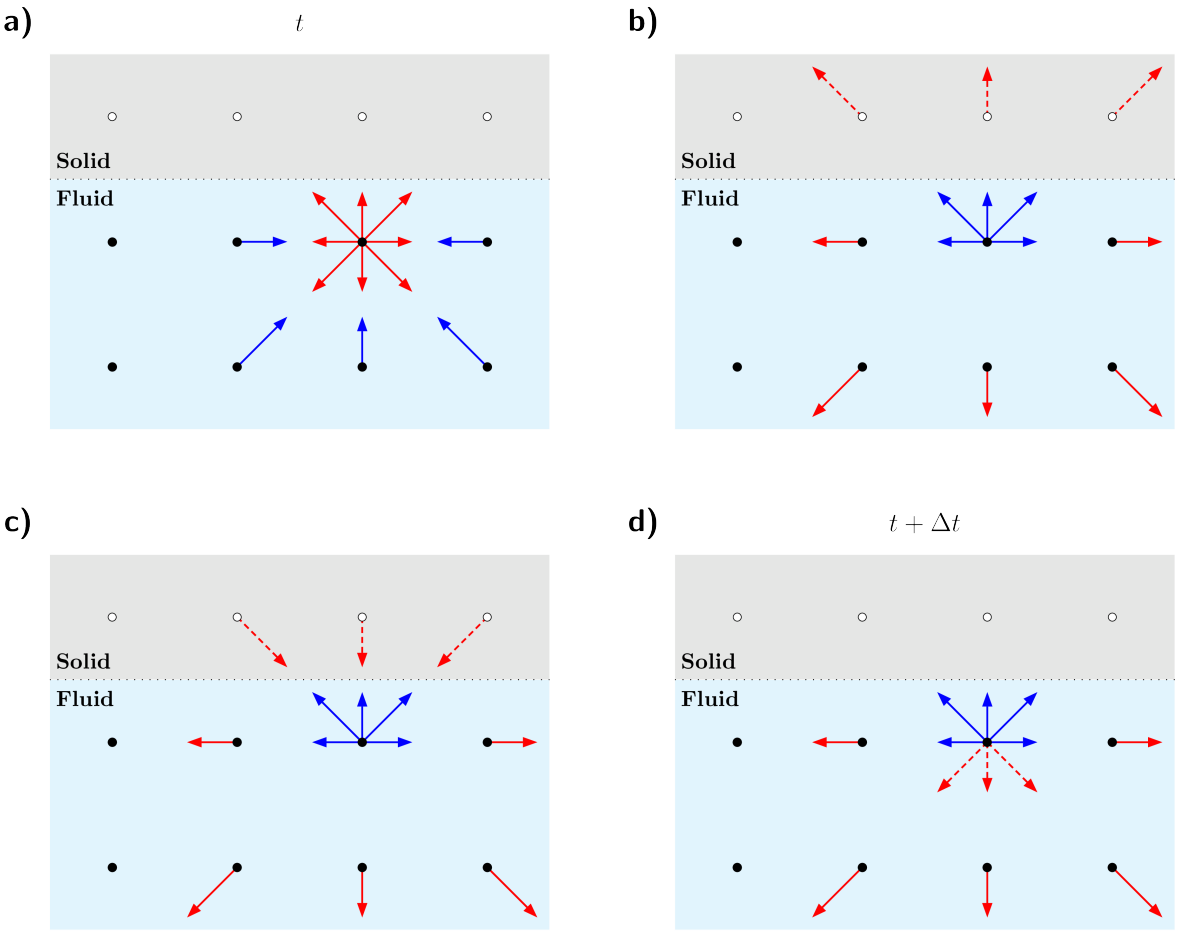

FIGURE B.3: Streaming process in the presence of a solid wall using the Bounce-Back model. **a)** A node (red arrows) interacts with its neighboring nodes (blue arrows) and the wall at time t. **b)** and **c)** are intermediate steps before the end of the process. **d)** End of process, the wall returns to the node the interactions in opposite sense $(t + \Delta t)$.

macroscopic velocity and the other distribution functions.

Then, the conditions of conservation (mass and momentum) are satisfied by Eq. 2.16. While, to satisfy the condition of equilibrium, the distribution functions with direction normal to the boundary must be equal to the equilibrium distribution function (Mohamad, 2011), as show below:

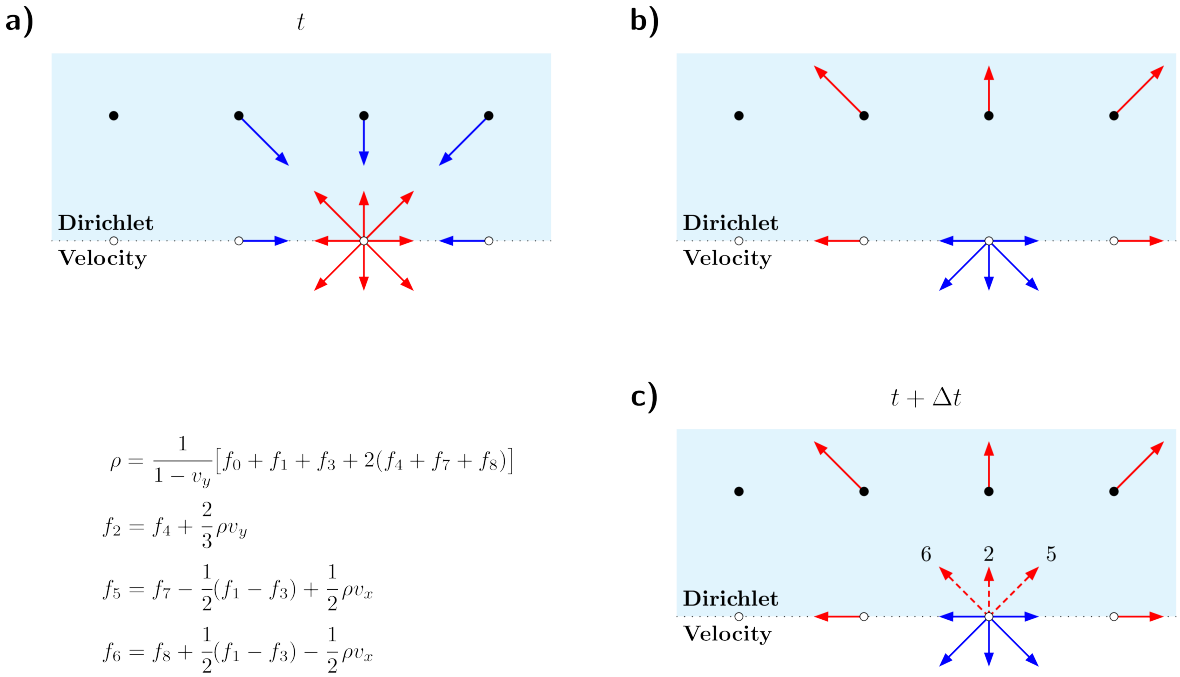

FIGURE B.4: Process streaming in the presence of a Dirichlet boundary (boundary velocity) that has a velocity $\boldsymbol{v}_o = v_x\hat{\imath} + v_y\hat{\jmath}$. **a)** A node (red arrows) interacts with its neighbors (blue arrows) and the velocity boundary at time t. **b)** is the intermediate step before the completion of the process. **c)** End of process, interactions missing in the node is completed by solving the equations relating macroscopic and microscopic quantities $(t + \Delta t)$.

a) Mass and momentum conservations:

$$\left.\begin{aligned} \rho &= \sum_{i=0}^{8} f_i = f_0 + f_1 + \cdots + f_8 \\ \rho\,\boldsymbol{v} &= \sum_{i=0}^{8} f_i\,\boldsymbol{c}_i = f_0\,\boldsymbol{c}_0 + f_0\,\boldsymbol{c}_0 + \cdots + f_8\,\boldsymbol{c}_8 \end{aligned}\right\} \tag{B.1}$$

b) Equilibrium condition:

$$f_2 - f_2^{\text{eq}} = f_4 - f_4^{\text{eq}} \tag{B.2}$$

Therefore, the unknown distribution functions f_2, f_5, f_6 and the density ρ are obtained by solving Eq. B.1 and Eq. B.2. The results are presented in Fig. B.4.

Appendix C

Simulation parameters

In a study of single-component fluid dynamics at macroscale, basically two physical magnitudes of the system are required: the density and viscosity of the fluid (Drazin, Riley, and Society, 2006). In contrast, in complex systems such as multi-component fluids, heterogeneous porous media, or at the microscopic scale, at least two additional magnitudes are necessary: interfacial tension between fluids and wettability of the porous media walls (Drikakis, Frank, and Tabor, 2019). These physical magnitudes can be obtained from experimental measurements or computational simulations such as Molecular Dynamics in combination with First Principles (Avendaño et al., 2019; Pereira, Lara, and Miranda, 2016).

C.1 Characteristic scale

The relationship between the LBM simulation parameters A^* and physical magnitudes A is defined in terms of a conversion factor C_A, as shown below:

$$A = C_A\, A^* \tag{C.1}$$

where C_A depends on the characteristic scale Γ determined by the set of variables characterizing a physical system: space, matter and time $(\Delta x, \Delta m, \Delta t)$.

The characteristic scale of the system under study can be determined by selecting a physical magnitude, assigning its corresponding simulation parameter, and conducting a simultaneous dimensional analysis of the system variables. For example, in a system defined solely by its geometry dimensions, a representative length of the system L is selected, and then the number of partitions N $(\equiv L^*)$ is conveniently assigned for the simulation. Therefore, the ratio L/N generates the spatial characteristic scale Δx. Because the system depends only on length, C_L is equivalent to the characteristic

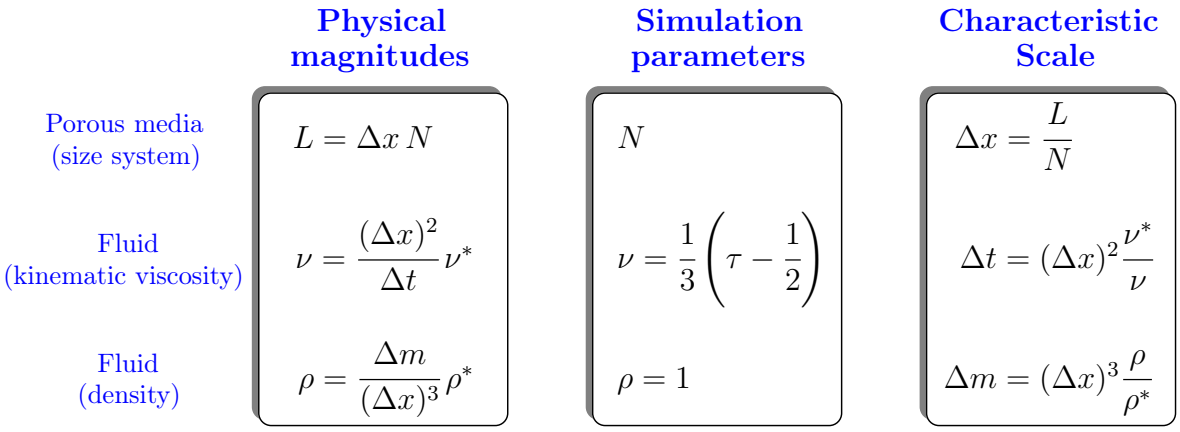

FIGURE C.1: Scheme for obtaining the characteristic scale Γ of a system based on physical magnitudes and simulation parameters, case: study of fluid dynamics using the LBM methodology.

scale. However, if the system depends on time and/or mass as well, the conversion factors may depend on several variables (see 1st column of Fig. C.1).

In fluid dynamics, the system is defined by the dimensions of the porous medium and the properties of the involved fluid, such as kinematic viscosity and density. If the system is approached using the LBM, the spatial discretization is chosen according to computational convergence criteria, the density value is set to 1, and viscosity is a function of the relaxation time restricted to values greater than 1/2, where the three parameters are dimensionless. Therefore, the characteristic scale $\Gamma \equiv (\Delta x, \Delta m, \Delta t)$ must be extracted based on the system properties and considerations of the LBM methodology, as shown in Fig. C.1.

C.2 Taxila-LBM values

A single-component, incompressible, and isothermal flow on a macroscopic scale can be described by the Navier-Stokes equations, where the system is entirely defined by the density and viscosity of the fluid. On a microscopic scale, where capillary phenomena such as interfacial tension and wettability become important, the LBM is an ideal methodology for describing multi-component flows in heterogeneous porous media with complex geometry. Within the LBM methodology, there are various qualitative methods to address capillary phenomena in fluid flow through porous media, such as Shan-Chen. Meanwhile, the Explicit Force method is quantitative and has its own software called Taxila-LBM (Porter et al., 2012; Coon, Porter, and Kang, 2014).

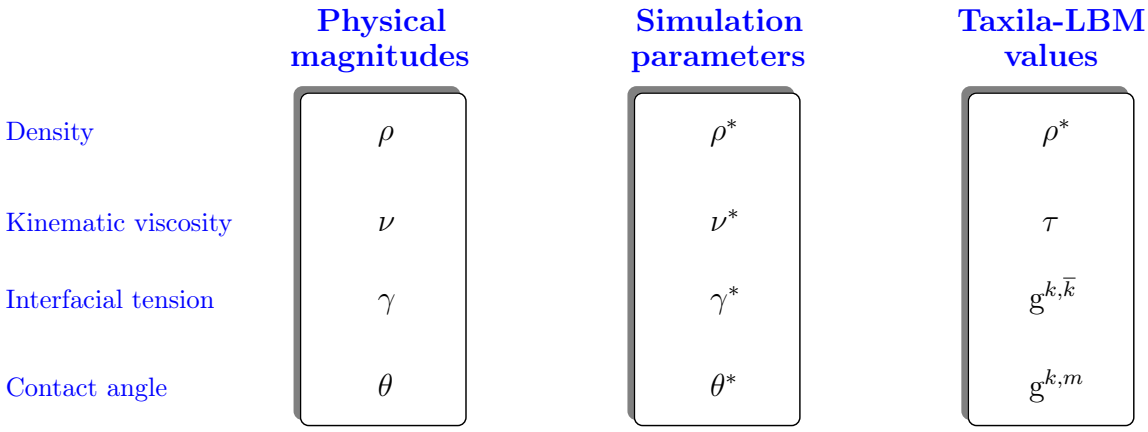

FIGURE C.2: Scheme of the conversion of physical magnitudes to dimensionless simulation parameters and their subsequent conversion to values of the Taxila-LBM software.

In numerical analysis applied to computational simulations, such as LBM simulations, the physical magnitudes of the system (porous medium dimension and fluid density-viscosity) are transformed into dimensionless simulation parameters (see Fig. C.1). Furthermore, if the fluid is multicomponent and at the micrometric scale, the Explicit Force method interprets the interfacial tension between fluids as fluid-fluid interactions denoted as $g^{k,\overline{k}}$, and the wetting behavior of the porous medium as fluid-solid interactions denoted as $g^{k,m}$ (see Fig. C.2).

Specifically, the fluid-fluid interaction force $g^{k,\overline{k}}$ is related to the dimensionless interfacial tension γ^*, which is obtained from the following relationship:

$$\gamma = \frac{\Delta m}{(\Delta t)^2}\,\gamma^* \tag{C.2}$$

where, $C_\gamma = \Delta m/(\Delta t)^2$ is the conversion factor between the physical magnitude γ and the simulation parameter γ^* (see Eq. C.1).

Porter *et.al* has shown that for the Explicit Force method, there is a unique relationship between the interfacial tension γ^* and the interaction strength $g^{k,\overline{k}}$ of a binary mixture $(k, \overline{k})$, which is independent of the chosen viscosity and viscosity ratio (Porter et al., 2012; Coon, Porter, and Kang, 2014). They determine a simple

quadratic fit rule that relates these two dimensionless quantities, as shown below:

$$1.361(\mathrm{g}^{k,\bar{k}})^2 - 1.721\,\mathrm{g}^{k,\bar{k}} + (1.178 + \gamma^*) = 0 \tag{C.3}$$

where, although the quadratic discriminant indicates that $\gamma^* \geqslant -0.862$, the Eq. C.2 show that the value must necessarily be positive.

On the other hand, the $\mathrm{g}^{k,m}$ parameter is obtained through simulations of fluids in contact and confined between parallel plates. There are no external forces on the system during the process until equilibrium (stationary state). The parameter value $\mathrm{g}^{k,m}$ is obtained from the simulation that is capable of reproducing the physical contact angle ($\theta \equiv \theta^*$). Therefore, we must perform several simulations for different values of $\mathrm{g}^{k,m}$ (but keeping the values of ρ_k^*, τ_k and $\mathrm{g}^{k,\bar{k}}$ constant) until obtaining the closest value to θ (Pereira, Lara, and Miranda, 2016).

C.3 Example: Molecular Dynamics data

The physical information required for LBM simulations can come from experimental measurements or computational simulations. For example, in the work performed by Pereira et al., the data or physical magnitudes are generated via Molecular Dynamics (Pereira, Lara, and Miranda, 2016). The physical system is composed of a porous structure of montmorillonite clay (MMT), the displaced fluid is light oil, and the injected fluid is API brine (8% NaCl and 2% $CaCl_2$). In addition to the pure brine solution (no-NP), there are three types of SiO_2 nanoparticle solutions:

COMPUTATIONAL SIMULATIONS DATA [a]

System	Brine		Oil		Brine-Oil-Clay	
	ρ_{b} $(\frac{kg}{m^3})$	ν_{b} $(10^{-6}\,\frac{m^2}{s})$	ρ_{o} $(\frac{kg}{m^3})$	ν_{o} $(10^{-6}\,\frac{m^2}{s})$	$\gamma_{\mathrm{b\text{-}o}}$ $(\frac{kg}{s^2})$	$\theta_{\mathrm{b\text{-}c}}$ $(\,^\circ)$
no NP	997	0.791	810	4.473	0.043	69
NP-H	1026	0.867	810	4.348	0.038	64
NP-SA	1037	0.867	810	4.395	0.033	57
NP-PEG2	1034	0.854	810	4.384	0.029	50

[a] Conducted by *NanoPetro Group* (Pereira, Lara, and Miranda, 2016).

TABLE C.1: Summary of molecular dynamics simulations performed for the case of a brine solution (with and without nanoparticles) in contact with oil confined between surfaces of the montmorillonite clay.

MAPPING COMPUTATIONAL DATA								
System	**Brine**		**Oil**		**Brine-Oil-Clay**			
	ρ_b^*	τ_b	ρ_o^*	τ_o	$\gamma_{b\text{-}o}^*$	$g^{b\text{-}o}$	$g^{b\text{-}c}$	$g^{o\text{-}c}$
no NP	1.000	1.230	0.894	4.628	0.100	0.190	−0.027	+0.027
NP-H	1.000	1.299	0.894	4.513	0.089	0.181	−0.031	+0.031
NP-SA	1.000	1.300	0.894	4.556	0.077	0.171	−0.033	+0.033
NP-PEG2	1.000	1.288	0.894	4.546	0.068	0.164	−0.034	+0.034

TABLE C.2: Summary of the molecular dynamics mapped parameters for the Explicit Force model and LBM simulations.

hydroxylated (NP-H), functionalized with sulfonic acid (NP-SA) and functionalized with polyethylene glycol (NP-PEG2), see details in Tab. C.1.

To obtain the characteristic spatial scale of the system, the physical dimension of the porous medium is defined as a square with a side length of $L = 5.68\,\mu m$ (physical magnitude), discretized or divided into $N = 256$ parts (simulation parameter). Meanwhile, for the temporal/material characteristic scale, brine is chosen as the reference fluid. Thus, starting from the physical viscosity $\nu = 0.791 \times 10^{-6}\,m^2/s$ and a relaxation time chosen as $\tau = 1.230$ (simulation viscosity as $\nu^* = 0.244$), the temporal characteristic scale is obtained. The material characteristic scale is obtained from the physical density $\rho = 997\,kg/m^3$, with the simulation density assigned as $\rho^* = 1$.

Finally, the dimensionless LBM parameters derived from the MD results are shown in Tab. C.2. The characteristic scale is: $\Delta x = 2.22 \times 10^{-8}\,m$, $\Delta t = 1.52 \times 10^{-10}\,s$ and $\Delta m = 9.91 \times 10^{-21}\,kg$. The methodology developed by Pereira *et al.* applies a multiscale hierarchical calculation protocol that combines LBM simulations and data generated by MD, where the data mapped as LBM input parameters (Pereira, Lara, and Miranda, 2016).

Bibliography

Adloo, Hadi and Behnam Abbasi (2021). "Some insights into the use of pore network simulations for predicting single-phase fluid flow in model porous media". In: *Microfluidics and Nanofluidics* 25.7, p. 61.

Aidun, Cyrus K and Jonathan R Clausen (2010). "Lattice-Boltzmann method for complex flows". In: *Annual review of fluid mechanics* 42, pp. 439–472.

Akai, Takashi, Branko Bijeljic, and Martin J. Blunt (2018). "Wetting boundary condition for the color-gradient lattice Boltzmann method: Validation with analytical and experimental data". In: *Advances in Water Resources* 116, pp. 56–66. ISSN: 0309-1708. DOI: https://doi.org/10.1016/j.advwatres.2018.03.014. URL: https://www.sciencedirect.com/science/article/pii/S030917081731028X.

Alamooti, Amirhossein Mohammadi and Farzan Karimi Malekabadi (2018). "Chapter One - An Introduction to Enhanced Oil Recovery". In: *Fundamentals of Enhanced Oil and Gas Recovery from Conventional and Unconventional Reservoirs*. Ed. by Alireza Bahadori. Gulf Professional Publishing, pp. 1–40. ISBN: 978-0-12-813027-8. DOI: https://doi.org/10.1016/B978-0-12-813027-8.00001-1. URL: https://www.sciencedirect.com/science/article/pii/B9780128130278000011.

Allen, P. and D.J. Tildesley (1989). *Computer Simulation of Liquids*. Oxford Science Publ. Clarendon Press. ISBN: 9780198556459. URL: http://books.google.es/books?id=O32VXB9e5P4C.

Alvim, Raphael S., Vladivostok Suxo, Oscar A. Babilonia, Yuri M. Celaschi, and Caetano R. Miranda (2017). "Nanoscience Applied to Oil Recovery and Mitigation: A Multiscale Computational Approach". In: *MRS Advances* 2.9, 477–482. DOI: 10.1557/adv.2017.28.

Amirpour, Masoud, Seyed Reza Shadizadeh, Hamid Esfandyari, and Saeid Ahmadi (2015). "Experimental investigation of wettability alteration on residual oil saturation using nonionic surfactants: Capillary pressure measurement". In: *Petroleum* 1.4, pp. 289–299. ISSN: 2405-6561. DOI: https://doi.org/10.1016/j.petlm.2015.11.003. URL: https://www.sciencedirect.com/science/article/pii/S2405656115000711.

Anderson, W.G. (Dec. 1987). "Wettability Literature Survey-Part 6: The Effects of Wettability on Waterflooding". In: *Journal of Petroleum Technology* 39.12, pp. 1605–1622. ISSN: 0149-2136. DOI: 10.2118/16471-PA. eprint: https://onepetro.org/JPT/article-pdf/39/12/1605/2220972/spe-16471-pa.pdf. URL: https://doi.org/10.2118/16471-PA.

Andrade, J. S., D. A. Street, T. Shinohara, Y. Shibusa, and Y. Arai (1995). "Percolation disorder in viscous and nonviscous flow through porous media". In: *Phys. Rev. E* 51 (6), pp. 5725–5731. DOI: 10.1103/PhysRevE.51.5725. URL: https://link.aps.org/doi/10.1103/PhysRevE.51.5725.

Ansarinasab, Javad and Mohammad Jamialahmadi (2016). "Investigating the effect of interfacial tension and contact angle on capillary pressure curve, using free energy Lattice Boltzmann Method". In: *Journal of Natural Gas Science and Engineering* 35, pp. 1146–1157. ISSN: 1875-5100. DOI: https://doi.org/10.1016/j.jngse.2016.09.055. URL: https://www.sciencedirect.com/science/article/pii/S1875510016306953.

Arfken, G.B., H.J. Weber, and F.E. Harris (2011). *Mathematical Methods for Physicists: A Comprehensive Guide*. Elsevier Science. ISBN: 9780123846556. URL: https://books.google.com.br/books?id=JOpHkJF-qcwC.

Avendaño, Jorge, Nicolle Lima, Antonio Quevedo, and Marcio Carvalho (2019). "Effect of Surface Wettability on Immiscible Displacement in a Microfluidic Porous Media". In: *Energies* 12.4. ISSN: 1996-1073. DOI: 10.3390/en12040664. URL: https://www.mdpi.com/1996-1073/12/4/664.

Balankin, Alexander S. and Benjamin Espinoza Elizarraraz (2012). "Map of fluid flow in fractal porous medium into fractal continuum flow". In: *Phys. Rev. E* 85 (5), p. 056314. DOI: 10.1103/PhysRevE.85.056314. URL: https://link.aps.org/doi/10.1103/PhysRevE.85.056314.

Bates, Paul D, Stuart N Lane, and Robert I Ferguson (2005). *Computational fluid dynamics: applications in environmental hydraulics*. John Wiley & Sons.

Bauer, D, L Talon, Y Peysson, HB Ly, G Batôt, T Chevalier, and M Fleury (2019). "Experimental and numerical determination of Darcy's law for yield stress fluids in porous media". In: *Physical Review Fluids* 4.6, p. 063301.

Bellomo, N. and M. Pulvirenti (2013). *Modeling in Applied Sciences: A Kinetic Theory Approach*. Modeling and Simulation in Science, Engineering and Technology. Birkhäuser Boston. ISBN: 9781461205135. URL: https://books.google.com.br/books?id=kv7ZBwAAQBAJ.

Berg, John (1993). *Wettability*. Vol. 49. CRC Press.

Bertrand, P., D.D. Sarto, and A. Ghizzo (2019). *The Vlasov Equation 1: History and General Properties*. Wiley. ISBN: 9781119662679. URL: https://books.google.com.br/books?id=LsWxDwAAQBAJ.

Bhatnagar, P. L., E. P. Gross, and M. Krook (May 1954). "A Model for Collision Processes in Gases. I. Small Amplitude Processes in Charged and Neutral One-Component Systems". In: *Phys. Rev.* 94.3, pp. 511–525. DOI: 10.1103/PhysRev.94.511. URL: http://link.aps.org/doi/10.1103/PhysRev.94.511.

Bourguignon, Marcelo, Maria do Carmo S Lima, Jeremias Leão, Abraão DC Nascimento, Luis Gustavo B Pinho, and Gauss M Cordeiro (2015). "A new generalized gamma distribution with applications". In: *American Journal of Mathematical and Management Sciences* 34.4, pp. 309–342.

Bradt, Hale and Stanislaw Olbert (2008). "Liouville's Theorem". In: *Supplement to*.

Bruus, Henrik (2008). *Theoretical microfluidics*. Vol. 18. Oxford university press Oxford.

Cercignani, C. (2013). *Mathematical Methods in Kinetic Theory*. Springer US. ISBN: 9781489972910. URL: https://books.google.co.mz/books?id=alH2BwAAQBAJ.

— (2014). *Kinetic Theory and Gas Dynamics*. CISM International Centre for Mechanical Sciences. Springer Vienna. ISBN: 9783709127629. URL: https://books.google.com.br/books?id=pcUrBAAAQBAJ.

Cercignani, Carlo (1988). "The Boltzmann Equation". In: *The Boltzmann Equation and Its Applications*. New York, NY: Springer New York, pp. 40–103. ISBN: 978-1-4612-1039-9. DOI: 10.1007/978-1-4612-1039-9_2. URL: https://doi.org/10.1007/978-1-4612-1039-9_2.

Chapman, S. and T.G. Cowling (1970). *The Mathematical Theory of Non-uniform Gases: An Account of the Kinetic Theory of Viscosity, Thermal Conduction and Diffusion in Gases*. Cambridge Mathematical Library. Cambridge University Press. ISBN: 9780521408448. URL: http://books.google.com.br/books?id=Cbp5JP2OTrwC.

Chapuis, Robert P and Michel Aubertin (2003). "On the use of the Kozeny Carman equation to predict the hydraulic conductivity of soils". In: *Canadian Geotechnical Journal* 40.3, pp. 616–628.

Chen, Jikai, Yanhui Dou, Yang Li, and Jiang Li (2016). "Application of Shannon wavelet entropy and Shannon wavelet packet entropy in analysis of power system transient signals". In: *Entropy* 18.12, p. 437.

Chung, TJ et al. (2002). *Computational fluid dynamics*. Cambridge university press.

Coelho, Rodrigo CV, Anderson S Ilha, and Mauro M Doria (2016). "A lattice Boltzmann method based on generalized polynomials and its application for electrons in metals". In: *EPL (Europhysics Letters)* 116.2, p. 20001.

Coon, Ethan T., Mark L. Porter, and Qinjun Kang (2014). "Taxila LBM: a parallel, modular lattice Boltzmann framework for simulating pore-scale flow in porous media". In: *Computational Geosciences* 18.1, pp. 17–27. ISSN: 1573-1499. DOI: 10.1007/s10596-013-9379-6. URL: https://doi.org/10.1007/s10596-013-9379-6.

Cover, Thomas M and Joy A Thomas (1991). "Information theory and statistics". In: *Elements of Information Theory* 1.1, pp. 279–335.

Crain, IK and RE Miles (1976). "Monte Carlo estimates of the distributions of the random polygons determined by random lines in a plane". In: *Journal of Statistical Computation and Simulation* 4.4, pp. 293–325.

Dandekar, Abhijit Y (2006). *Petroleum reservoir rock and fluid properties*. CRC press.

— (2013). "Petroleum Reservoir Rock and Fluid Properties". In:

Degond, P., L. Pareschi, and G. Russo (2012). *Modeling and Computational Methods for Kinetic Equations*. Modeling and Simulation in Science, Engineering and Technology. Birkhäuser Boston. ISBN: 9780817682002. URL: https://books.google.com.br/books?id=YvrZBwAAQBAJ.

Dolomite, Microfluidics (2023). *Dolomite Microfluidics*. https://www.dolomite-microfluidics.com. accessed on 17 September 2023.

Donaldson, Erle C and Waqi Alam (2013). *Wettability*. Elsevier.

Drazin, P.G., N. Riley, and London Mathematical Society (2006). *The Navier-Stokes Equations: A Classification of Flows and Exact Solutions*. London Mathematical Society Lecture Note Series v. 13. Cambridge University Press. ISBN: 9780521681629. URL: http://books.google.com.br/books?id=9SHzrFhVO30C.

Drikakis, Dimitris, Michael Frank, and Gavin Tabor (2019). "Multiscale computational fluid dynamics". In: *Energies* 12.17, p. 3272.

Du Plessis, J. Prieur and Jacob H. Masliyah (1988). "Mathematical modelling of flow through consolidated isotropic porous media". In: *Transport in Porous Media* 3.2, pp. 145–161. ISSN: 1573-1634. DOI: 10.1007/BF00820342. URL: https://doi.org/10.1007/BF00820342.

Duda, Artur, Zbigniew Koza, and Maciej Matyka (2011). "Hydraulic tortuosity in arbitrary porous media flow". In: *Physical Review E* 84.3, p. 036319.

Durán, Juan Manuel (2018). *Computer simulations in science and engineering: Concepts-Practices-Perspectives*. Springer.

Fagbemi, Samuel, Pejman Tahmasebi, and Mohammad Piri (2018). "Interaction between fluid and porous media with complex geometries: A direct pore-scale study". In: *Water Resources Research* 54.9, pp. 6336–6356.

Fani, Mahmood, Peyman Pourafshary, Peyman Mostaghimi, and Nader Mosavat (2022). "Application of microfluidics in chemical enhanced oil recovery: A review". In: *Fuel* 315, p. 123225. ISSN: 0016-2361. DOI: https://doi.org/10.1016/j.fuel.2022.123225. URL: https://www.sciencedirect.com/science/article/pii/S0016236122000965.

Galdi, G.P. (2011). *An Introduction to the Mathematical Theory of the Navier-Stokes Equations: Steady-State Problems*. Springer Monographs in Mathematics. Springer-Verlag. ISBN: 9780387096209. URL: http://books.google.es/books?id=dXCFbCJGsi8C.

Green, Don W, G Paul Willhite, et al. (1998). *Enhanced oil recovery*. Vol. 6. Henry L. Doherty Memorial Fund of AIME, Society of Petroleum Engineers ...

Harris, S. (2004). *An Introduction to the Theory of the Boltzmann Equation*. Dover books on physics. Dover Publications. ISBN: 9780486438313. URL: https://books.google.com.br/books?id=KfYK1lyq3VYC.

Hinde, AL and RE Miles (1980). "Monte Carlo estimates of the distributions of the random polygons of the Voronoi tessellation with respect to a Poisson process". In: *Journal of statistical computation and simulation* 10.3-4, pp. 205–223.

Huang, Haibo, Michael Sukop, and Xiyun Lu (2015). "Multiphase lattice Boltzmann methods: Theory and application". In:

Iglauer, S., M.A. Fernø, P. Shearing, and M.J. Blunt (2012). "Comparison of residual oil cluster size distribution, morphology and saturation in oil-wet and water-wet sandstone". In: *Journal of Colloid and Interface Science* 375.1, pp. 187–192. ISSN: 0021-9797. DOI: https://doi.org/10.1016/j.jcis.2012.02.025. URL: https://www.sciencedirect.com/science/article/pii/S0021979712001816.

Islam, M Rafuqul, Jamal H Abou-Kassem, ME Hossain, S Hossien Mousavizadegan, and Shabbir Mustafiz (2016). *Advanced petroleum reservoir simulation: Towards developing reservoir emulators*. John Wiley & Sons.

Jackson, J David (2007). "Electrodynamics". In: *The Optics Encyclopedia: Basic Foundations and Practical Applications*.

Jadhunandan, P. P. and N. R. Morrow (Feb. 1995). "Effect of Wettability on Waterflood Recovery for Crude-Oil/Brine/Rock Systems". In: *SPE Reservoir Engineering* 10.01, pp. 40–46. ISSN: 0885-9248. DOI: 10.2118/22597-PA. eprint: https://onepetro.org/RE/article-pdf/10/01/40/2602471/spe-22597-pa.pdf. URL: https://doi.org/10.2118/22597-PA.

James, L. and I. Chatzis (2004). "Details of gravity drainage of heavy oil during vapour extraction". In: *Dimensions* 3.4, p. 4.

Jeans, James (1982). *An Introduction to the Kinetic Theory of Gases*. Cambridge Science Classics. Cambridge University Press. DOI: 10.1017/CBO9780511628849.

Kaufmann, William J and Larry L Smarr (1995). "Supercomputing and the Transformation of Science". In: *La Météorologie*.

Kemper, Timothy G. (2020). "Oil Extraction". In: *Bailey's Industrial Oil and Fat Products*. John Wiley & Sons, Ltd, pp. 1–38. ISBN: 9780471678496. DOI: https://doi.org/10.1002/047167849X.bio013.pub2. eprint: https://onlinelibrary.wiley.com/doi/pdf/10.1002/047167849X.bio013.pub2. URL: https://onlinelibrary.wiley.com/doi/abs/10.1002/047167849X.bio013.pub2.

Khodabina, Morteza and Alireza Ahmadabadib (2010). "Some properties of generalized gamma distribution". In:

Kim, Deok-Soo, Donguk Kim, and Kokichi Sugihara (2001). "Voronoi diagram of a circle set from Voronoi diagram of a point set: I. Topology". In: *Computer Aided Geometric Design* 18.6, pp. 541–562.

Kirch, Alexsandro, Naiyer Razmara, Vladivostok Franz Suxo Mamani, Julio Romano Meneghini, and Caetano Rodrigues Miranda (2020). "Multiscale Molecular Modeling Applied to the Upstream Oil & Gas Industry Challenges". In: *Polytechnica* 3.1, pp. 54–65. ISSN: 2520-8063. DOI: 10.1007/s41050-019-00019-w. URL: https://doi.org/10.1007/s41050-019-00019-w.

Koltun, Vladlen and Micha Sharir (2004). "Polyhedral Voronoi diagrams of polyhedra in three dimensions". In: *Discrete & Computational Geometry* 31.1, pp. 83–124.

Körner, Carolin, Thomas Pohl, Ulrich Rüde, Nils Thürey, and Thomas Zeiser (2006). "Parallel Lattice Boltzmann Methods for CFD Applications". In: *Numerical Solution of Partial Differential Equations on Parallel Computers*. Ed. by Are Magnus Bruaset and Aslak Tveito. Berlin, Heidelberg: Springer Berlin Heidelberg, pp. 439–466. ISBN: 978-3-540-31619-0.

Krüger, T., H. Kusumaatmaja, A. Kuzmin, O. Shardt, G. Silva, and E.M. Viggen (2016). *The Lattice Boltzmann Method: Principles and Practice*. Graduate Texts in Physics. Springer International Publishing. ISBN: 9783319446493. URL: https://books.google.com.br/books?id=S-d0DQAAQBAJ.

Lake, Larry W, Russell Johns, Bill Rossen, Gary A Pope, et al. (2014). *Fundamentals of enhanced oil recovery*. Vol. 1. Society of Petroleum Engineers Richardson, TX.

Landau, L.D. and E.M. Lifshits (1959). *Fluid Mechanics, by L.D. Landau and E.M. Lifshitz*. Teoreticheskai a fizika. Pergamon Press. URL: http://books.google.com.br/books?id=CVbntgAACAAJ.

Leach, Andrew R. (2001). *Molecular Modelling: Principles and Applications*. Pearson Education. Prentice Hall. ISBN: 9780582382107. URL: http://books.google.com.br/books?id=kB7jsbV-uhkC.

Lee, Hyundo, Seung Goo Lee, and Patrick S. Doyle (2015). "Photopatterned oil-reservoir micromodels with tailored wetting properties". In: *Lab Chip* 15 (14), pp. 3047–3055. DOI: 10.1039/C5LC00277J. URL: http://dx.doi.org/10.1039/C5LC00277J.

Liang, Mingchao, Yinhao Gao, Shanshan Yang, Boqi Xiao, Zhankui Wang, and Yongfeng Li (2018). "An analytical model for two-phase relative permeability with Jamin effect in porous media". In: *Fractals* 26.03, p. 1850037.

Liu, Guangfeng, Hengli Wang, Jiachao Tang, Zongke Liu, and Daoyong Yang (2023). "Effect of wettability on oil and water distribution and production performance in a tight sandstone reservoir". In: *Fuel* 341, p. 127680. ISSN: 0016-2361. DOI: https://doi.org/10.1016/j.fuel.2023.127680. URL: https://www.sciencedirect.com/science/article/pii/S0016236123002934.

Liu, Siyan, Chi Zhang, and Reza Barati Ghahfarokhi (2021). "A review of lattice-Boltzmann models coupled with geochemical modeling applied for simulation of advanced waterflooding and enhanced oil recovery processes". In: *Energy & Fuels* 35.17, pp. 13535–13549.

Mark, Daniel, Stefan Haeberle, Günter Roth, Felix Von Stetten, and Roland Zengerle (2010). "Microfluidic lab-on-a-chip platforms: requirements, characteristics and applications". In: *Microfluidics based microsystems*, pp. 305–376.

Martys, Nicos S., Xiaowen Shan, and Hudong Chen (1998). "Evaluation of the external force term in the discrete Boltzmann equation". In: *Phys. Rev. E* 58 (5), pp. 6855–6857. DOI: 10.1103/PhysRevE.58.6855. URL: http://link.aps.org/doi/10.1103/PhysRevE.58.6855.

Matyka, Maciej and Zbigniew Koza (2012). "How to calculate tortuosity easily?" In: *AIP Conference Proceedings 4*. Vol. 1453. 1. American Institute of Physics, pp. 17–22.

McNamara, Guy R and Gianluigi Zanetti (1988). "Use of the Boltzmann equation to simulate lattice-gas automata". In: *Physical review letters* 61.20, p. 2332.

Mendoza, M, BM Boghosian, Hans Jürgen Herrmann, and S Succi (2010). "Fast lattice Boltzmann solver for relativistic hydrodynamics". In: *Physical review letters* 105.1, p. 014502.

Merriam, D.F. (2012). *Random Processes in Geology*. Springer Berlin Heidelberg. ISBN: 9783642661464. URL: https://books.google.com.br/books?id=26PrCAAAQBAJ.

Michalowicz, J.V., J.M. Nichols, and F. Bucholtz (2013). *Handbook of Differential Entropy*. Taylor & Francis. ISBN: 9781466583160. URL: https://books.google.com.br/books?id=_Xr6AQAAQBAJ.

Mohamad, A.A. (2011). *Lattice Boltzmann Method: Fundamentals and Engineering Applications with Computer Codes*. SpringerLink : Bücher. Springer London. ISBN: 9780857294555. URL: https://books.google.com.br/books?id=5gGFlf-tAIQC.

Morrow, N.R. (1990). *Interfacial Phenomena in Petroleum Recovery*. Surfactant Science. Taylor & Francis. ISBN: 9780824783853. URL: http://books.google.com.br/books?id=Jz70HZMPGWoC.

Munshi, A. M., V. N. Singh, Mukesh Kumar, and J. P. Singh (2008). "Effect of nanoparticle size on sessile droplet contact angle". In: *Journal of Applied Physics* 103.8, p. 084315. DOI: 10.1063/1.2912464. eprint: https://doi.org/10.1063/1.2912464. URL: https://doi.org/10.1063/1.2912464.

Neuman, Shlomo P (1977). "Theoretical derivation of Darcy's law". In: *Acta mechanica* 25.3-4, pp. 153–170.

Omelyan, I. P., I. M. Mryglod, and R. Folk (2002). "Optimized Verlet-like algorithms for molecular dynamics simulations". In: *Phys. Rev. E* 65 (5), p. 056706. DOI: 10.1103/PhysRevE.65.056706. URL: https://link.aps.org/doi/10.1103/PhysRevE.65.056706.

Pathria, R.K. and P.D. Beale (2011). *Statistical Mechanics*. Elsevier Science. ISBN: 9780123821898. URL: http://books.google.com.br/books?id=KdbJJAXQ-RsC.

Pereira, Aline O., Lucas S. Lara, and Caetano R. Miranda (2016). "Combining molecular dynamics and lattice Boltzmann simulations: a hierarchical computational protocol for microfluidics". In: *Microfluidics and Nanofluidics* 20.2, p. 36. ISSN: 1613-4990. DOI: 10.1007/s10404-016-1704-7. URL: https://doi.org/10.1007/s10404-016-1704-7.

Popov, P., G. Qin, L. Bi, Y. Efendiev, Z. Kang, and J. Li (Apr. 2009). "Multiphysics and Multiscale Methods for Modeling Fluid Flow Through Naturally Fractured Carbonate Karst Reservoirs". In: *SPE Reservoir Evaluation and Engineering* 12.02, pp. 218–231. ISSN: 1094-6470. DOI: 10.2118/105378-PA. eprint: https://onepetro.org/REE/article-pdf/12/02/218/2531186/spe-105378-pa.pdf. URL: https://doi.org/10.2118/105378-PA.

Porter, Mark L., E. T. Coon, Q. Kang, J. D. Moulton, and J. W. Carey (2012). "Multicomponent interparticle-potential lattice Boltzmann model for fluids with large viscosity ratios". In: *Phys. Rev. E* 86 (3), p. 036701. DOI: 10.1103/PhysRevE.86.036701. URL: https://link.aps.org/doi/10.1103/PhysRevE.86.036701.

Press, W.H. (2007). *Numerical Recipes 3rd Edition: The Art of Scientific Computing*. Cambridge University Press. ISBN: 9780521880688. URL: http://books.google.es/books?id=1aAOdzK3FegC.

Rao, Feixiong, Andrey V. Kuznetsov, and Yan Jin (2020). "Numerical Modeling of Momentum Dispersion in Porous Media Based on the Pore Scale Prevalence Hypothesis". In: *Transport in Porous Media* 133.2, pp. 271–292. ISSN: 1573-1634. DOI: 10.1007/s11242-020-01423-y. URL: https://doi.org/10.1007/s11242-020-01423-y.

Robin, M. (2001). "Interfacial Phenomena: Reservoir Wettability in Oil Recovery". In: *Oil & Gas Science and Technology - Rev. IFP* 56.1, pp. 55–62. DOI: 10.2516/ogst:2001007. URL: https://doi.org/10.2516/ogst:2001007.

Rycroft, Chris H. (2009). "VORO++: A three-dimensional Voronoi cell library in C++". In: *Chaos: An Interdisciplinary Journal of Nonlinear Science* 19.4, p. 041111. DOI: 10.1063/1.3215722. eprint: https://doi.org/10.1063/1.3215722. URL: https://doi.org/10.1063/1.3215722.

Sangani, A.S. and A. Acrivos (1982). "Slow flow through a periodic array of spheres". In: *International Journal of Multiphase Flow* 8.4, pp. 343–360. ISSN: 0301-9322. DOI: https://doi.org/10.1016/0301-9322(82)90047-7. URL: https://www.sciencedirect.com/science/article/pii/0301932282900477.

Sangtani Lakhwani, NM, FCGA Nicolleau, and Wernher Brevis (2019). "Lattice Boltzmann Method simulations of high Reynolds number flows past porous obstacles". In: *International Journal of Applied Mechanics* 11.03, p. 1950028.

Sarr, A (1983). "Mechanisms of the displacement of one fluid by another in a network of capillary ducts". In: *Journal of Fluid Mechanics* 135, pp. 337–353.

Scheid, F. (1988). *Schaum's Outline of Numerical Analysis*. Schaum's Outline Series. McGraw-Hill Education. ISBN: 9780070552210. URL: http://books.google.com.br/books?id=j1QIhvihBO4C.

Scheid, Francis (1968). *Schaum's Outline Series Theory and Problems of Numerical Analysis*. McGraw-Hill Book Company.

Scheidegger, Adrian E (2020). *The physics of flow through porous media*. University of Toronto press.

Schön, Jürgen H (2015). *Physical properties of rocks: Fundamentals and principles of petrophysics*. Elsevier.

Senechal, Marjorie (1993). "Spatial tessellations: Concepts and applications of voronoi diagrams". In: *Science* 260.5111, pp. 1170–1173.

Shan, Xiaowen and Hudong Chen (1993). "Lattice Boltzmann model for simulating flows with multiple phases and components". In: *Phys. Rev. E* 47 (3), pp. 1815–1819.

DOI: 10.1103/PhysRevE.47.1815. URL: https://link.aps.org/doi/10.1103/PhysRevE.47.1815.

Shannon, Claude Elwood (1948). "A mathematical theory of communication". In: *The Bell system technical journal* 27.3, pp. 379–423.

Sheng, James J. (2020). "Chapter Nine - EOR mechanisms of wettability alteration and its comparison with IFT". In: *Enhanced Oil Recovery in Shale and Tight Reservoirs*. Ed. by James J. Sheng. Gulf Professional Publishing, pp. 213–278. ISBN: 978-0-12-815905-7. DOI: https://doi.org/10.1016/B978-0-12-815905-7.00009-8. URL: https://www.sciencedirect.com/science/article/pii/B9780128159057000098.

Soto, R. (2016). *Kinetic Theory and Transport Phenomena*. Oxford Master Series in Physics. OUP Oxford. ISBN: 9780191025143. URL: https://books.google.com.br/books?id=SsJLDQAAQBAJ.

Stacy, Edney W et al. (1962). "A generalization of the gamma distribution". In: *The Annals of mathematical statistics* 33.3, pp. 1187–1192.

Succi, S. (2001). *The Lattice Boltzmann Equation: For Fluid Dynamics and Beyond*. Numerical Mathematics and Scientific Computation. Clarendon Press. ISBN: 9780198503989. URL: https://books.google.com.br/books?id=0C0Sj_xgnhAC.

Sukop, M.C. and D.T. Thorne (2007). *Lattice Boltzmann Modeling: An Introduction for Geoscientists and Engineers*. Springer Berlin Heidelberg. ISBN: 9783540279822. URL: https://books.google.com.br/books?id=35SWbKnPb5IC.

Suleimanov, Baghir A, FS Ismailov, and EF Veliyev (2011). "Nanofluid for enhanced oil recovery". In: *Journal of Petroleum Science and Engineering* 78.2, pp. 431–437.

Surmas, R. (2010). "Simulação de fenômenos termo-fluidodinâmicos pelo emprego dos métodos de diferencias finitas à solução da equação de Boltzmann". PhD thesis. Universidade Federal de Santa Catarina.

Suxo, Vladivostok and Caetano Miranda (Jan. 2017). "Multiscale fluid dynamics in porous media: applications in enhanced oil recovery". In: DOI: 10.20906/CPS/CILAMCE2017-0357.

Tanemura, Masaharu (2003). "Statistical distributions of Poisson Voronoi cells in two and three dimensions". In: *FORMA-TOKYO-* 18.4, pp. 221–247.

Temam, Roger (2001). *Navier-Stokes equations: theory and numerical analysis*. Vol. 343. American Mathematical Soc.

Tiab, Djebbar and Erle C Donaldson (2015). *Petrophysics: theory and practice of measuring reservoir rock and fluid transport properties*. Gulf professional publishing.

Tian, Lei and Liuchao Qiu (2022). "Modeling the Wettability of Microstructured Hydrophobic Surface Using Multiple-relaxation-time Lattice Boltzmann Method". In: *Journal of Bionic Engineering* 19.5, pp. 1460–1471.

Trojer, Mathias, Michael L. Szulczewski, and Ruben Juanes (2015). "Stabilizing Fluid-Fluid Displacements in Porous Media Through Wettability Alteration". In: *Phys. Rev. Appl.* 3 (5), p. 054008. DOI: 10.1103/PhysRevApplied.3.054008. URL: https://link.aps.org/doi/10.1103/PhysRevApplied.3.054008.

Vishnyakov, Vladimir, Baghir Suleimanov, Ahmad Salmanov, and Eldar Zeynalov (2020). "7 - Oil recovery stages and methods". In: *Primer on Enhanced Oil Recovery*. Ed. by Vladimir Vishnyakov, Baghir Suleimanov, Ahmad Salmanov, and Eldar Zeynalov. Gulf Professional Publishing, pp. 53–63. ISBN: 978-0-12-817632-0. DOI: https://doi.org/10.1016/B978-0-12-817632-0.00007-4. URL: https://www.sciencedirect.com/science/article/pii/B9780128176320000074.

Welander, P (Jan. 1954). "On The Temperature Jump in a Rarefied Gas". In: *Arkiv Fysik* 7. URL: https://www.osti.gov/biblio/4395580.

Wu, Mengjie, Feng Xiao, Rebecca M. Johnson-Paben, Scott T. Retterer, Xiaolong Yin, and Keith B. Neeves (2012). "Single- and two-phase flow in microfluidic porous media analogs based on Voronoi tessellation". In: *Lab Chip* 12 (2), pp. 253–261. DOI: 10.1039/C1LC20838A. URL: http://dx.doi.org/10.1039/C1LC20838A.

Yang, Qian, Xiaolong He, Haonan Peng, and Jianmin Zhang (2022). "Wall wettability effect on process of collapse of single cavitation bubbles in near-wall region using pseudo-potential lattice Boltzmann method". In: *Heliyon* 8.12.

Yilmaz, Burak and Fazilet Yilmaz (2018). "Chapter 8 - Lab-on-a-Chip Technology and Its Applications". In: *Omics Technologies and Bio-Engineering*. Ed. by Debmalya Barh and Vasco Azevedo. Academic Press, pp. 145–153. ISBN: 978-0-12-804659-3. DOI: https://doi.org/10.1016/B978-0-12-804659-3.00008-7. URL: https://www.sciencedirect.com/science/article/pii/B9780128046593000087.

Yu, Zhao, Hui Yang, and Liang-Shih Fan (2011). "Numerical simulation of bubble interactions using an adaptive lattice Boltzmann method". In: *Chemical Engineering Science* 66.14. 10th International Conference on Gas–Liquid and Gas–Liquid–Solid Reactor Engineering, pp. 3441–3451. ISSN: 0009-2509. DOI: https://doi.org/10.1016/j.ces.2011.01.019. URL: https://www.sciencedirect.com/science/article/pii/S0009250911000297.

Zhang, Xiqi, Hongliang Liu, and Lei Jiang (2019). "Wettability and Applications of Nanochannels". In: *Advanced Materials* 31.5, p. 1804508. DOI: https://doi.org/10.1002/adma.201804508. eprint: https://onlinelibrary.wiley.com/doi/

pdf/10.1002/adma.201804508. URL: https://onlinelibrary.wiley.com/doi/abs/10.1002/adma.201804508.

Zhao, Benzhong, Christopher W MacMinn, and Ruben Juanes (2016). "Wettability control on multiphase flow in patterned microfluidics". In: *Proceedings of the National Academy of Sciences* 113.37, pp. 10251–10256.

Zhao, Jianlin, Qinjun Kang, Youping Wang, Jun Yao, Lei Zhang, and Yongfei Yang (2020). "Viscous Dissipation and Apparent Permeability of Gas Flow in Nanoporous Media". In: *Journal of Geophysical Research: Solid Earth* 125.2, e2019JB018667.

Zhou, Kan, Carolyn Coyle, Junye Li, Jacopo Buongiorno, and Wei Li (2017). "Flow boiling in vertical narrow microchannels of different surface wettability characteristics". In: *International Journal of Heat and Mass Transfer* 109, pp. 103–114. ISSN: 0017-9310. DOI: https://doi.org/10.1016/j.ijheatmasstransfer.2017.01.111. URL: https://www.sciencedirect.com/science/article/pii/S001793101634011X.

Zhou, Zhuhuang, Chih-Chung Huang, K Kirk Shung, Po-Hsiang Tsui, Jui Fang, Hsiang-Yang Ma, Shuicai Wu, and Chung-Chih Lin (2014). "Entropic imaging of cataract lens: an in vitro study". In: *PLoS One* 9.4, e96195.